NAVAL POSTGRADUATE SCHOOL

MONTEREY, CALIFORNIA

THESIS

MODELING LASER EFFECTS ON MULTI-JUNCTION SOLAR CELLS USING SILVACO ATLAS SOFTWARE FOR SPACECRAFT POWER BEAMING APPLICATIONS

by

Jamie E. VanDyke

June 2010

Thesis Advisor: Sherif Michael
Second Reader: Alan Scott

Approved for public release; distribution is unlimited

THIS PAGE INTENTIONALLY LEFT BLANK

REPORT DOCUMENTATION PAGE		*Form Approved OMB No. 0704-0188*
Public reporting burden for this collection of information is estimated to average 1 hour per response, including the time for reviewing instruction, searching existing data sources, gathering and maintaining the data needed, and completing and reviewing the collection of information. Send comments regarding this burden estimate or any other aspect of this collection of information, including suggestions for reducing this burden, to Washington headquarters Services, Directorate for Information Operations and Reports, 1215 Jefferson Davis Highway, Suite 1204, Arlington, VA 22202-4302, and to the Office of Management and Budget, Paperwork Reduction Project (0704-0188) Washington DC 20503.		
1. AGENCY USE ONLY *(Leave blank)*	**2. REPORT DATE** June 2010	**3. REPORT TYPE AND DATES COVERED** Master's Thesis
4. TITLE AND SUBTITLE Modeling Laser Effects on Multi-Junction Solar Cells Using Silvaco ATLAS Software for Spacecraft Power Beaming Applications		**5. FUNDING NUMBERS**
6. AUTHOR(S) Jamie E. VanDyke		
7. PERFORMING ORGANIZATION NAME(S) AND ADDRESS(ES) Naval Postgraduate School Monterey, CA 93943-5000		**8. PERFORMING ORGANIZATION REPORT NUMBER**
9. SPONSORING /MONITORING AGENCY NAME(S) AND ADDRESS(ES) N/A		**10. SPONSORING/MONITORING AGENCY REPORT NUMBER**
11. SUPPLEMENTARY NOTES The views expressed in this thesis are those of the author and do not reflect the official policy or position of the Department of Defense or the U.S. Government. IRB Protocol number _____.		
12a. DISTRIBUTION / AVAILABILITY STATEMENT Approved for public release; distribution is unlimited		**12b. DISTRIBUTION CODE** A

13. ABSTRACT (maximum 200 words)

This thesis explores the possibility of power beaming from terrestrial sites to orbiting spacecraft. Solar cell annealing to repair radiation damaged cells and power augmentation for satellites that are battery limited are two of the possible uses for power beaming. Through modeling and simulation a more complete understanding of the expected system response was obtained. A virtual wafer fabrication tool (VWFT) called Silvaco ATLAS was used to simulate a previously optimized InGaP/GaAs/Ge triple junction solar cell's response to a three laser system. The software was used to determine the optimum wavelength for each layer of the cell and then the intensity of the lasers was determined to achieve the same output of the cell as experienced under solar illumination, thereby replacing the sun. The original cell boasted 36.29% efficiency under solar illumination, but by applying the laser system the same cell operated at 51.15% efficiency. The approach and lessons learned can be applied to any solar cell design.

14. SUBJECT TERMS Solar Cell, Photovoltaic, Directed Energy, Power Beaming, Wireless Power Transfer, Multi-junction, Laser, Silvaco, Modeling, Simulation		**15. NUMBER OF PAGES** 141
		16. PRICE CODE
17. SECURITY CLASSIFICATION OF REPORT Unclassified	**18. SECURITY CLASSIFICATION OF THIS PAGE** Unclassified	**19. SECURITY CLASSIFICATION OF ABSTRACT** Unclassified	**20. LIMITATION OF ABSTRACT** UU

THIS PAGE INTENTIONALLY LEFT BLANK

Approved for public release; distribution is unlimited

MODELING LASER EFFECTS ON MULTI-JUNCTION SOLAR CELLS USING SILVACO ATLAS SOFTWARE FOR SPACECRAFT POWER BEAMING APPLICATIONS

Jamie E. VanDyke
Lieutenant, United States Navy
B.S., University of Missouri-Rolla, 2002

Submitted in partial fulfillment of the
requirements for the degree of

MASTER OF SCIENCE IN SPACE SYSTEMS OPERATIONS

from the

**NAVAL POSTGRADUATE SCHOOL
June 2010**

Author: Jamie E. VanDyke

Approved by: Sherif Michael
                 Thesis Advisor

                 Alan Scott
                 Second Reader

                 Rudolf Panholzer
                 Chairman, Space Systems Academic Group

THIS PAGE INTENTIONALLY LEFT BLANK

ABSTRACT

This thesis explores the possibility of power beaming from terrestrial sites to orbiting spacecraft. Solar cell annealing to repair radiation damaged cells and power augmentation for satellites that are battery limited are two of the possible uses for power beaming. Through modeling and simulation a more complete understanding of the expected system response was obtained. A virtual wafer fabrication tool (VWFT) called Silvaco ATLAS was used to simulate a previously optimized InGaP/GaAs/Ge triple junction solar cell's response to a three laser system. The software was used to determine the optimum wavelength for each layer of the cell and then the intensity of the lasers was determined to achieve the same output of the cell as experienced under solar illumination, thereby replacing the sun. The original cell boasted 36.29% efficiency under solar illumination, but by applying the laser system the same cell operated at 51.15% efficiency. The approach and lessons learned can be applied to any solar cell design.

THIS PAGE INTENTIONALLY LEFT BLANK

TABLE OF CONTENTS

THIS PAGE INTENTIONALLY LEFT BLANK

LIST OF FIGURES

THIS PAGE INTENTIONALLY LEFT BLANK

LIST OF TABLES

THIS PAGE INTENTIONALLY LEFT BLANK

EXECUTIVE SUMMARY

The Naval Postgraduate School has had two power beaming theses under the auspices of Professor Sherif Michael. In addition, Professor Michael has advised numerous theses using Silvaco ATLAS as a virtual wafer fabrication tool to simulate and optimize multi-junction solar cells. This thesis serves as the link between these two research interests of Professor Michael's. Through modeling and simulation, a better understanding of the solar cell response to laser illumination was obtained.

The fundamental concept of power beaming is the use of terrestrial-based high-energy lasers to send a coherent directed beam of photonic energy to orbiting spacecraft. Several possible applications for this energy source are outlined in this thesis. Power augmentation was the largest category explored. Satellite uses for this power could be to supplement for solar cell degradation, overcome battery failure, expedite battery conditioning operations and expand payload options for space. The possibility also exists to realize a revolutionary architecture shift in satellite design, if the secondary power source (batteries) were replaced with a globally dispersed network of ground sites. This would provide significant weight savings and eliminate one of the predominate sources of satellite failure modes. The use of ion engines has a multitude of benefits compared to chemical bi-propellant systems. Power beaming to enhance the capability of these ion engines could lead to their increased use over chemical bi-propellant systems in future satellite designs. Finally, solar cell degradation from radiation in the space environment can be reversed through solar cell annealing using lasers. Prior research under Professor Michael has demonstrated that these cells can be restored to near beginning of life (BOL) efficiency levels, providing yet another possible power beaming application.

The quest for higher efficiency solar cells has led to the development of multi-junction solar cells. These cells are designed to utilize a greater percentage of the available solar spectrum. The previous power beaming theses were centered around single junction solar cells with the idea of providing power to our costly aging satellite systems. The future applicability of power beaming will be determined by the ability to transfer energy to multi-junction solar cells since all new satellites are being launched

with them. The construction of these solar cells require a system of lasers to be used and the optimization of this system will most likely determine if power beaming is a cost effective means of satellite lifetime extension.

This research designed a theoretical three laser system to effectively replace the sun for a triple-junction solar cell. The triple-junction solar cell design used in the analysis was designed and optimized by Michael Tsutagawa. Unfortunately, due to proprietary reasons, an actual triple-junction cell could not be modeled. The analysis was accomplished by determining the optimum operating frequencies for each layer of the solar cell and then varying the laser intensities to achieve the same cell output as the cell produced under solar illumination. The laser system yielded an operating efficiency of 51.15% under laser illumination, whereas under solar illumination the cell yielded 36.28%.

The system of lasers designed required variable wavelength and intensity lasers to achieve this efficiency, which is unrealistic in the near future. Therefore, an example using the Air Force's Airborne Laser (ABL) program was used that imparted real world constraints to the power beaming challenge.

This research was concluded with several proposed model upgrades. These upgrades would utilize additional simulation software, namely Satellite Tool Kit (STK), to accurately model changing satellite parameters. The possibility to model varying satellite range, laser energy propagation through the atmosphere and angle of incidence would permit the Silvaco ATLAS software to predict the solar cell response as a function of time.

The purpose of this paper was to enhance the previous research performed under the direction of Professor Michael by incorporating multi-junction solar cells and modeling and simulation. Therefore, the information that was adequately addressed in the two previous power beaming theses was not reproduced here. Instead, this thesis was written such that only the necessary concepts were discussed so that the reader would have sufficient knowledge of the overall power beaming challenge to understand the research performed.

LIST OF ACRONYMS AND ABBREVIATIONS

ABL	Airborne Laser
AFB	Air Force Base
AFRL	Air Force Research Lab
AMOS	Air Force Maui Optical Station
AM0	Air Mass Zero
AO	Adaptive Optics
BILL	Beacon Illuminating Laser
BOL	Beginning of Life
BSF	Back Surface Field
COIL	Chemical Oxygen Iodine Laser
DoD	Department of Defense
EM	Electromagnetic
EOL	End of Life
FEL	Free Electron Laser
GEO	Geosynchronous Earth Orbit
GUI	Graphic User Interface
HEO	Highly Elliptical Earth Orbit
LASER	Light Amplification by Stimulated Emission of Radiation
LEO	Low Earth Orbit
LINAC	Linear Electron Accelerator
MDA	Missile Defense Agency
NREL	National Renewable Energy Laboratory
NPS	Naval Postgraduate School

RF   Radio Frequency

SOR   Star-fire Optical Range

SSAG   Space Systems Academic Group

SSL   Solid State Laser

SSM   Satellite Survivability Module

STK   Satellite Tool Kit

TILL   Tracking Illuminating Laser

VWFT   Virtual Wafer Fabrication Tool

ACKNOWLEDGMENTS

I would like to first thank my wife for her seemingly endless supply of patience when it came to me finishing this thesis. Her love and support through this process has been instrumental to my successful completion of this research.

There is no way to verbalize the amount of help and guidance that I was provided by my thesis advisor, Professor Sherif Michael. His knowledge and energy were invaluable throughout the process.

I would also like to thank the entire faculty and staff in the Space Systems Academic Group (SSAG) for the superb Master's experience I have had at the Naval Postgraduate School. In particular, I would like to thank Professor Alan Scott, who on numerous occasions served as a sounding board for my ideas. His real-world experience has greatly enhanced my educational experience. Also, I would like to thank Professor Richard Olsen, in the physics department, who spent a great deal of time outside of class assisting me throughout my core space curriculum classes and during my thesis work.

THIS PAGE INTENTIONALLY LEFT BLANK

I. INTRODUCTION

A. THESIS OBJECTIVE

The focus of this research was to advance previous research through simulation and to incorporate the use of multi-junction solar cells. The discussion will be centered on a previously optimized triple-junction solar cell, but the approach and lessons learned can be applied to any solar cell design.

B. PREVIOUS WORK

This thesis serves as the link between two of Professor Michael's research interests of solar cell simulation and power beaming. Two previous power beaming theses written under the auspice of Professor Sherif Michael have paved the way for this research. The first thesis, by Richard C. Luce, Jr. is entitled, "Spacecraft Power Beaming and Solar Cell Annealing Using High-Energy Lasers." His work explained why power beaming from ground-based high-energy lasers to on-orbit spacecraft was advantageous. A follow-on thesis by Christopher M. Guoan provided a more in-depth look at each of the technologies involved and included some preliminary cost benefit analysis. Due to proprietary restrictions, the specifications for an actual solar cell were unavailable for this research. Instead, Michael H. Tsutagawa's previously optimized triple-junction solar cell was used to design a laser system. This was accomplished using a VWFT, called Silvaco ATLAS. The three laser system was designed to achieve the same output that the original cell produced when illuminated with the intensity of one sun.

C. BACKGROUND

Through modeling and simulation a better understanding of the entire power beaming challenge can be attained. In order to first be permitted to lase a satellite and subsequently be able to interpret the results, a great many questions must be answered. For example, the laser beam angle of incidence on the solar panels will greatly affect the amount of reflection and therefore the amount of energy transferred. Also, the amount of atmosphere the laser energy must traverse will alter the on-orbit energy supplied to the

solar panels. Simple assumptions like pointing the solar panels at the laser ground site to ensure a 90-degree incident angle and lasing a Geosynchronous Earth Orbit (GEO) satellite will hold both of these variables relatively constant. When the test being contemplated is lasing a "CubeSat" with body mounted solar arrays in Low Earth Orbit (LEO), both of the assumptions fall apart and the only way to fully predict the results and later interpret them is through modeling and simulation.

Beaming power to multi-million dollar satellites requires a complete understanding of the expected satellite system response. Power system specifics limiting the amount of voltage differential or current limitations that protect the wiring insulation must be assessed. Simply increasing the intensity of the laser until something adverse occurs is not an option available to an on-orbit satellite. Initial testing can be conducted on satellites that are near end of life (EOL) and open to testing, but with each candidate the type of solar cell and power system design (to include solar panel pointing ability) will differ greatly. A target satellite that is continuously changing range and the amount of atmosphere that must be traversed by the laser energy must be modeled to ensure limits are not exceeded or energy wasted.

The quest for higher efficiency solar cells has led developers to multi-junction cells. These stacked cells are capable of utilizing a greater percentage of the solar spectrum available, which results in satellite designers realizing significant weight savings or simply more power production capability. Due to their construction, multi-junction solar cells require the use of multiple lasers simultaneously. The viability of power beaming for future applications depends on the optimization of the laser system for these multi-junction solar cells.

D.   AUDIENCE

This thesis is written as a continuation of the previous work performed under Professor Michael. The necessary background for a thorough understanding of the work done is provided. Information required for a complete understanding of the power beaming process that was adequately addressed in the two previous theses will not be regenerated. The reader is encouraged to seek out further details on specific areas as

required by referring to the references in this thesis or the two power beaming theses that were previously written. This thesis was written to communicate the ideas necessary for a complete understanding of the work performed without the reader having advance knowledge of solar cell construction or lasers.

E.   ORGANIZATION

The thesis is organized into chapters, with sections within chapters, and subsections within sections. Chapter II covers some of the possible power beaming applications. Chapter III introduces basic physics concepts necessary for the follow-on discussions for solar cells and lasers. Chapter IV discusses applicable solar cell fundamentals such as semiconductors, p-n junctions, cell construction and solar cell parameters of interest. Chapter V introduces the generic laser to the reader. Chapter VI outlines the Silvaco ATLAS modeling and simulation software used in this research. Chapter VII describes the three laser system design process and results. Chapter VIII contains a realistic example using the Airborne Laser Program platform to provide more real world constraints. Chapter IX provides conclusions and outlines future work to be performed.

THIS PAGE INTENTIONALLY LEFT BLANK

II.   POWER BEAMING

A.   CHAPTER OVERVIEW

Space-based architectures are used when they are the cheapest or the only solution to the problem due to the inherent risk and cost of space-based assets. When problems arise, the very same characteristic that provides protection to the system also creates a major repair problem, its distance from Earth. Power beaming to space assets can help overcome this limitation by extending the life expectancy of our costly space systems. The possibility of power beaming to communications satellites was proposed by Geoffrey Landis in 1989. At the time, limitations in laser power and adaptive optics prevented the idea from being cost effective. This chapter will examine some of the possible applications of power beaming to orbiting solar cell arrays. Christopher M. Guoan's thesis, "Ground-Based High Energy Power Beaming In Support of Spacecraft Power Requirements," provided a detailed look into each of the possible power beaming applications. That work will not be duplicated in this chapter, rather an overview will be provided. For a more in-depth analysis the reader is encouraged to seek out the Guoan thesis.

B.   POWER AUGMENTATION

1.   Solar Panel Degradation

The use of laser power to augment the power received from the sun is a possible mission for power beaming. Due to the harsh radiation environment that satellites operate in, the solar arrays inevitably degrade over the lifetime of the spacecraft. In fact, the inability of a satellite's solar panels to provide the necessary power for the bus means a loss of capability for the spacecraft as it ages. For instance, a communications satellite near EOL may only be capable of producing sufficient power to operate a reduced number of transponders. In some cases, this leaves otherwise perfectly capable transponders (sources of income) idle due to the limited solar panel output. Beaming power to a satellite can provide the degraded solar arrays a source of energy of greater than one sun, which will allow the solar panels to produce the amount of energy required

to operate the otherwise power limited equipment. The amount of restored income or utility of the recovered assets when compared against the cost of beaming the sufficient amount of power will determine whether power beaming is a cost effective means of satellite lifetime extension.

2. Expanded Payload Options

Power augmentation also opens the possibility for power hungry payloads that were once unrealizable for use in space. The space based laser is a good example of such a payload. The amount of power required to pump the laser for any extent of time requires a great deal of fuel to be carried to orbit. If the pumping source could be supplemented by power beaming energy from a terrestrial based laser then the mission now becomes a reality.

3. Power Through Eclipse

Battery failure is currently the biggest limitation on satellite lifetime (Luce 33). Satellite battery capacity decreases over the lifetime of the satellite due to the build-up of internal resistance. Once the battery is incapable of providing sufficient power to the satellite during the eclipse period the satellite is normally put out to pasture. The possibility of powering the satellite through the eclipse period using globally dispersed laser sites could extend the useful life of these satellites by no longer requiring the use of the batteries. In the future, the satellite could be launched with this in mind from the start. The satellite could rely on this system of ground sites to provide power during eclipse starting from the first orbit. This will eliminate the need for large batteries onboard the satellite and result in significant weight savings.

4. Battery Recovery

Frequent charging and discharging of Nickel-Cadmium batteries can have detrimental long-lasting effects (Wertz 421). The battery can be thought of as having a memory of the cycle. For example, a battery that is not fully discharged or fully charged will "remember" the partial states and thereby be incapable of charging to full capacity ("Memory Effect"). The operating characteristics of a LEO satellite require that the

battery be partially discharged several times a day. The satellite batteries require frequent conditioning in order to reset the battery memory and maintain full capacity. This conditioning requires that the batteries be deeply discharged and then fully recharged. The time required to fully recharge a fully discharged battery can impact mission performance. For instance, the battery recharging efforts may preclude the solar arrays from supplying power to the payload for a period of time. The use of laser power to decrease the battery recharging times may be beneficial by allowing shorter down times of the mission payload.

C.   SOLAR CELL ANNEALING

Space is far from a perfect vacuum; in fact the amount of radiation and other particles present detrimentally impacts the lifetime and power output of satellite solar panels. The incident radiation damages the crystalline structure of the solar cells. Depending on the type of radiation (electron, proton, neutron, gamma rays, alpha particles, etc.), the damage incurred can be in the form of crystal lattice displacement or ionization damage. Displacement damage occurs when the crystalline lattice structure is altered by physically relocating an atom in the structure. This relocation leaves a vacancy in the structure and normally results in the atom moving to an interstitial location to create a semi-stable position (Chase 35). Ionization damage alters the majority and minority carrier concentrations within a cell when an incident particle removes orbital electrons. As a result, the solar cell will have a reduced voltage or current output.

This damage can be repaired by either thermal or current annealing. Thermal annealing raises the temperature of the solar cell to sufficient levels to re-grow the crystalline structure, thereby restoring the solar cell efficiency. Current annealing is accomplished by applying a large electrical flow into the solar cell. In both methods, the increase in energy excites the substrate electrons, which moves them into previously damaged locations (Luce 46). Using high-energy lasers to repair these solar arrays has the ability of restoring them to near BOL condition.

D.   PROPULSION

Beaming power to be used for on-orbit propulsion needs can provide significant weight savings. Orbital maneuvering to change or maintain orbital parameters currently requires additional fuel to be carried into orbit. Satisfaction of unforeseen propulsion needs, such as changing a satellite's subsatellite point to adjust to a change in mission requirements, is currently limited due to fuel budget constraints. Additionally, evasive maneuvering is becoming more commonplace due to the ever-expanding amount of debris, which is causing fuel mass budgets to grow.

Electric propulsion is capable of providing these capabilities at considerable weight savings. Electric propulsion provides high specific impulse (I_{sp}) compared to bi-propellant reaction engines, though at the expense of thrust.   Thrust levels of approximately 165 Newton meters and I_{sp}s of 3800 seconds are capable of providing on-orbit propulsion needs. Significant weight savings can be obtained when using an ion engine versus chemical bi-propellant engines. This savings comes from the size of the ion engine and the amount of fuel required. The ion engine requires approximately 10% of the propellant mass that a chemical bi-propellant system would use for a satellite designed for a 12- to 15-year lifetime (Guoan 13). "The weight savings in using an ion engine versus the chemical bi-propellant is typically 4 to 5 times that of the payload carried" (Guoan 16). While the low thrust on the ion engine prevents it from reaching orbital velocities inside the atmosphere of the earth, the weight savings for launch of the satellite would result in significant cost savings or allow for the launching of additional capability (more transponders, etc.).

E.   MANEUVER TIMES REDUCED

The current use of ion engines to raise orbits is severely limited due to the available onboard power. The use of power beaming can provide the satellite's ion engine with coherent and conditioned power at a higher power level than the sun. Also, the ion engine could be powered through eclipse periods allowing for further reduction of the maneuver time. For example, the current timetable for a LEO to GEO transfer using an ion engine is approximately 60 days. By providing the ion engine more power and

enabling its use during eclipse periods, the possibility exists to reduce the time to 20–30 days depending on the weight of the spacecraft (Guoan 15).

F.   SUMMARY

This chapter discussed possible power beaming applications. Some of the applications require a rethinking of how satellites are built and flown, while others are instances that could be used on currently orbiting satellites. Electric propulsion and powering a satellite through eclipse have the possibility of significantly altering the current satellite design process by offering significant weight savings. Other ideas, such as power augmentation and solar cell annealing, could result in significant service life extensions of aging satellites.

Prior research in this field has been done using single junction solar cells; however the future trend in solar cell technology will undoubtedly be centered on the use of multi-junction solar cells in space due to their increased efficiency. Power beaming to multi-junction cells requires the combination of multiple lasers at different wavelengths. Laser system optimization will help determine the cost effectiveness of power beaming for future use.

THIS PAGE INTENTIONALLY LEFT BLANK

III. POWER BEAMING PHYSICS FUNDAMENTALS

A. CHAPTER OVERVIEW

This chapter will cover the basic physics relevant to both solar cells and lasers. The discussion will begin with an overview of the atomic structure. Then electron quantized energy states, sometimes referred to as energy wells, will be introduced. Finally, the electromagnetic spectrum will be covered to include the solar spectrum and light propagation mechanisms. This chapter is not intended to be a comprehensive review of the material, rather an overview to prepare the reader for the chapters that follow. For further understanding the reader is encouraged to seek out the references cited in this chapter.

B. ATOMIC STRUCTURE

The Periodic Table in Figure 1 contains the atomic properties of all of the identified elements. The atomic structures of these elements are made up of positively charged protons, neutral neutrons and negatively charged electrons. The nucleus of each element consists of protons and neutrons held together by nuclear forces. The atomic number of each element (located in the upper left hand corner of each box) is determined by the number of protons present in the nucleus.
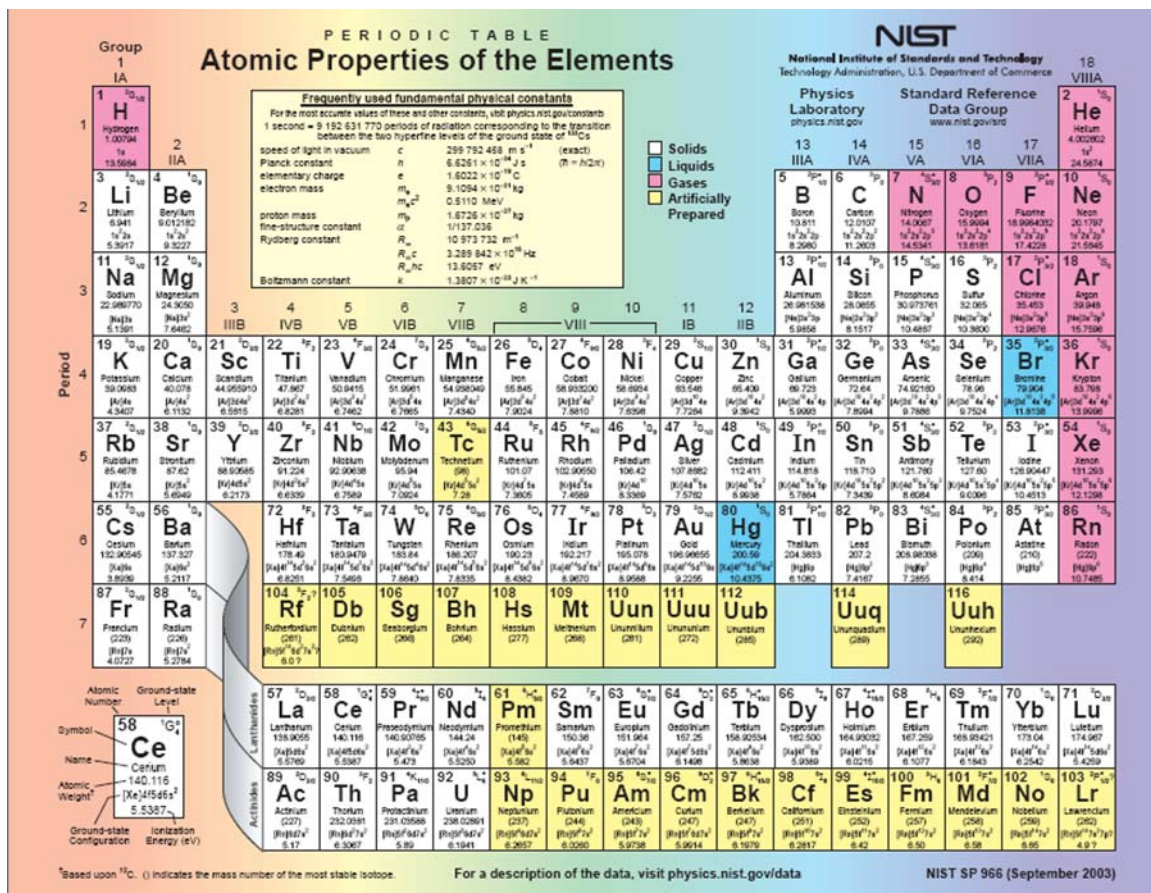
Figure 1.   Periodic Table by NIST (From Tsutagawa 3)

In order for the element to be neutrally charged, the number of electrons orbiting the nucleus of an element must be equal to the number of protons in the nucleus. It is accepted that these orbiting electrons exist in orbiting shells, with each shell consisting of a set number of orbital slots. The innermost shell has two orbital slots and the remaining outer shells have eight orbital slots. The outermost shell is called the valence shell and the number of electrons present in this shell determines the atomic stability of an element. The periodic table in Figure 1 is organized into columns, annotated by roman numerals, called groups. The group number is the number of electrons that exist in the valence shell and can be used to predict the stability of the elements. Elements attempt to create a full outer shell or valence shells to achieve atomic stability, in doing this they will give up, gain or share electrons. For example, Group III elements in the periodic table have three electrons in their outer shell and to achieve a full valence shell the element will give

up 3 electrons resulting in a net positive charge on the element. Group V and higher will attempt to gain electrons to achieve a full outer shell, thereby resulting in a negative net charge on the element. Group IV elements are most likely to share electrons in order to achieve atomic stability through a full outer shell.

C.   ELECTRON ENERGY STATES

Electrons orbiting the nucleus of an atom in an inner shell have a defined amount of energy (E_1) and are capable of absorbing energy to transition to outer shells at higher energy shells (E_2). The energy transferred to the electron can be in the form of heat or photons. The amount of energy between the two energy states is termed the bandgap energy. This electron transition to a higher energy state is termed excitation. The electron conversely can then transition back to the lower energy state by emitting a photon of equal energy, termed de-excitation. This ability to transition between energy states will be essential in the majority of laser designs.

The electron energy levels at the various orbiting shells can also be thought of as an energy well. The electrons are being held by the atom with a set amount of energy at each state. The electrons can be given enough energy to transition between shells and can also be given enough energy to be stripped from the atom completely. For example, Figure 2 is an energy-level diagram of a hydrogen atom.
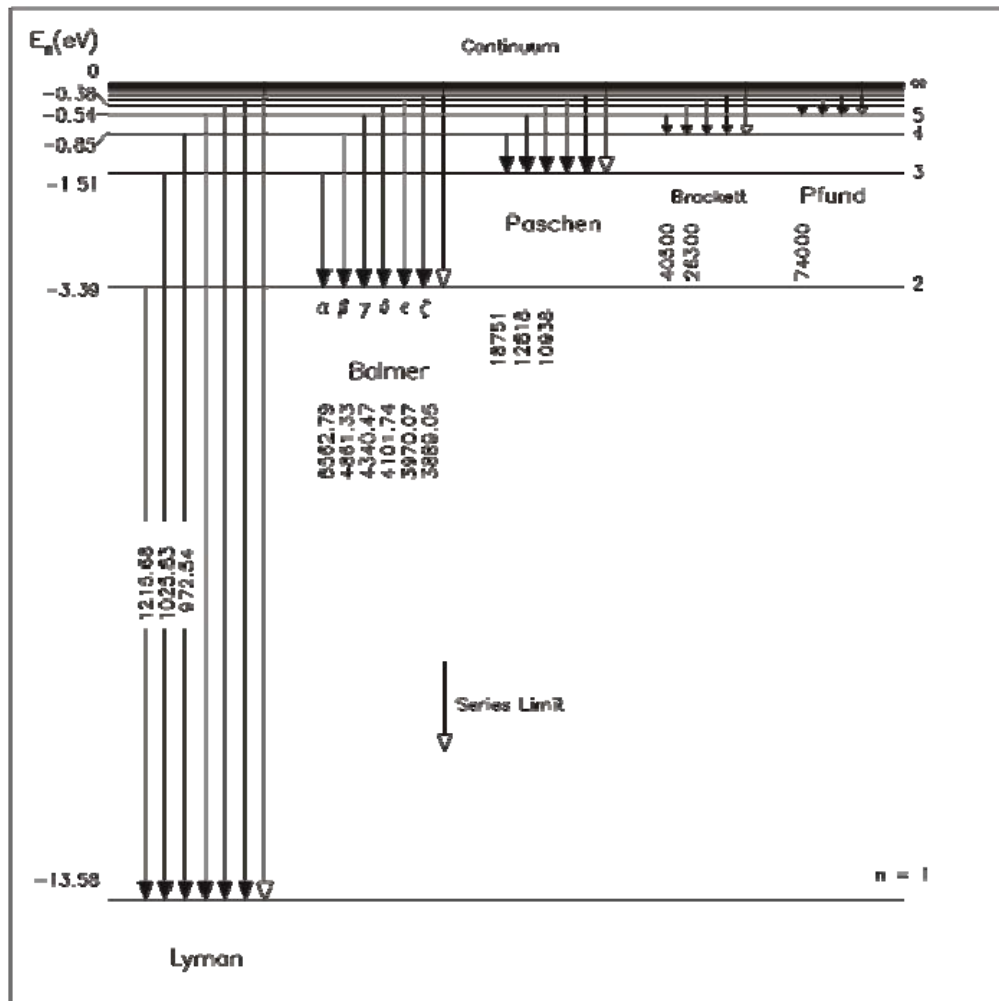
Figure 2.   Energy-level diagram of the hydrogen atom (From Olsen 41)

The hydrogen atom only has one electron and when it is in its ground state the electron contains -13.58 eV of energy. In order to free the electron from the atom, a photon of at least 13.58 eV is necessary, which equates to a wavelength of 91 nanometers (nm). The amount of energy required to strip electrons from various elements determines the conductivity of the element and will be essential in our discussion of semi-conductors with respect to solar cells.

D.   ELECTROMAGNETIC SPECTRUM

The energy in electromagnetic (EM) radiation is an important concept for both solar and laser energy. The electromagnetic spectrum can be described using wave

theory and particle theory. Wave theory leads to the description of the energy in terms of wavelength and frequency; however, when examining the process of the photoelectric effect in solar cells it is more useful to describe electromagnetic energy as particles, otherwise known as photons. Photon energy is a function of the frequency of the light given by Equation 3.1.

$$E = hf \tag{2.1}$$

f = frequency of the EM wave (Hz)

h = Planck's constant = 6.626×10^{-34} J*s = 4.136×10^{-15} eV*s

Figure 3 shows a portion of the EM spectrum with wavelength, frequency and energy plotted vertically along with the common names of each region.
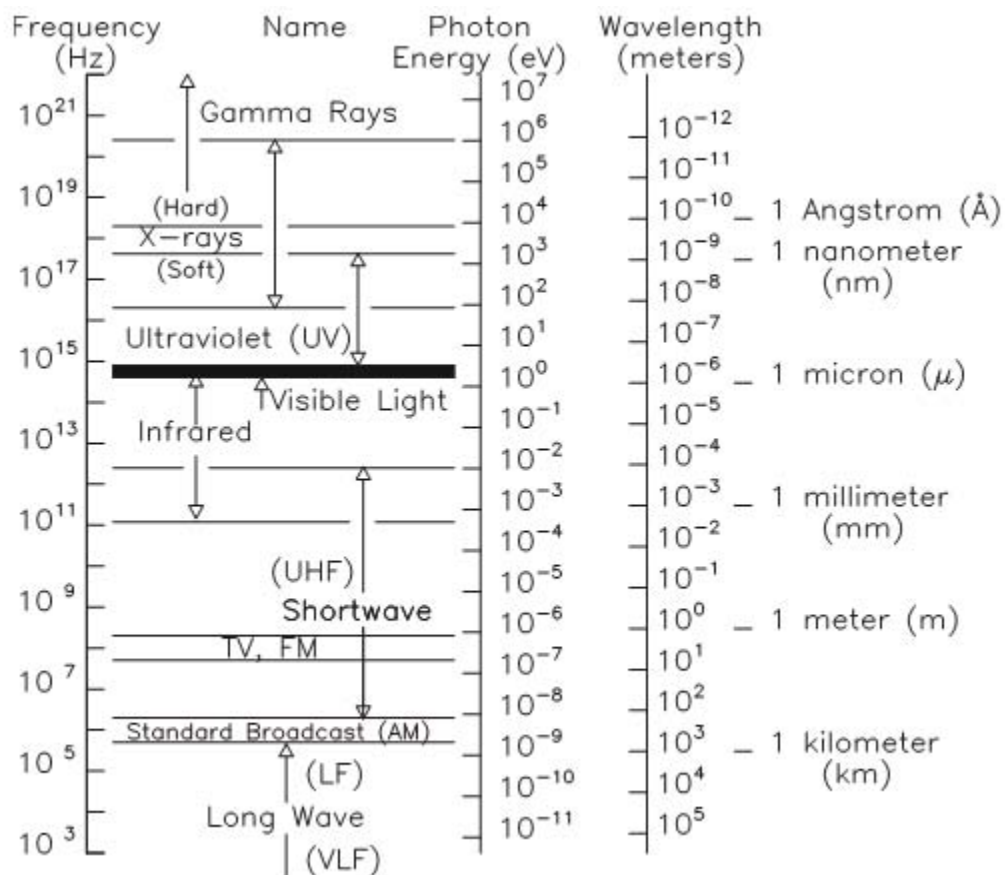
Figure 3.   Electromagnetic Spectrum (From Olsen 34)

1. Solar Spectrum

The EM energy provided by the sun to satellites is known as the Air Mass Zero (AM0) solar spectrum. The data used to produce Figure 4 was measured by the National Renewable Energy Laboratory (NREL) and shows the Spectral Irradiance (W/m^2/µm) versus photon wavelength (µm) for the AM0 solar spectrum.
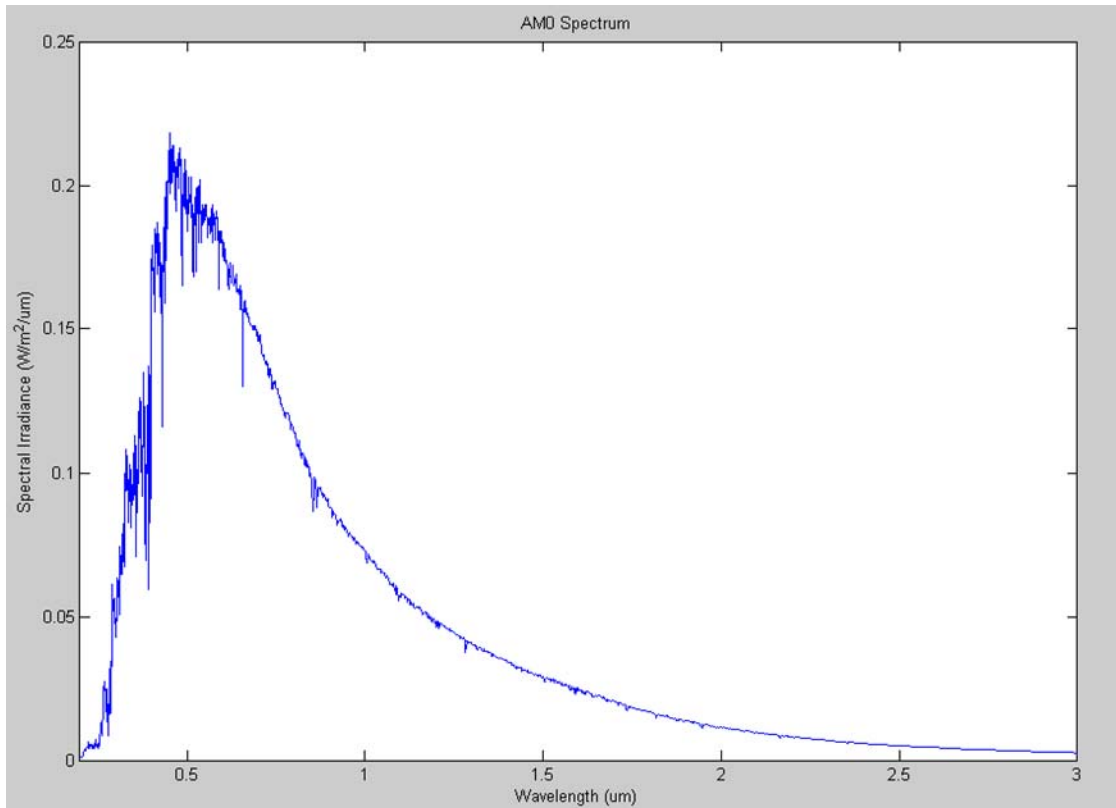
Figure 4.   AM0 Spectrum vs. Wavelength (From Davenport 9)

As discussed previously, the energy of an incident photon on a solar cell must be greater than the bandgap energy for the material in order to free an electron. For this reason, it is useful to plot the AM0 spectrum as a function of energy (see Figure 5).
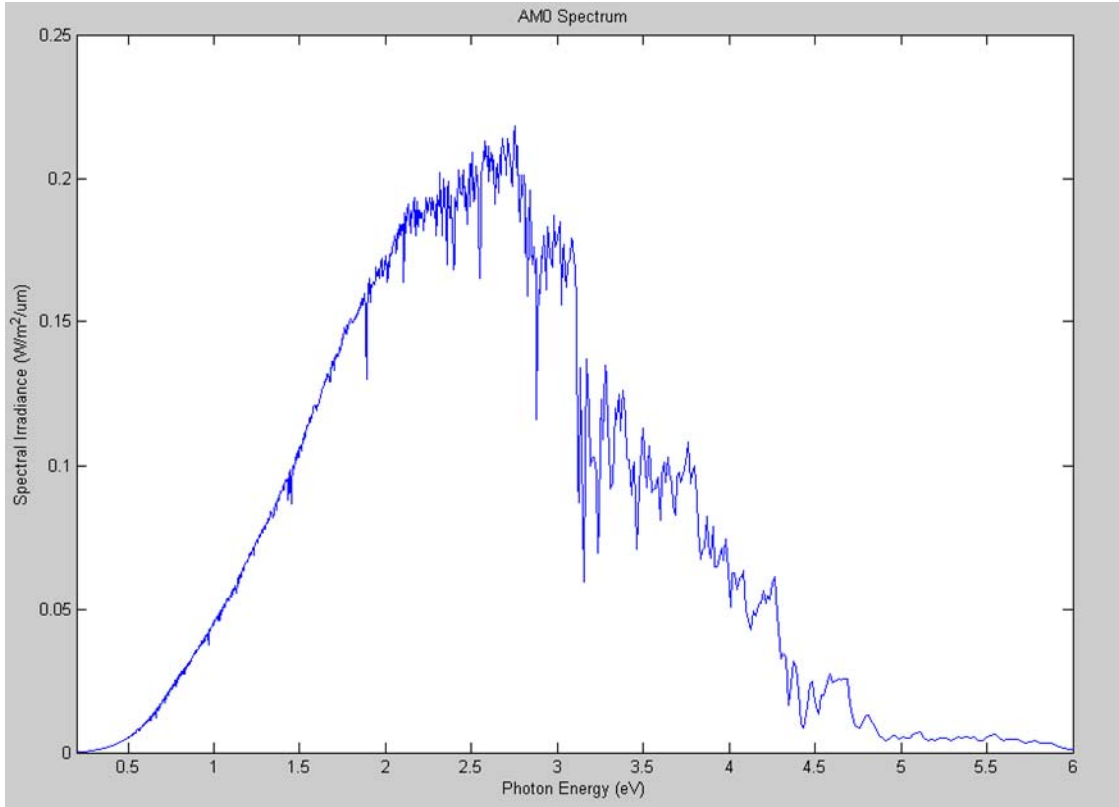
Figure 5.   AM0 Spectrum vs. Photon Energy (From Davenport 10)

The relationship between wavelength and energy is described by Equation 3.2.

$$E = \frac{hc}{\lambda} \tag{2.2}$$

h = Planck's constant

c = speed of light

Another easy-to-remember equation that gives the photon energy in electron volts is shown in Equation 3.3.

$$E(eV) \approx \frac{1.24(eV \cdot \mu m)}{\lambda(\mu m)} \tag{2.3}$$

2.   Atmospheric Absorption, Scattering and Turbulence

Solar cells designated for use in space are designed to receive unfiltered sunlight, but for terrestrial based lasers used for power beaming it is important to consider the filtering effects of the atmosphere. Ground-based high-energy laser systems must first

17

traverse a certain portion of the atmosphere. In doing this there are losses associated, mainly absorption, scattering and turbulence. Turbulence for the most part can be corrected using adaptive optics systems, which will be discussed in Chapter V. Atmospheric absorption and scattering of laser energy have the ability to preclude the use of certain wavelength lasers. Figure 6 shows the percent of transmission verses wavelength through one U.S. standard atmosphere taking into account absorption.
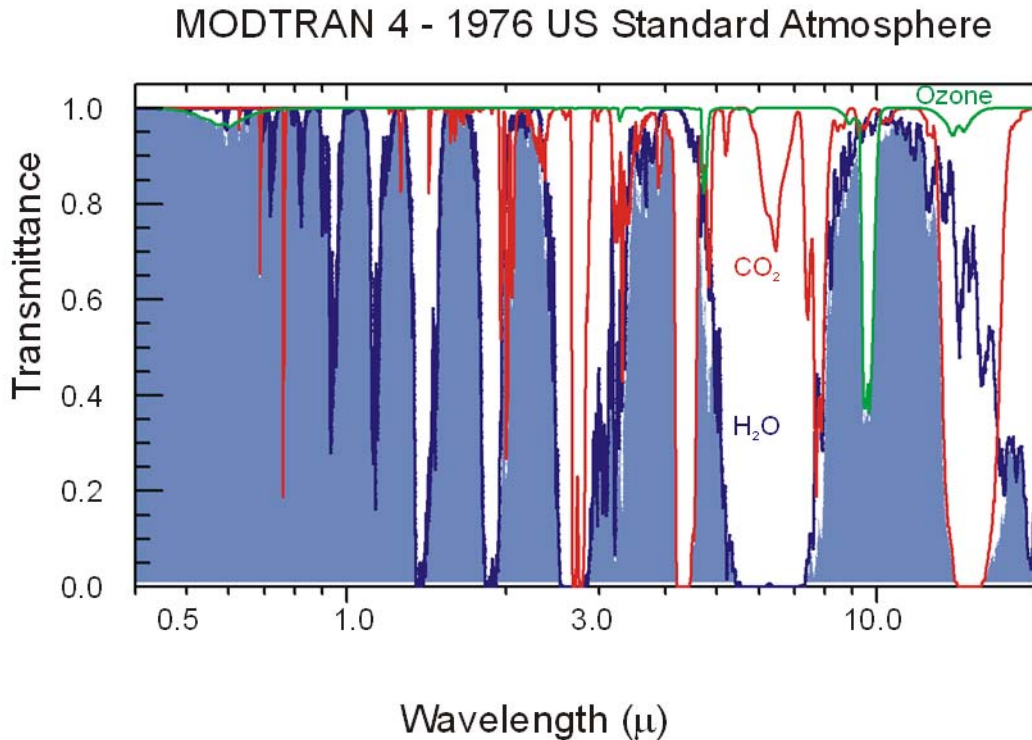
Figure 6.   Atmospheric Absorption (From Olsen 63)

In the visible spectrum, which contains the majority of the solar spectrum of interest, the atmosphere is relatively transparent with respect to absorption. However, as shown in Figure 7, the transmittance drastically decreases when scattering is taken into account.
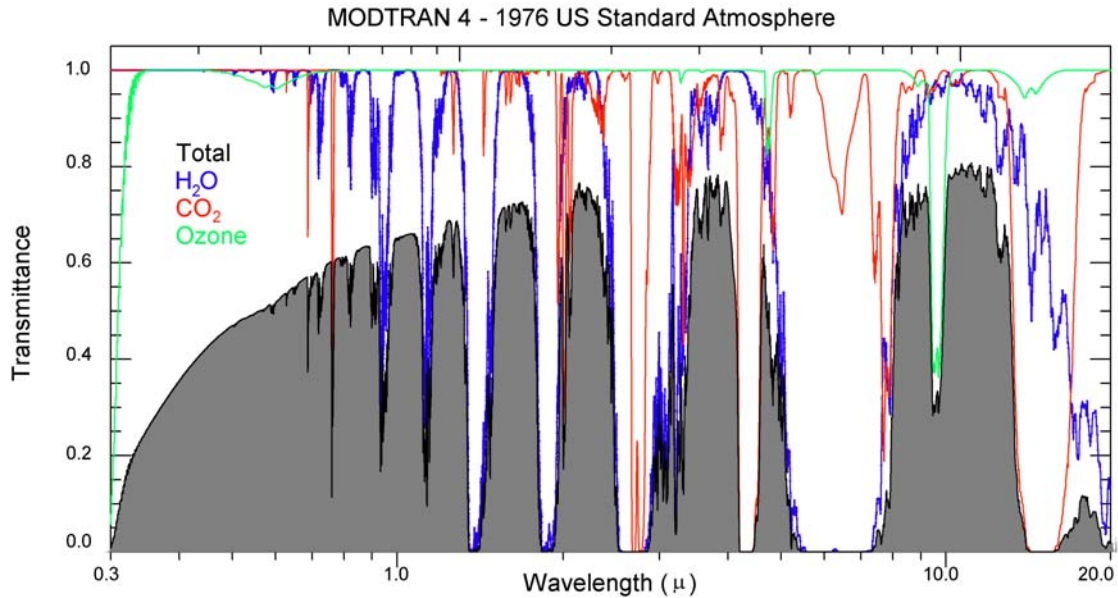
Figure 7.   Combined Effects of Scattering and Absorption (From Olsen 65)

Figure 7 shows the combination of absorption and scattering through one U.S. standard atmosphere. In the visible spectrum, the transmittance drops below 60%, which creates a great deal of loss for ground-based lasers. Although ground-based power can be thought of as unlimited in quantity, it is not with respect to cost. For instance, if the cost of projecting 1 Watt/m^2 is too expensive many of the possible applications of power beaming will not be realizable.   The price must make business sense for most applications. However, some space assets have a mission that is non-commercial. For example, how much would a pound of national security be worth? The extensive amount of scattering can be minimized by placing the laser sites at high altitudes, for example at the Air Force Maui Optical Station (AMOS).   The AMOS is at an altitude of approximately 10,000 feet, which permits the beam to project through much less than one atmosphere and can increase the percent of transmittance significantly.

E.   SUMMARY

This chapter provided some general background information that is necessary for the development of the subsequent chapters. A brief summary of the atomic structure was discussed to set the stage for the introduction of electron energy states. This concept is important for both laser and solar cell topics. Also, an overview of the EM spectrum was provided that included the AM0 solar spectrum and the interactions of light with the atmosphere. Satellite solar cells receive unfiltered sunlight, but the use of ground-based high-energy lasers for power beaming will require the laser to first propagate through the Earth's atmosphere.

IV.   SOLAR CELLS

A.   CHAPTER OVERVIEW

This chapter will cover the solar cell fundamentals needed to understand the phenomenon behind solar cell technology to a degree that will enable the reader to comprehend the research performed. This chapter is not a comprehensive review of all solar cell construction and optimization facets, but rather a general overview.   To facilitate greater understanding of solar cell technology the reader is encouraged to seek out the references cited in this chapter.

B.   SEMICONDUCTOR MATERIALS

Solar cell research requires a fundamental understanding of semiconductor materials. The following section provides an overview of the necessary concepts that will be discussed throughout the remainder of the paper. Semiconductor materials are the cornerstone to the construction of solar cells. Semiconductor materials, as the name implies, fall somewhere between the physical properties of a conductor and an insulator. For example, a conductor such as copper has conductivity of approximately 10^6 mho/cm and an insulator such as quartz (SiO_2) has conductivity of approximately 10^{-16} mho/cm. Semiconductors range in conductivity from 10^{-4}-10^4 mho/cm.

In the previous chapter, the fact that electrons exist in quantized energy states was introduced. It was explained that the electrons orbiting an atom reside in energy wells and require photons of sufficient energy to be freed from the atom, and that amount of energy was termed bandgap energy. Another way to illustrate the concept of bandgap energy is with energy bands. Free or unbound electrons require a certain amount of energy to remain free and serve as majority or minority carriers. This band of energies is termed the conduction band (see Figure 8).
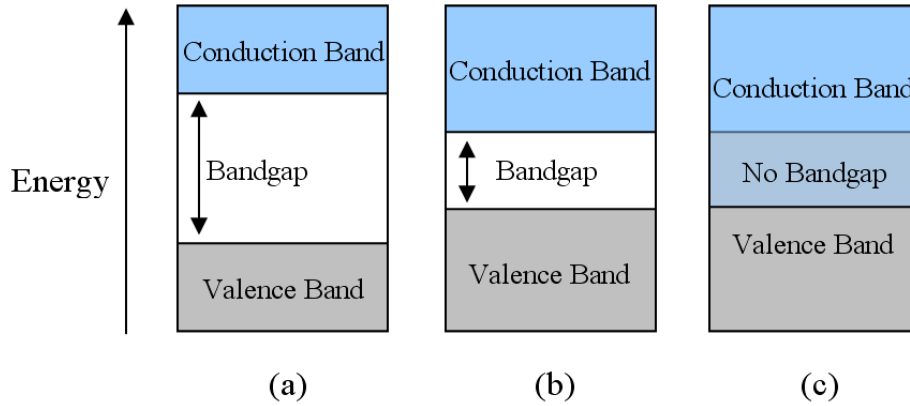
Figure 8.   Band structure of an (a) insulator, (b) semiconductor, and (c) conductor.
(From Bates 4)

The band of energies when the electron is still bound to the atom is termed the valence band.   The difference between the two energy bands is called the bandgap energy. Materials that have zero or negative bandgaps are called conductors (see Figure 8.c). Materials with relatively high bandgap energies are classified as insulators (see Figure 8.a). Materials somewhere between the two extremes are known as semiconductors (see Figure 8.b).

Semiconductors such as Silicon (Si) and Germanium (Ge) are Group IV elements that contain 4 electrons in their valence shells. In a pure Si crystal each atom shares two covalent electrons with its four closest neighboring atoms, thus achieving a stable eight electron outer shell. In order to separate an electron from the nuclei of the Si atom it takes 1.14 eV, known as the bandgap energy (E_g). Typical bandgap energies for semiconductors can be seen in Table 1.

Table 1.   Material Bandgap Energies (After Guoan 74)

Si	1.14 eV
Ge	0.67 eV
InN	0.7 eV
InGaN	0.7 - 3.4eV
InP	1.34 eV
GaAs	1.43 eV
AlGaAs	1.42 - 2.16 eV
AlAs	2.16 eV
InSb	0.17 eV
SiC 6H	3.03 eV
SiC 4H	3.28 eV
GaN	3.37 eV
Diamond	5.46-6.4 eV

The freed electron leaves behind a positively charged hole in the Si structure that can subsequently be filled by a neighboring atom. This progressive movement of holes through the Si structure is in essence current flow. In pure, or intrinsic, semiconductors the concentration of electrons (n) and holes (p) are equal, and have the following relationship (Hu 41):

$$np = Be^{-E_g/kT} \equiv n_i^2 \qquad (3.1)$$

B = approx. 10^{39} (cm^{-6})

k = Boltzmann's constant

n_i = intrinsic carrier concentration

The conductivity of a semiconductor can be increased through doping. For example, if Phosphorus (P) or Arsenic (As), group V elements, are added to Si it will result in an extra electron in the outer shell, which can be easily stripped away. Since the added group V elements donate electrons they are referred to as *donors*. Now the electron density (N_d) is much greater than the density of holes (p) and the material is called an n-type semiconductor where the electrons are the majority carriers and the holes are the minority carriers.

Similarly, the material could be doped with a group III element, such that additional holes are created. Since these dopants accept additional electrons they are referred to as *acceptors*. Now the hole density (N_a) is much greater than the electron density (n) and the materials are called p-type semiconductors. In p-type semiconductors the holes are the majority carriers and the electrons are the minority carriers.

C.   P-N JUNCTION

The p-n junction was invented by William B. Shockley at Bell Labs in 1949 (Tsutagawa 17). A basic understanding of the p-n junction is essential for studying all semiconductor device applications that rely on this phenomenon. The junction is formed when two semiconducting materials are connected, one of which is doped p-type and the other side is doped n-type. At the junction of the two materials, an equilibrium condition is established when the p-type holes diffuse to the n-side and the n-type electrons diffuse to the p-side. This localized diffusion at the junction of the two materials sets up a depletion region where the separation of charge establishes an electric field (see Figure 9).
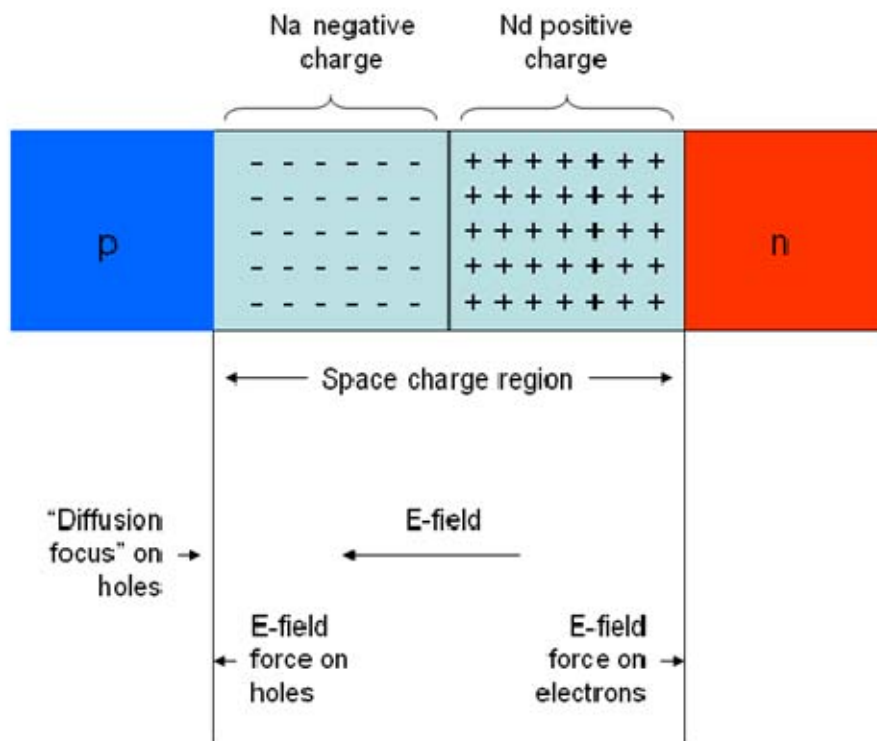
Figure 9.   Depletion Region of P-N Junction (From Lavery 24)

The potential voltage associated with the electric field is called the built-in voltage (V_{bi}) and is dependent on the doping concentrations, temperature and intrinsic concentration of the material. Equation 4.2 can be used to find the built-in voltage.

$$V_{bi} = \frac{kT}{q} \ln\left(\frac{N_a N_d}{n_i^2}\right)$$

(3.2)

$k = 1.38 \text{ X } 10^{-23}$ (J/K)

T = temperature (K)

q = charge (J)

N_a = acceptor concentration

N_d = donor concentration

n_i^2 = majority minority carrier concentration product (cm^{-3})

The only effects of the laser on this built-in voltage will be an increase in the temperature of the p-n junction caused by lattice vibration. This temperature increase will result in a larger built-in voltage and a reduction in solar cell efficiency.

D. PHOTOVOLTAIC SOLAR CELLS

The photovoltaic effect is a basic physical process that allows solar cells to convert light into electrical current. Photovoltaics or solar power generation devices use sunlight to create electron-hole pairs in a p-n junction. The p-n junction forms the foundation for a simple solar cell. As described previously, photovoltaics developed for space applications are constructed to maximize the amount of energy that can be captured from the AM0 solar spectrum. Cells constructed for use in space do not receive the same atmosphere filtered solar spectrum that terrestrial based solar cells receive. Therefore, the solar cells are able to take advantage of energy that the atmosphere filters out for terrestrial cells. For our purposes the sun outside the Earth's atmosphere supplies approximately 1350 Watts/m^2 (Michael, 2010).

1.   Performance Parameters

Solar cells exhibit current and voltage characteristics unique to their construction. Under no illumination at a temperature above absolute zero the I-V characteristic relationship is known as the dark I-V curve. This curve exists due to the thermal energy present in the cell that results in dark current. Figure 10.a shows the dark I-V curve in blue. When the solar cell is illuminated, the photogeneration in the cell develops the light I-V curve relationship; see the red line in Figure 10.a. Figure 10.b illustrates the major performance parameters for solar cells.
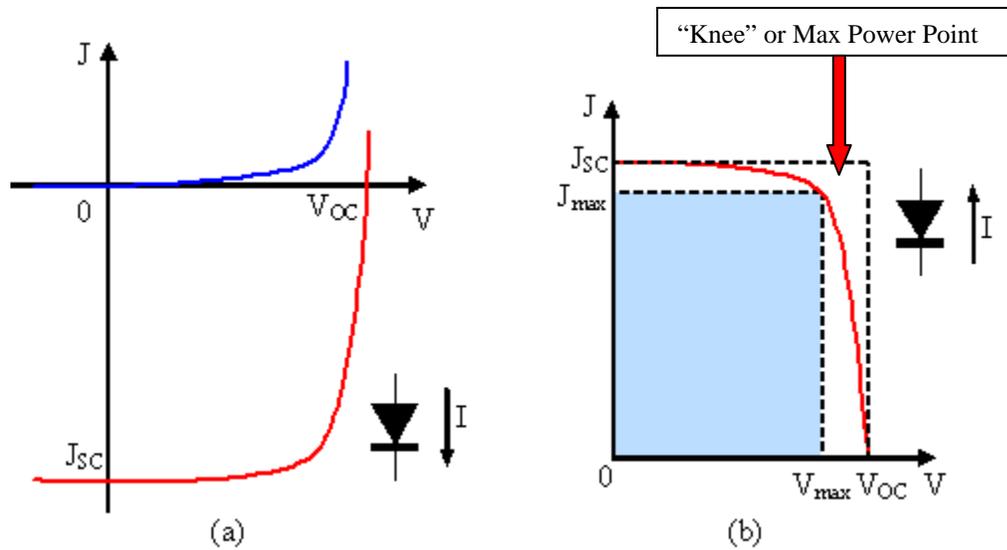
Figure 10.   Dark (blue) and Light (red) I-V Curves (From Tsutagawa 29)

The light I-V curve in Figure 10.b has been inverted for visualization purposes. The open circuit voltage (V_{oc}) and short circuit current density (J_{sc}) are where the I-V curve intersect the x and y axes, respectively.   The maximum voltage (V_{max}) and maximum current density (J_{max}) occur at the knee of the I-V curve where the maximum power output of the solar cell is achieved. The fill factor is the ratio of the max power rectangle ($V_{max}J_{max}$) to the ideal power rectangle ($V_{oc}J_{sc}$), given by Equation 4.3 reported as a percentage.

$$FF = \frac{P_{max}}{P_{V_{OC}-J_{SC}}} \times 100 = \frac{V_{max} \cdot J_{max}}{V_{OC} \cdot J_{SC}} \times 100 \tag{3.3}$$

Solar cell efficiency (η) is another important parameter than determines the cell's power conversion efficiency, given by Equation 4.4 reported as a percentage.

$$\eta = \frac{P_{max}}{P_{inc}} \times 100 = \frac{FF \times V_{OC} \times I_{SC}}{P_{inc}} \times 100 \qquad (3.4)$$

2.   Solar Cell Efficiency Factors

There are many factors that affect the efficiency of a solar cell (EC3230, 2009).

a.   *Reflection*

The reflection of light off the cell surface prevents the energy from being converted. Several factors affect the amount of reflection that occurs. The amount of reflected energy can be reduced by using antireflective coatings or surface texturing.

b.   *Electrical Conductors*

Electrical conductors used to collect electrons are opaque materials and cover approximately 8% of the cell surface. The spacing of the conductors is extremely important in the solar cell design to prevent electron-hole recombination; therefore, the surface area required cannot be reduced. Therefore, 8% of the incident energy is effectively prevented from entering the cell structure and results in a reduction in solar cell efficiency.

c.   *Temperature*

Operating solar cells at other than optimum temperatures (higher or lower) interferes with the flow of charge due to lattice vibrations. Several events can result in an increase in temperature. Internal resistance to charge and current flow produces heat. Also, photons of greater than or less than the bandgap energy required can result in the production of heat. The ability of the laser energy to provide precisely the optimum photon energy limits the temperature increase from this contributing source.

d.   *Defects*

Imperfections in the cell material cause dangling bonds from impurities and defects in the crystalline structure cause recombination problems. The number of defects in the cell structure increases as the cell is irradiated in the space environment.

e.   *Recombination*

Direct or indirect internal recombination of electron-hole pairs can occur prior to utilization. Prevention of premature recombination dictates the size and spacing of cell contacts.

E.   MULTI-JUNCTION SOLAR CELLS

The fact that solar cells only utilize a small portion of the solar spectrum accounts for much of the inherent inefficiency, which can be alleviated through the use of multi-junction solar cells. The use of multi-junction or multi-layered cells enables the conversion of more of the solar spectrum. This is accomplished by layering cells with differing bandgap energies. Each subsequent layer of the cell contains a p-n junction that requires lower bandgap energy, thereby utilizing lower energy photons that the layers above could not. Figure 11 shows the Indium Gallium Phosphide (InGaP)-Gallium Arsenide (GaAs)- Germanium (Ge) solar cell utilization of the solar spectrum.
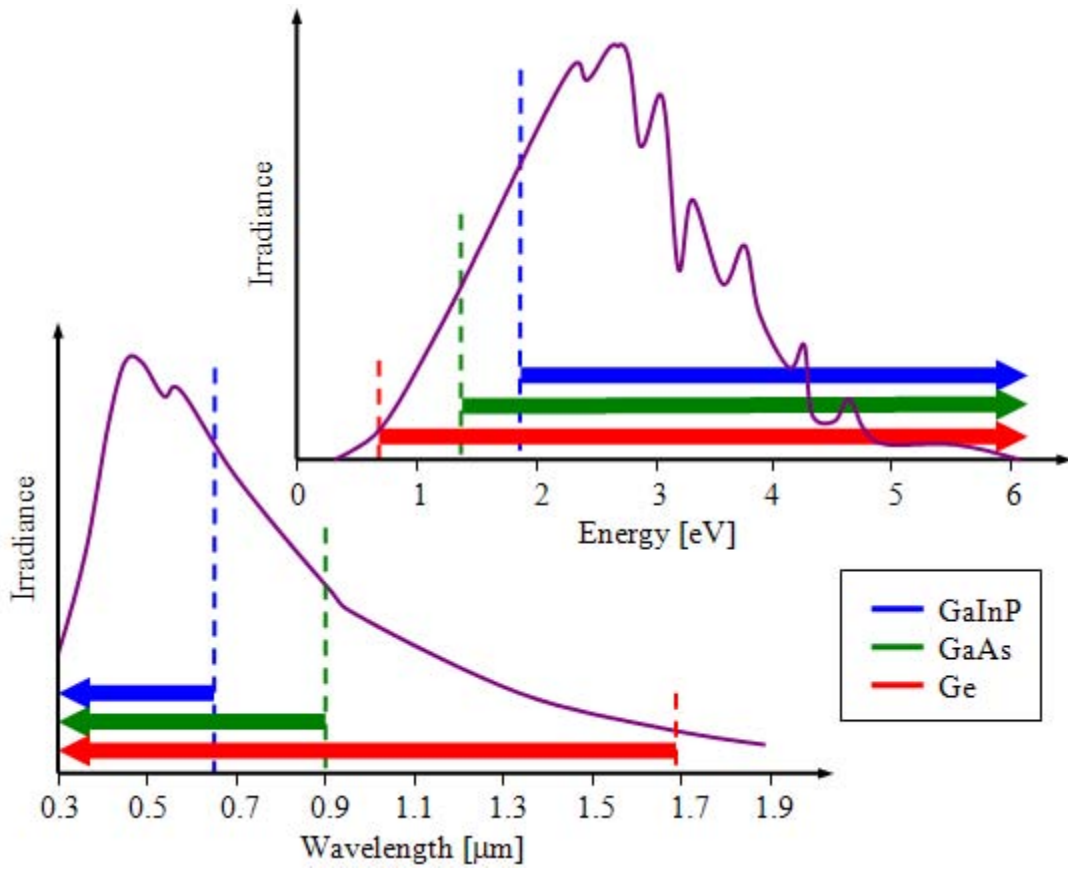
Figure 11.   Solar Spectrum Utilization (From Michalopoulous 63)

The solar spectrum is shown in purple. The top p-n junction (InGaP) requires photons of greater energy (or shorter wavelength) than the GaAs layer as does each subsequent layer.   "In order to avoid a current bottleneck, the junction layer with the lowest current producing capability is placed at the top of the cell, where it receives the full light from the source, and can therefore produce current to its full capacity" (Bates 13).

In multi-junction solar cells the cells are stacked on top of each other and are connected in series. The fact that the individual layers are connected in series results in the total current output of the cell to be the minimum of the layered cells and the voltages of the layered cells to add. The generic I-V curves for typical solar cell materials are shown in Figure 12.
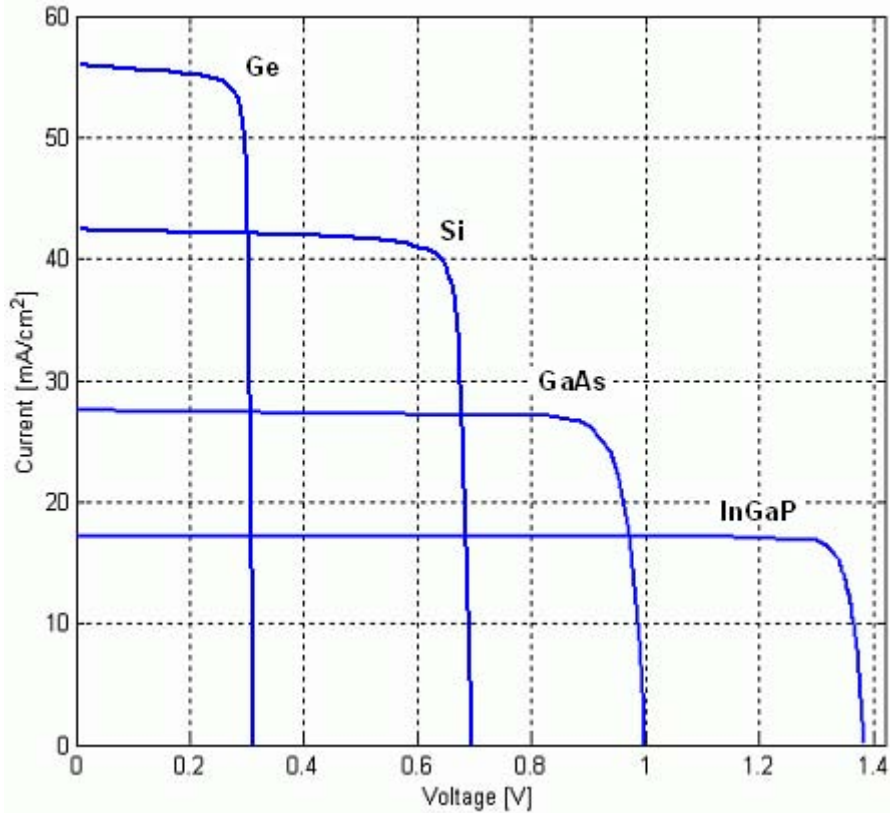
Figure 12. I-V Curves for InGaP, GaAs, Si, and Ge (From Tsutagawa 33)

For example, if the materials in Figure 12 were used to create an InGaP/GaAs/Ge triple-junction solar cell the J_{sc} would be equal to that of the InGaP layer at approximately 18 mA/cm^2 and the V_{oc} would be the sum of the individual open circuit voltages, equal to 2.7 volts.

F. CELL COMPONENTS

This section will introduce terminology necessary for understanding solar cell construction. The cell structure will be discussed from top to bottom. Figure 13 illustrates the construction of a triple-junction solar cell.

Top InGaP Layer	Window	n+ AlInP	0.01µm	5e19cm⁻³
	Emitter	n+ InGaP	0.17µm	4.64e17cm⁻³
	Base	p+ InGaP	0.63µm	1e17cm⁻³
	BSF	p+ InGaP	0.01µm	5e19cm⁻³
	Buffer	p+ AlInP	0.3µm	1e18cm⁻³
Tunnel Junction	Tunnel Emitter	p+ InGaP	0.015µm	8e18cm⁻³
	Tunnel Base	n+ InGaP	0.015µm	1e19cm⁻³
Middle GaAs Layer	Window	n+ AlInP	0.01µm	4.64e17cm⁻³
	Emitter	n+ GaAs	0.01µm	4.64e15cm⁻³
	Base	p+ GaAs	3.87µm	1e17cm⁻³
	BSF	p+ InGaP	0.01µm	5e19cm⁻³
	Buffer	p+ GaAs	0.3µm	7e18cm⁻³
Tunnel Junction	Tunnel Emitter	p+ GaAs	0.015µm	8e18cm⁻³
	Tunnel Base	n+ GaAs	0.015µm	1e19cm⁻³
Bottom Ge Layer	Window	n+ GaAs	0.05µm	7e18cm⁻³
	Emitter	n+ Ge	0.1µm	3e18cm⁻³
	Substrate	p+ Ge	300µm	3e18cm⁻³

Figure 13.   Tsutagawa's Champion Triple-Junction Solar Cell Structure (After Tsutagawa 72)

1.   Contacts

The contacts (not shown) are physically located on the top and bottom surfaces of the solar cell. The contacts serve as drains for the majority and minority carriers, from which they would be channeled to a load to provide electrical power. The top contact would cover anywhere from 2–8% of the surface of the cell to minimize shadowing and

prevent recombination. The bottom contact would cover the entire bottom surface of the cell to prevent recombination and act as a reflective surface to force the light back into the solar cell.

2.   Window

The solar cell window layer is highly conductive to allow electrons to flow to the electrical contact without increasing the solar cell's series resistance. The materials selected have very high bandgap energies that allow them to be nearly transparent to light.

3.   Emitter and Base

The emitter and base layers are the simple n-p junction introduced earlier. "Following the naming convention for bipolar junction transistors, the n-type region in an n-on-p solar cell is called the emitter. Similarly, the p-type region is referred to as the base" (Bates 7).

4.   Back Surface Field

The back surface field (BSF) introduces another junction into the cell structure, creating n-p-p^+ combination. The BSF layer, or p-p^+ junction, makes two contributions to the cell structure. First, the addition of the BSF layer shares the applied voltage between the n-p and p-p^+ junction, which decreases the dark current in the cell. Second, the built-in electric field in the p-p^+ junction reflects the minority carriers, thereby increasing the short circuit voltage of the solar cell.

5.   Tunnel Junctions

Multi-junction solar cells require an interface between the n-p layers to prevent the formation of a parasitic p-n junction that would be formed if the layers were simply stacked on top of one another. The voltage drop across this forward biased parasitic p-n junction would be too large to overcome in the top n-p layer. To solve this problem a thin, highly doped p-n junction is placed between the two n-p layers to serve as a transition layer. The tunnel junction has a drastically smaller forward bias voltage drop

compared to the p-n junction that would have been formed if the cells were simply stacked. "With the use of tunnel junctions, multi-junction solar cells of up to three junctions are commercially available. Four-junction solar cells are being researched, but are not yet in production" (Bates 12).

6. Buffer

The buffer layer is incorporated to achieve higher open circuit voltages.

G. SUMMARY

This chapter covered some of the fundamental concepts necessary for the study of solar cells. Semiconductors are used to construct p-n junctions, which are then used to build solar cells. Also, introduced were parameters used to describe solar cells. Among them were solar cell efficiency and fill factor, which are widely used for comparison purposes for solar cells. Then an introduction into the factors that affect a solar cell's ability to convert incident energy was discussed. Finally, the multi-junction solar cell was discussed. The quest for higher efficiency solar cells has led to the use of multi-junction cells. Due to the construction of multi-junction solar cells their current and future use will require a system of lasers to generate the required bus power. The ability to optimize the ground based laser system could determine whether power beaming is a viable future endeavor.

THIS PAGE INTENTIONALLY LEFT BLANK

V.   LASERS

A.   CHAPTER OVERVIEW

This chapter will develop for the reader some fundamental laser concepts that will be required for a greater understanding of the researched performed. The discussion by no means will be all inclusive, for a more thorough understanding the reader is encouraged to seek out the references cited in this chapter.

B.   LASER FUNDAMENTALS

This section will introduce a generic laser and the applicable concepts for this research. The subsequent sections will discuss more specifically the different types of lasers.

The word *laser* is actually an acronym for Light Amplification by Stimulated Emission of Radiation (LASER). "A laser is a device that amplifies light and produces a highly directional, high-intensity beam that most often has a very pure frequency or wavelength" (Silfvast 1). Most lasers are constructed of three elements, a gain material, a pumping source, and a resonant cavity (Kuhn 19). Laser gain materials contain the atoms that will be excited to a higher energy state, and subsequently produce a photon when the electrons transition to their ground state. "Lasers can be constructed from solids, liquids, gases, or plasmas. In all cases laser action occurs because photons are emitted as the system transitions between two energy states" (Kuhn 9).   When an electron spontaneously decays from one energy state E_2 to a lower energy state E_1, it emits a photon of the energy difference between the two states where (Kuhn 11):

$$E = hv = E_2 - E_1 \qquad\qquad (4.1)$$

h = Planck's constant

v = frequency of the laser light

A conversion between the energy difference between the two states in electron volts and the wavelength of the emitted photon in micro-meters is given below.

$$\lambda(\mu m) = \frac{1.24(eV * \mu m)}{E(eV)} \tag{4.2}$$

Lasers use a process called stimulated emission, in which an incident photon of wavelength hv forces an electron in energy state E_2 to decay to energy state E_1. The incident photons of wavelength hv are generated from previous electrons decaying or from an external source, known as a pumping source, that are contained within a resonant cavity in most cases. The resonant cavity is usually a series of highly reflective mirrors that establish a regenerative path for the photons to follow forcing them to pass through the gain material a fixed number of times before escaping the resonant cavity. As the population of photons of energy state E_2 becomes greater than photons of energy state E_1 in the gain material a process known as population inversion occurs. The Boltzman equation governs the population ratio of the two energy states in thermal equilibrium (Kuhn 13):

$$\frac{N_2}{N_1} = e^{-(E_2 - E_1)/k_B T} \tag{4.3}$$

N_2 = population of photons in energy state E_2

N_1 = population of Photons in energy state E_1

k_B = Boltzman's constant

T = temperature (degrees Kelvin)

This equation implies that N_2 greater than N_1 only occurs when the temperature of the material is negative, which is physically impossible. This requires that lasers operate in non-equilibrium conditions and therefore require a pumping source to elevate the population of atoms in energy state E_2. Lasers can use chemical reactions, external light sources or electric sparks for pumping sources.

Different types of lasers are only capable of lasing at specific wavelengths. These wavelengths are dependent on the cavity length and the gain material.

> A laser can only lase at those wavelengths for which an integral multiple of half-wavelengths precisely fit into the cavity. The set of possible integral multiples of the cavity length is termed the set of longitudinal electromagnetic modes of the cavity (or simply the longitudinal modes). (Kuhn, p. 21)

The frequencies of these modes are given by:

$$v = \frac{pc_o}{2nL} \tag{4.4}$$

$p = 1, 2, 3, \ldots$

n_r = index of refraction of the cavity

c_o = speed of light in a vacuum (m/s)

L = cavity length (meters)

Another often reported stat for lasers is the longitudinal mode spacing given by (Kuhn 22):

$$\Delta v_{FSR} = \frac{c_o}{2nL} \tag{4.5}$$

This information alone is not very useful without an understanding of the frequency dependence of the gain material, termed the gain profile. There are an infinite number of possible longitudinal modes, but the intersection of these modes with the gain profile will determine the output of the laser. The bottom of Figure 14 illustrates the useful frequencies and the corresponding intensity of a generic laser.
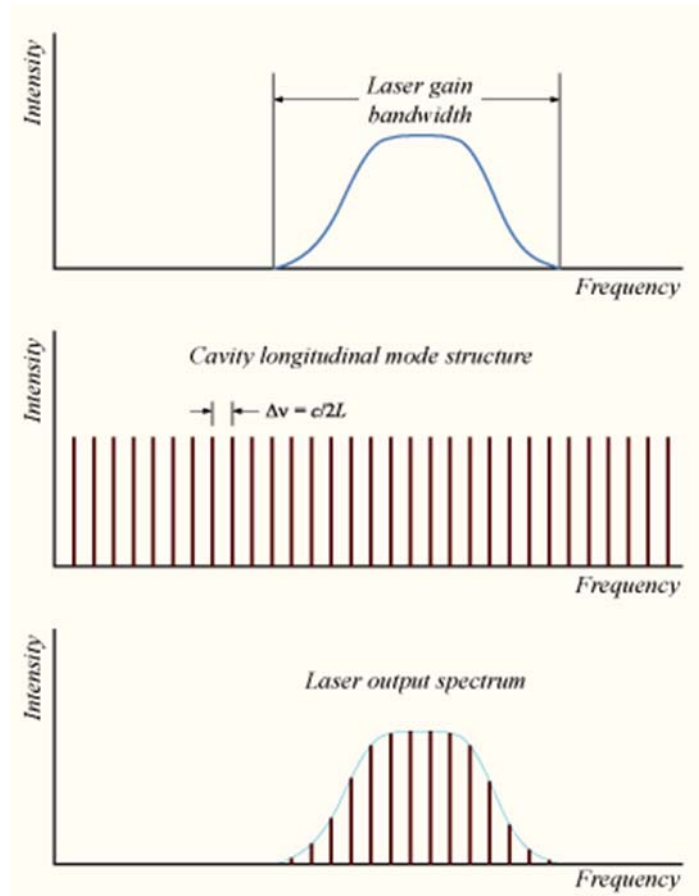
Figure 14.   Useful Laser Frequencies (From "Mode-locking" 2010)

The efficiency of the laser will depend on where in the gain profile the laser is operated. Any of the modes located on the center frequency will produce the greatest amount of intensity, whereas operating the laser at frequencies on the leading or trailing edge of the gain profile will result in significantly lower output.

The selection of a laser for power beaming applications requires the determination of the optimum frequency taking into account the laser capabilities, solar cell response and atmospheric transmission. Another consideration for testing is availability, meaning do the possible sites already possess a laser of sufficient energy at a frequency of interest for the cell that is to be illuminated. To further complicate the issue, with a multi-junction solar cell multiple lasers are required since the solar cell output is dependent on the current output of the limiting layer. Therefore, a laser of sufficiently larger power would be appropriate for the limiting layer of a multi-junction cell.

C. TYPES OF LASERS

Laser operating frequencies are largely dependent on the gain material of the laser. Not all materials are capable of serving as laser gain materials. Table 2 shows some of the most common high energy laser materials and their primary operating frequency.

Table 2. Common High Energy Lasers (After Luce 6)

Laser Material	Wavelength (μm)
Neodymium: YAG (Nd: YAG)	1.064
Chemical Oxygen Iodine (I)	1.315
Hydrogen Fluoride (HF)	2.8
Deuterium Fluoride (DF)	3.8
Carbon Dioxide (CO_2)	10.6

1. Chemical Lasers

Chemical lasers use a consumable pumping source that results in relatively short duration beams. "It uses an exothermic (energy liberating) reaction as an energy source to pump a low pressure gas phase gain medium" (Guoan 36). The short duration firing times for the high energy chemical lasers makes their application limited in power beaming. However, the current power levels available with the Chemical Oxygen Iodine Lasers (COIL), which are in the megawatt class, may have applicability in solar cell annealing. This laser will be discussed further in Chapter VIII.

2. Solid State Lasers

Solid state lasers (SSL) use solid crystalline materials as their gain material. The SSL can be either optically or electrically pumped. The optically pumped SSL are low power lasers up to just a few watts. Electrically pumped or diode lasers use a forward biased p-n junction to inject electron-hole pairs into a semiconductor to create light. Again,

the electrically pumped SSL are low power, but the lasers can be built into large arrays to achieve higher powers. The only limitation on the number of diode lasers that could be assembled together would be the ability to dissipate the heat generated (Guoan 38).

3.   Free Electron Laser

The free electron laser (FEL), otherwise known as Xaser, is tunable from millimeter to x-ray wavelengths (Guoan 35). The FEL differ from the generic laser discussed previously, in that, it uses a relativistic electron beam as the lasing medium vice bound atomic or molecular state electrons. Without the predetermined energy states of the bound electrons, the FEL can achieve a virtually infinite number of lasing frequencies.

The FEL laser uses a linear electron accelerator (LINAC) and a wiggler section of alternating polarity magnets to accomplish a coherent laser beam. The sheer size of the FEL laser system is currently on the order of football fields. Therefore, although the possibility of using a FEL exists for a single junction solar cell it is highly unlikely that multiple FELs will coexist on the same site for some time to come. The U.S. Navy has recently conducted a preliminary design review of the Boeing FEL design for use on ships, which should continue to push the size and cost down to realistic levels for implementation for future power beaming applications (Boeing, 2010). The ability to tune the laser frequency makes the FEL an excellent candidate for satellite power beaming since the variations in on-orbit satellite solar cells will require multiple frequencies in order to fully optimize the system for each type of cell.
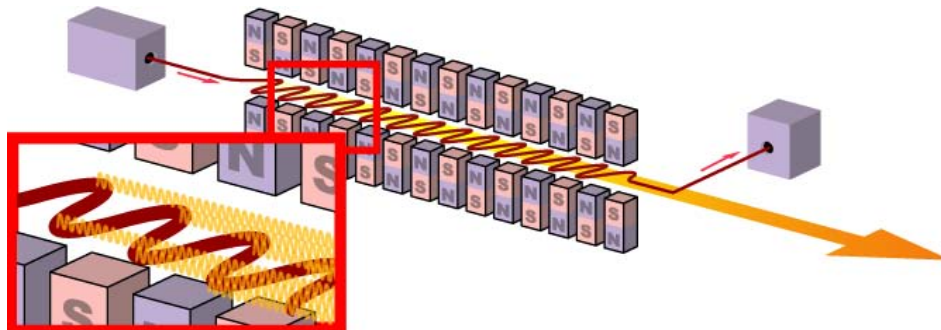
Figure 15.   FEL Schematic (From "Free Electron Laser" 2010)

D. BEAM PROPAGATION

1. Adaptive Optics

Adaptive optics systems correct for optical distortions that occur when the laser wavefront traverses through changes in the density of the atmosphere or wind speed, which cause atmospheric turbulence. "Adaptive optics works by measuring the distortions in a wavefront and compensating for them with a spatial phase modulator such as a deformable mirror or a liquid crystal array" ("Adaptive Optics"). The Guoan thesis provided an overview of available adaptive optics packages, sufficient for our purposes. In order to model the positive effects of an adaptive optics system on laser propagation the Strehl ratio is used.

> The effectiveness of the adaptive optic system is characterized by a Strehl ratio, which is the ratio of the actual peak intensity produced by the laser to the ratio which would be produced with no atmospheric distortion. For perfect compensation, the Strehl ratio would be unity. For systems of the type likely to be constructed in the near future, a Strehl ratio of 0.85 could be expected for a vertical beam, decreasing to 0.65 at 60° zenith angle. (Landis 7)

A more accurate model can be produced when the adaptive optics package to be used for power beaming has been determined. The relationship for how the Strehl ratio varies as a function of zenith angle will aid in developing a more accurate model.

2. Laser Power Requirements Example

This section will systematically step through the laser power requirement calculations to illuminate a satellite. The equations and approach are a reproduction of work by Geoffrey Landis, in which power beaming to GEO communication satellites was approximated. This example allows for a simplification of the LEO power beaming problem by holding the distance between the laser site and the target constant, along with the amount of atmosphere that must be traversed through. The diffraction limited spot radius (r_{spot}) is determined using the inverse-square law of propagation, shown in Equation 5.6 (Landis 6).

$$r_{Spot} = \frac{0.61 d \lambda}{r_{lens}} \qquad (4.6)$$

d = target distance (m)

λ = laser wavelength (m)

r_{lens} = radius of telescope aperture (m)

A GEO communications satellite is approximately 36,000 kilometers from the laser ground site. Using the spectral response for silicon solar cells at approximately 800 nm and a telescope of radius 2.5 meters, the calculated spot radius is 7 meters. "The spot radius is here defined as the first zero in the diffraction pattern; this contains 84% of the beam energy" (Landis 6). This equates to illuminating an area of 150 m^2 at GEO. Solar cell efficiency under laser illumination at wavelength (λ) can be determined using (Landis 5).

$$\eta_{Laser} = \frac{\eta_{Solar} P_{Sun} SR(\lambda)}{J_{SC}} \qquad (4.7)$$

η_{Solar} = Solar cell efficiency under solar illumination (%)

P_{sun} = Average solar density (Watts/m^2)

$SR(\lambda)$ = Spectral Response of solar cell (A/W)

J_{sc} = Short circuit current of solar cell (Amps)

Our hypothetical GEO communications satellite is currently operating at 8% solar efficiency (η_{Solar}), with a spectral response of 0.5 A/W for a 800 nm laser (SR(800 nm)) and EOL short circuit current density (J_{sc}) of 0.029 A/cm^2. Estimating the average solar density at 1350 W/m^2 results in a 19% efficiency of the solar cell under laser illumination. Therefore, the required power at the satellite to obtain the equivalent of one sun of intensity is 580 W/m^2.

Approximating the Strehl ratio of a vertical beam to be 0.85 with the available adaptive optics and assuming the 16% loss of the power that fell outside the first zero of the diffraction pattern, the required ground-based laser would be approximately 120 kW.

The 120 kW ground based laser would illuminate a 150 m^2 area that encompasses the target satellite and provides a power density of 580 W/m^2.

E.   BEAM COLLIMATION

As discussed previously multi-junction solar cells require unique wavelengths of energy for each layer, therefore the collimation of laser beams is required to beam power to multi-junction cells. This can be accomplished through the use of fiber optics or multiple laser feeds into a single tracking telescope.

1.   Fiber Optic

Combining multiple wavelengths of light into a fiber optic strand allows a single telescope to be used.

2.   Multiple Laser Feeds

This configuration would require additional optics to feed multiple lasers into a single telescope

F.   SUMMARY

This chapter covered the necessary laser concepts for the remainder of the thesis discussion. The proposed model for power beaming begins with the output of the laser. Therefore, only the applicable laser fundamentals were discussed. These included the ability to operate lasers at other than optimum frequencies at reduced efficiency, types of lasers and energy propagation. The reader should understand that operating a laser at other than optimum frequencies would need to be included into any future cost benefit analysis when selecting a system of lasers for power beaming to a multi-junction solar cell.

THIS PAGE INTENTIONALLY LEFT BLANK

VI. SILVACO MODELING SOFTWARE

A. CHAPTER OVERVIEW

The use of sophisticated modeling software to design and optimize solar cells is still developing with many solar cell producers still fabricating actual cells for testing. This chapter will introduce the reader to Silvaco modeling software that has been used to model many electro-optical devices such as solar cells. In addition, the previous work will be discussed for a complete understanding of the programming methodology for future contributors.

B. SILVACO SIMULATION ENVIRONMENT

The DeckBuild run time environment was used to write the command file for the VWFT. This command file allows the user to build a virtual solar cell that can then be illuminated using a power file that simulates the AM0 solar spectrum in the ATLAS device simulator. The simulator provides runtime outputs, along with output files that can then be interpreted using programs such as TonyPlot or Matlab for visualization. Figure 16 shows an overview of the Silvaco ATLAS inputs and outputs.
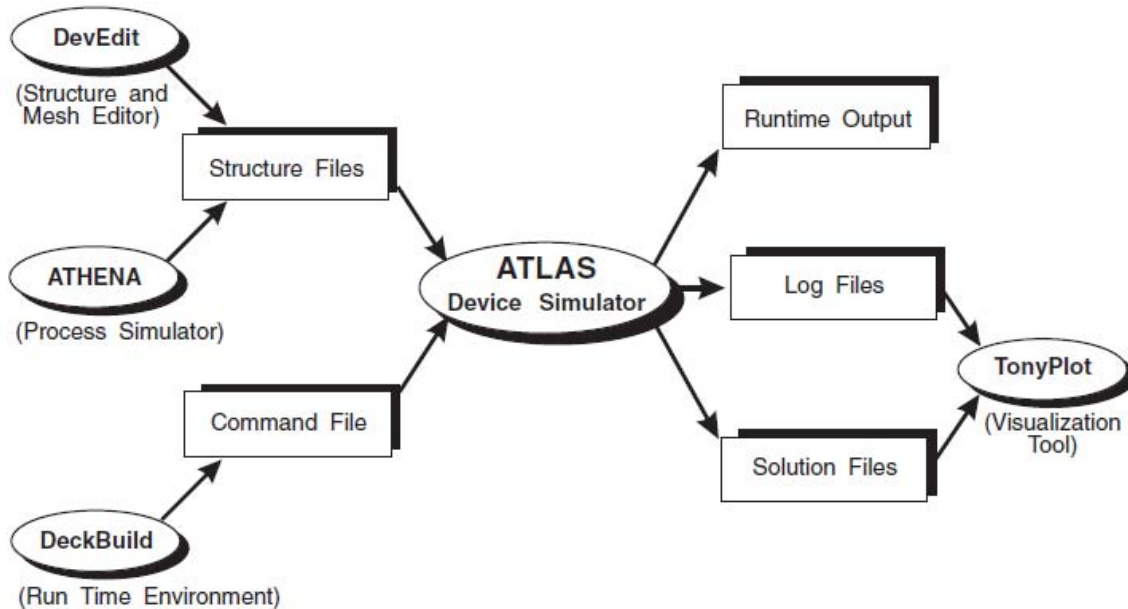
Figure 16.   ATLAS Inputs and Outputs (From SILVACO 2010)

45

C. SILVACO PROGRAMMING OVERVIEW

The Silvaco modeling software was used to model and optimize the design of solar cells virtually. This optimization was accomplished by altering the thicknesses and doping concentrations of the different layers. The modeling and simulation allowed for thousands of combinations to be investigated without the costly fabrication of the actual solar cells.

1. Simulation Source Code

This section will introduce the scheme that was followed when writing the Silvaco program files. This introduction is meant to enhance the understanding for future developers and aid in avoiding repetition. All Silvaco files are divided into the following main sections:

```
# Mesh
# X-Mesh
# Y-Mesh
# Regions
# Electrodes
# Doping
# Material properties
# Models
# Light beams
# Solving
```

First the mesh that the cell will be constructed on is defined. This mesh consists of numerous triangles, the density of which determines the resolution of the simulation. The resolution will determine how accurately the solar cell is represented and the amount of time required for each iteration of the program. Figure 17 shows a typical mesh division that the solar cell would be built upon.
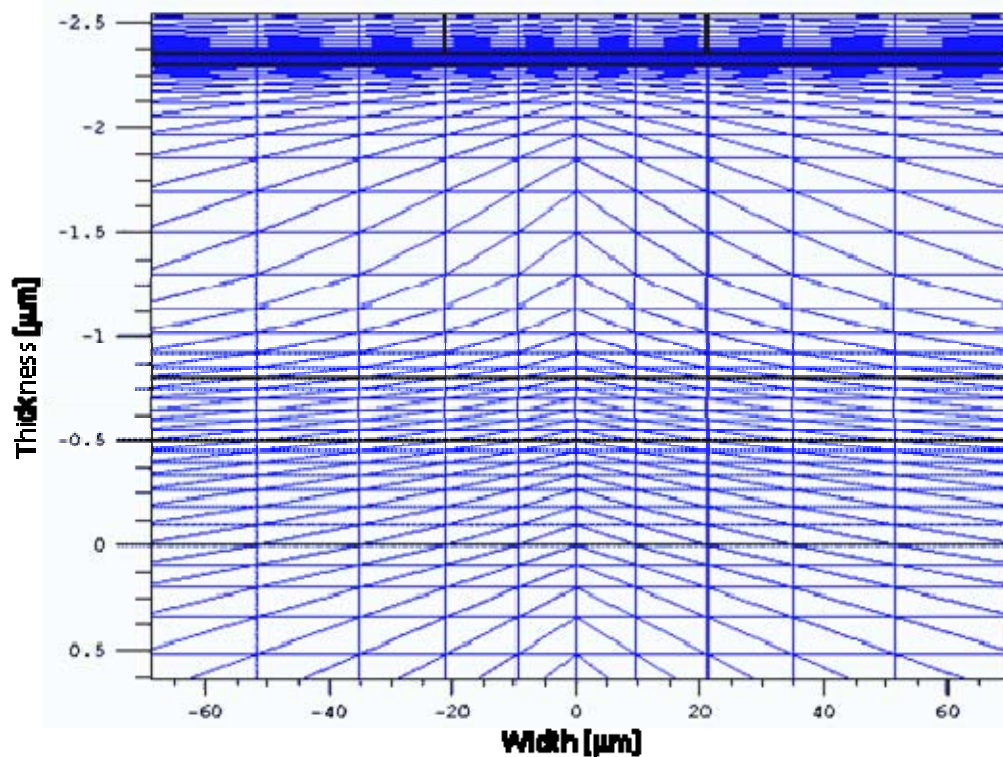
Figure 17.   Typical Structure Mesh (From Michalopoulos 75)

Of note, the density of mesh can be varied to provide finer resolution where the majority of the electron-hole production occurs. If the resolution is too crude the simulation results can be misleading and if the resolution is too fine the amount of time required to run the simulation can overwhelm an average computer. Next the cell is divided into regions with each region assigned a material. Then the electrodes that connect each cell in series are defined. The amount of doping for each region is assigned in the next section. Then the material properties to be used by the program are defined. The common materials are contained within a library, but the more exotic materials used in solar cell construction can also be defined by the user. The user defined materials require that an optical file be generated (.opt) that specifies the real and imaginary portions of the index of refraction. Next the model to be used to evaluate the structure is called. There are more than 70 different models available, with each having the ability to gain a better understanding of the phenomenology. The model used to evaluate the simulated cell in this thesis was the Shockley-Read-Hall model. The Shockley-Read-Hall

47

model was determined to provide, "the best results closest to the experimental cell" (Tsutagawa 41). Next, the light source is developed. This will be described in more detail in a subsequent section. Finally, the solve statement is used to evaluate the structure at each triangle intersection and generate output files.

2. Software Validation

The Silvaco ATLAS software was first used to model a Japanese dual junction solar cell for validation by Tsutagawa. The Japanese paper published the required cell parameters (doping levels and thicknesses) along with the cell output parameters (V_{oc}, J_{sc}, P_{max}, V_{max}, J_{max}, FF, and efficiency) that were required. Due to proprietary reasons, the required data for a triple-junction cell was unavailable. After the Silvaco ATLAS code results for the simulated solar cell were determined to accurately predict the actual bench testing, the solar cell was then optimized. This process verified that the simulated cell displayed the same output characteristics as the fabricated solar cell.

3. Cell Optimization

The laser system designed in this thesis was for a triple-junction solar cell that had been optimized by Michael Tsutagawa. The original Silvaco ATLAS code for Tsutagawa's triple-junction solar cell, otherwise known as the "Champion" cell, can be found in Appendix A. To accomplish the optimization Tsutagawa started with Michalopoulos' cell and used a novel approach of current matching in layers by varying the layer thicknesses. The InGaP has the lowest current density (J_{sc}) and was therefore the limiting layer. Assuming optimum doping concentration in the layers the thickness was incrementally increased until the choke point was reached, which is the thickness at which the J_{sc} of the GaAs layer was matched to the InGaP layer. By increasing the thickness of the limiting layer of the solar cell to that point the maximum achievable output could be obtained. Finally, by matching the J_{sc} of the Ge layer the third layer was incorporated to complete the triple- junction solar cell.

4.   Defining Light Sources

As discussed previously, solar cells are designed to maximize output when illuminated by the AM0 solar spectrum. Silvaco contains a built-in power file for the solar spectrum, but the fidelity of this file was insufficient. Therefore, Andrew Bates generated a more accurate representation of the AM0 solar spectrum by increasing the fidelity of the power file. The beam statement below was used in Tsutagawa's code to illuminate the solar cell.

```
beam num=1 x.origin=0 y.origin=-5 angle=90 back.refl \
      power.file=AM0nrel.spec wavel.start=0.12 wavel.end=2.4 wavel.num=1500
```

This statement defines the origin of the beam for 2D optical sources; see `x.origin` and `y.origin` with the units being microns. Also, the statement describes the angle of incidence; see `angle`. A 90-degree angle of incidence indicates that the beam was perpendicular to the surface of the solar cell. The `back.refl` statement allows the beam to reflect back into the cell off the bottom contact of the solar cell. The power file, `power.file=AM0nrel.spec`, causes ATLAS to read the multi-spectral file created to simulate solar illumination. This file contains ordered pairs of wavelengths and irradiance levels. The wavelengths in these files are given in microns and the irradiance levels are provided in watts per square centimeter per micron ($W/cm^2/\mu m$). The final portion of the beam statement indicates the starting and ending wavelengths along with the number of wavelengths to sample.

For the purposes of simulating laser sources, nearly monochromatic light source power files were generated that incorporated a 2 nm line-width laser source. When modeling an actual experiment it will be necessary to use the actual line width of the lasers to be used.

D.   SUMMARY

This chapter discussed the Silvaco ATLAS simulation software used. An overview of the simulation environment was provided. Then several aspects specific to the programming methodology were introduced including program structuring, validation and beam statements.

THIS PAGE INTENTIONALLY LEFT BLANK

VII.   LASER SYSTEM OPTIMIZATION

A.   CHAPTER OVERVIEW

This section will cover the approach and methodology used to replace the AM0 solar spectrum with a system of three lasers. The coding involved was simply the dissection of Michael Tsutagawa's "Champion" solar cell and the replacement of the illuminating source with a nearly monochromatic light source.

B.   OPTIMIZED SOLAR CELL

Tsutagawa's optimized cell was an InGaP/GaAs/Ge triple-junction solar cell that was originally designed by Panayiotis Michalopoulos. Tsutagawa's original code can be found in Appendix A. Tsutagawa's optimized triple junction solar cell had an incredible efficiency of greater than 36%. A summary of the cell's outputs are shown in Table 3.

Table 3.   Tsutagawa Triple Junction Cell Outputs

V_{oc}	2.76425	Volts
J_{sc}	19.8531	mA/cm^2
V_{max}	2.525	Volts
J_{max}	19.4419	mA/cm^2
P_{max}	0.0490907	W/cm^2
Fill Factor	89.4527	%
Efficiency	36.2829	%

The materials, thicknesses and doping concentrations of the champion cell are shown in Figure 18.

Layer				
Top InGaP Layer	Window	n+ AlnP	0.01µm	$5e19cm^{-3}$
	Emitter	n+ InGaP	0.17µm	$4.64e17cm^{-3}$
	Base	p+ InGaP	0.63µm	$1e17cm^{-3}$
	BSF	p+ InGaP	0.01µm	$5e19cm^{-3}$
	Buffer	p+ AlnP	0.3µm	$1e18cm^{-3}$
Tunnel Junction	Tunnel Emitter	p+ InGaP	0.015µm	$8e18cm^{-3}$
	Tunnel Base	n+ InGaP	0.015µm	$1e19cm^{-3}$
Middle GaAs Layer	Window	n+ AlnP	0.01µm	$4.64e17cm^{-3}$
	Emitter	n+ GaAs	0.01µm	$4.64e15cm^{-3}$
	Base	p+ GaAs	3.87µm	$1e17cm^{-3}$
	BSF	p+ InGaP	0.01µm	$5e19cm^{-3}$
	Buffer	p+ GaAs	0.3µm	$7e18cm^{-3}$
Tunnel Junction	Tunnel Emitter	p+ GaAs	0.015µm	$8e18cm^{-3}$
	Tunnel Base	n+ GaAs	0.015µm	$1e19cm^{-3}$
Bottom Ge Layer	Window	n+ GaAs	0.05µm	$7e18cm^{-3}$
	Emitter	n+ Ge	0.1µm	$3e18cm^{-3}$
	Substrate	p+ Ge	300µm	$3e18cm^{-3}$

Figure 18.   Tsutagawa's Champion Triple Junction Solar Cell Structure (After Tsutagawa 72)

C.   SOLAR CELL DISSECTION

In order to determine the peak spectral response of each layer of the triple junction solar cell the cell had to be divided into three separate cells. The code used to model each layer can be found in Appendix E. In addition, the code was modified in order to determine the cell's response to a unity intensity beam over the wavelengths of interest for each cell. This was accomplished by altering the power file intensity values.

For example, the InGaP cell was illuminated with wavelengths between 350–600 nm at 1 W/cm^2/μm and the results are shown in Figure 19.
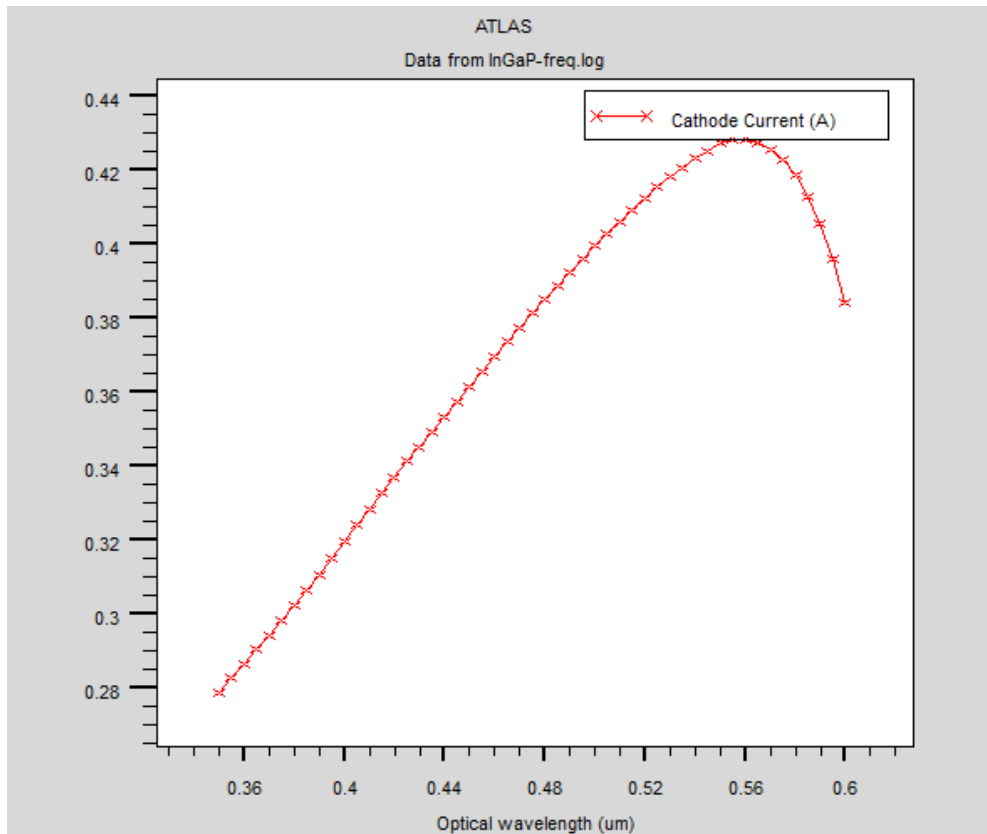
Figure 19.   InGaP Layer Frequency Response

The peak for the InGaP layer was determined to be 555 nm. The GaAs layer was illuminated with wavelengths between 350-900 nm at 1 W/cm^2/μm (see Figure 20).

53

Data from GaAs-freq.log
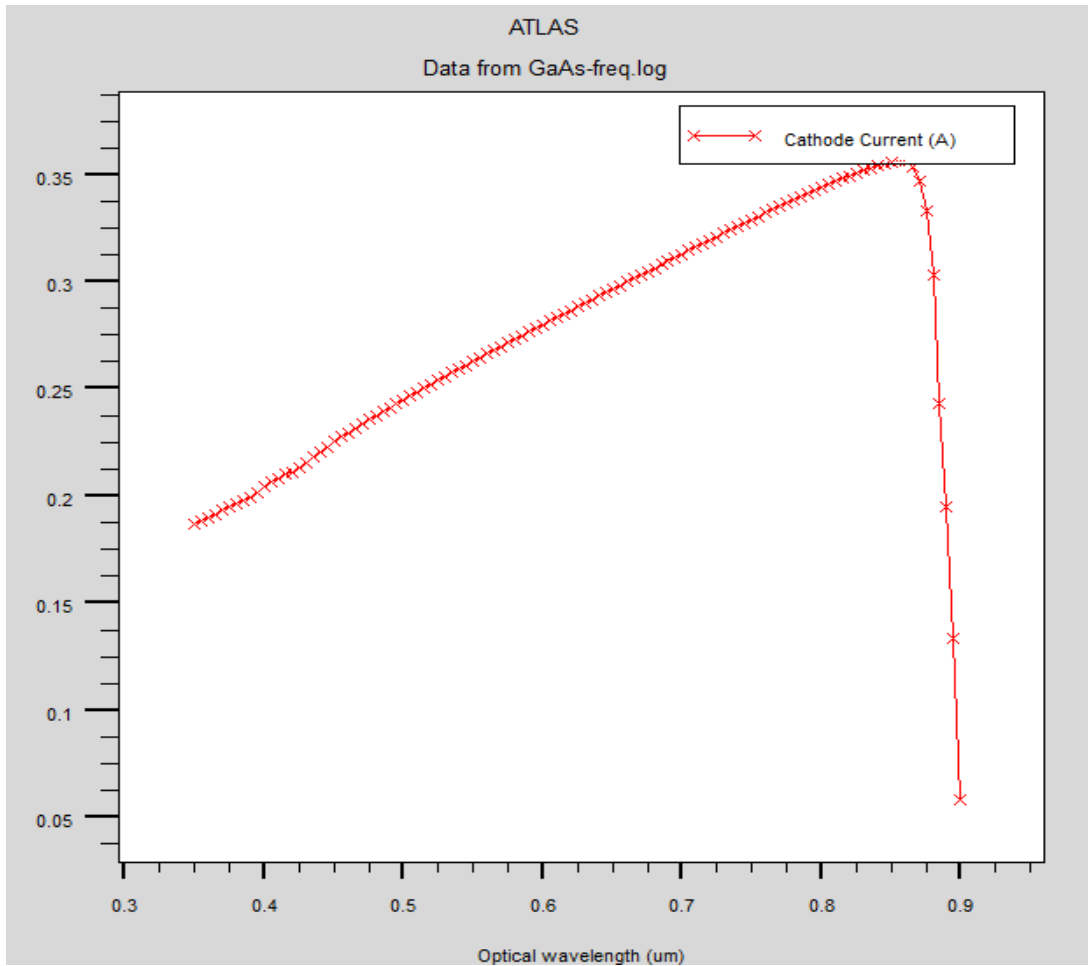
Figure 20.　GaAs Layer Frequency Response

The peak for the GaAs layer was determined to be 860 nm and photons of greater than 0.9 microns were shown to be incapable of generating an electron-hole pair. The Ge layer was illuminated with wavelengths between 350–1700 nm at 1 W/cm^2/μm (Figure 21).
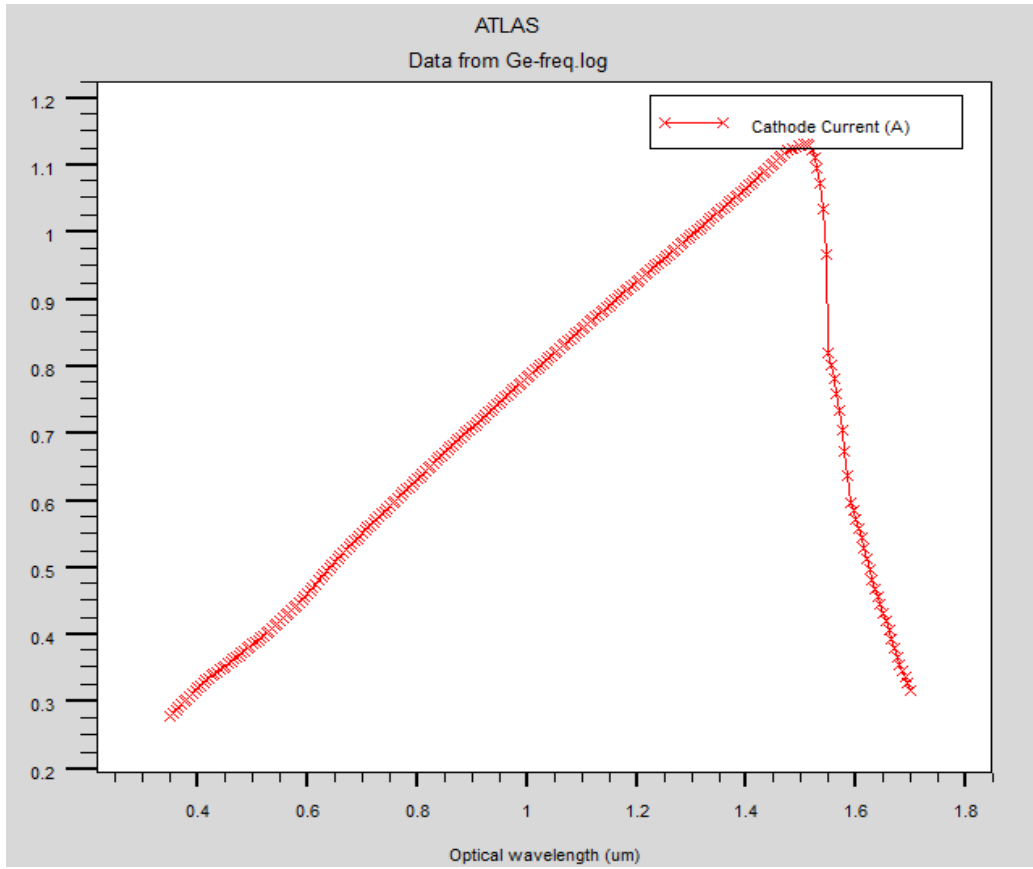
Figure 21.   Ge Layer Frequency Response

The peak for the Ge layer was determined to be 1510 nm and photons of greater than 1.7 microns do not contain sufficient energy to generate an electron-hole pair.

The dissection of the triple-junction cell required that the tunnel junctions be omitted with the results of the omission to be determined once the entire cell was reconstructed and illuminated with the three laser system.   The tunnel junctions in Tsutagawa's code were non-functional, therefore their inclusion would have only allowed for the possibility of shadowing.

D.   INTENSITY DETERMINATION

As discussed previously the solar cell short circuit current density (J_{sc}) is the result of the minimum of the three layers in a triple-junction solar cell since they are connected in series. Therefore, using the peak values obtained in the above analysis the next step was to determine the laser intensity required to obtain a short circuit current

equivalent to the J_{sc} of the champion cell, approximately 20 mA/cm^2. Figure 22 shows the TonyPlot of the I-V curve for the InGaP layer with the y-axis measured in milliamps and the x-axis measured in volts.
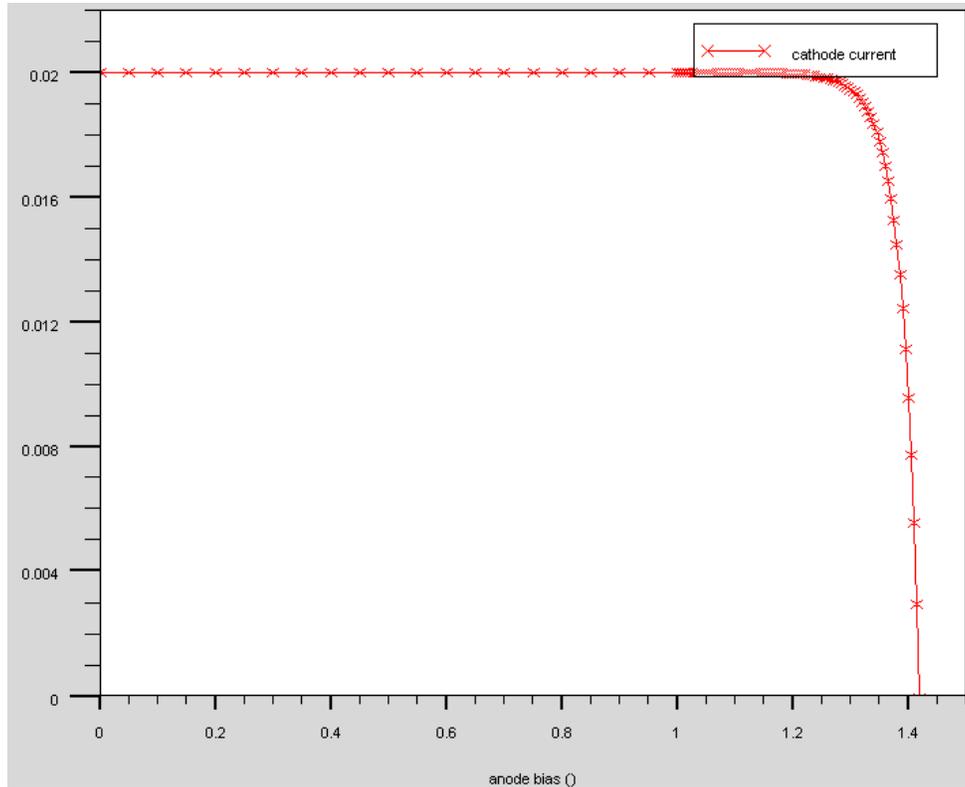
Figure 22.   InGaP Intensity Determination

Using a 2 nm line-width laser centered at 554 nm the intensity required to achieve a 20 mA/cm^2 short circuit current density in the InGaP layer was 23.35 W/cm^2/μm. A comparison between the InGaP solar cell under solar and laser illumination is shown in Table 4.

Table 4.   InGaP Solar and Laser Illumination Comparison

	Sun	Laser	Units	%Difference
V_{oc}	1.41965	1.41989	Volts	0.0169
J_{sc}	19.8526	19.9998	mA/cm^2	0.7415
V_{max}	1.3	1.3	Volts	0.0000
J_{max}	19.2868	19.4339	mA/cm^2	0.7627
P_{max}	0.025073	0.0252641	W/cm^2	0.7626
Fill Factor	88.9623	88.9659	%	0.0040
Efficiency	18.5313	54.0987	%	191.9315

The laser power provided to the InGaP solar cell was 0.0467 W/cm^2, which is approximately equal to 35% of one sun. The considerable increase in the reported efficiency of the cell comes from the fact that it is provided with the optimum frequency of light required to generate an electron-hole pair and nothing else. Of note, all of the cell output parameter percent differences were less than 1%. Figure 23 shows a TonyPlot of the I-V curve for the GaAs layer with the y-axis measured in milliamps and the x-axis measured in volts.
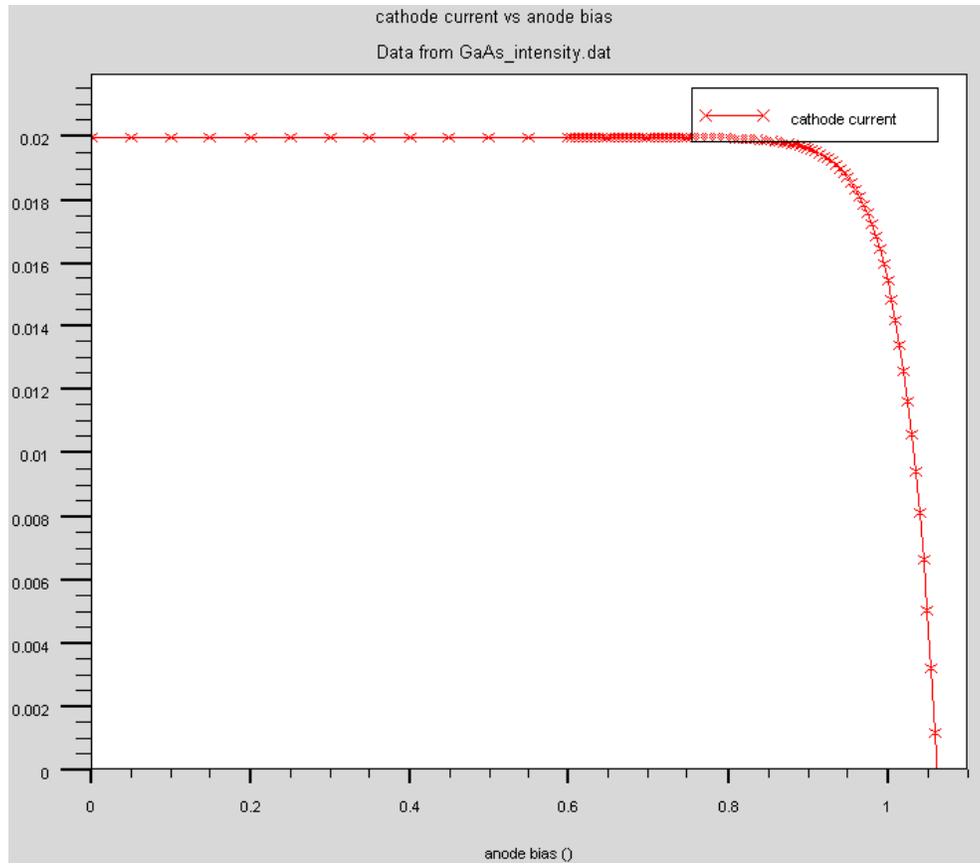
Figure 23.   GaAs Intensity Determination

Using a 2 nm line-width laser centered at 861 nm the intensity required to achieve a 20 mA/cm^2 short circuit current density in the GaAs layer was 14.97 W/cm^2/μm. A comparison between the GaAs solar cell under solar and laser illumination is shown in Table 5.

Table 5.   GaAs Solar and Laser Illumination Comparison

	Sun	Laser	Units	%Difference
V_{oc}	1.08034	1.0625	Volts	1.6513
J_{sc}	39.3149	19.9968	mA/cm^2	49.1368
V_{max}	0.919988	0.929985	Volts	1.0866
J_{max}	37.1821	19.2189	mA/cm^2	48.3114
P_{max}	0.034207	0.0178733	W/cm^2	47.7497
Fill Factor	80.5376	84.1231	%	4.4520
Efficiency	25.2824	59.6971	%	136.1212

The laser power provided to the GaAs solar cell was 0.02994 W/cm^2, which is approximately equal to 22% of one sun. The larger percent differences are due to the fact that the GaAs layer was illuminated with the AM0 power file, whereas in the actual triple-junction cell it would have been shadowed from the InGaP layer. Figure 24 shows a TonyPlot of the I-V curve for the Ge layer with the y-axis measured in milliamps and the x-axis measured in volts.
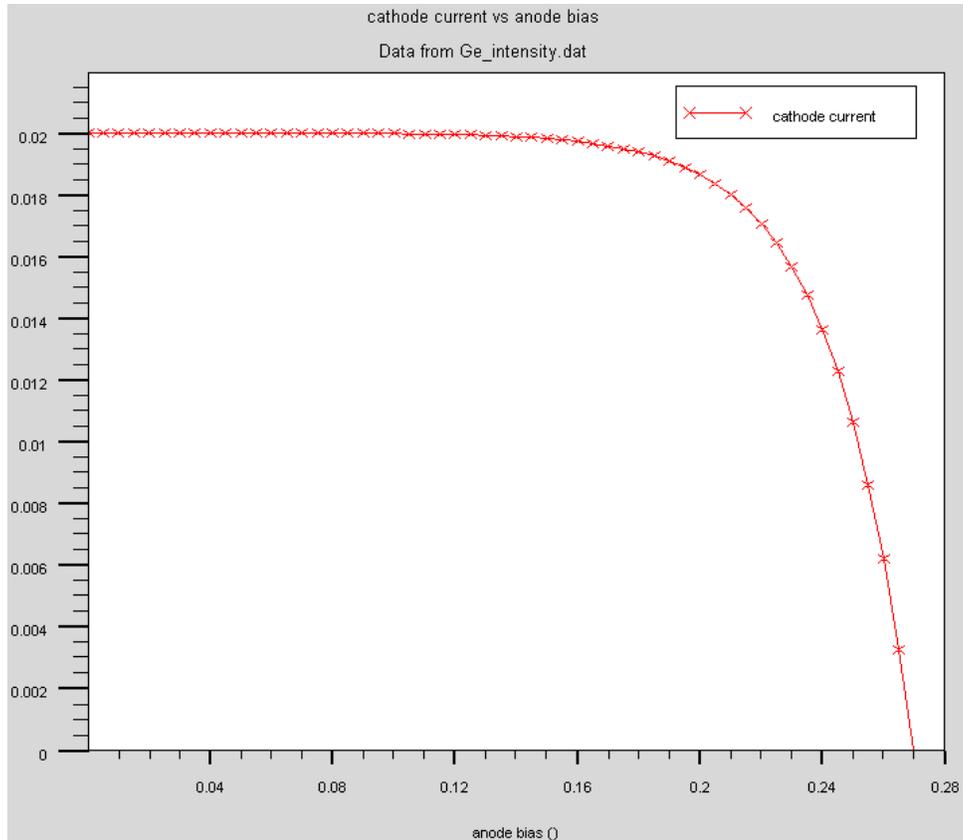

Figure 24.   Ge Intensity Determination

Using a 2 nm line-width laser centered at 1511 nm the intensity required to achieve a 20 mA/cm^2 short circuit current density in the Ge layer was 8.85 W/cm^2/μm. A comparison between the Ge solar cell under solar and laser illumination is shown in Table 6.

Table 6.   Ge Solar and Laser Illumination Comparison

	Sun	Laser	Units	%Difference
V_{oc}	0.302459	0.269605	Volts	10.8623
J_{sc}	71.6097	20.0346	mA/cm^2	72.0225
V_{max}	0.24	0.209999	Volts	12.5004
J_{max}	65.1267	18.03	mA/cm^2	72.3155
P_{max}	0.01563	0.0037863	W/cm^2	75.7761
Fill Factor	72.1658	70.0979	%	2.8655
Efficiency	11.5524	21.3915	%	85.1693

The laser power provided to the Ge solar cell was 0.0177 W/cm^2, which is approximately equal to 13% of one sun. Again, the increase in the percent differences are due to shadowing from the top two layers of the solar cell. An overlay plot of the three layers can be seen in Figure 25.
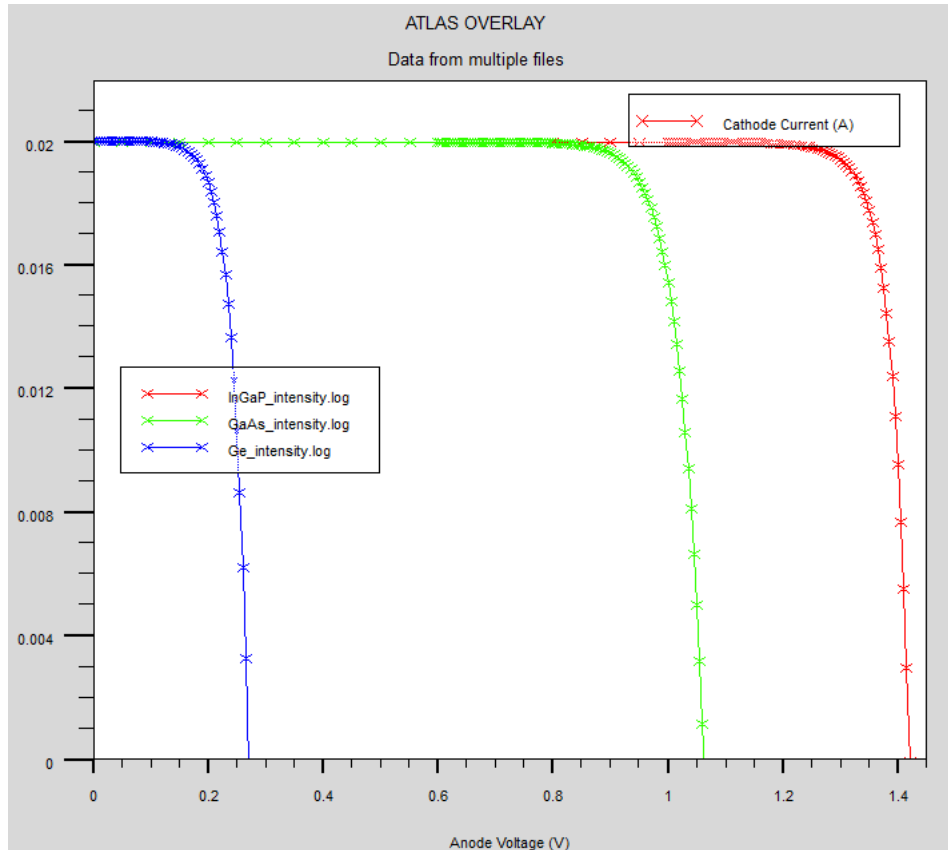
Figure 25.   I-V Curve Overlay of Three Layers

Next the three laser system was applied to the original triple-junction "Champion" cell. The three beam statements used are shown below:

```
beam num=1 x.origin=0 y.origin=-5 angle=90 back.refl \
      power.file=AM0nrel1.spec wavel.start=0.553 wavel.end=0.555 wavel.num=1
beam num=2 x.origin=0 y.origin=-5 angle=90 back.refl \
      power.file=AM0nrel1.spec wavel.start=0.860 wavel.end=0.862 wavel.num=1
beam num=3 x.origin=0 y.origin=-5 angle=90 back.refl \

      power.file=AM0nrel1.spec wavel.start=1.51 wavel.end=1.512 wavel.num=1
```

The expectation was that the short circuit current density would be approximately 20 mA/cm^2 and the open circuit voltages of the three layers should add to achieve approximately 2.8 V. Figure 26 shows that the results were as expected.
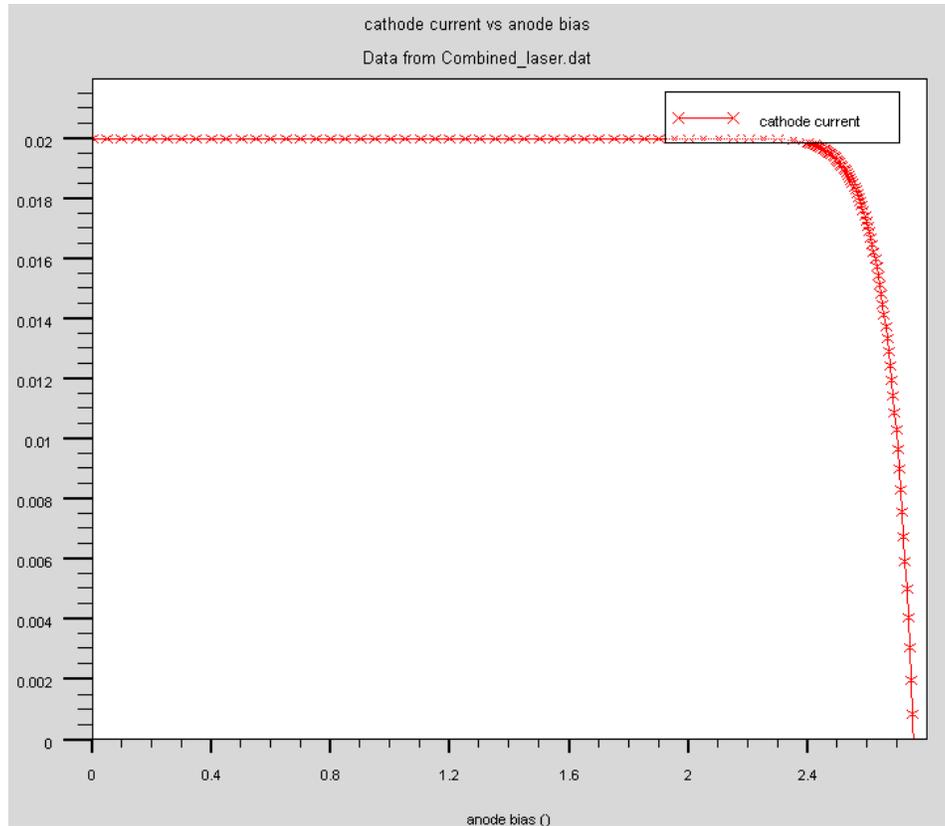
Figure 26.   Champion Cell Under Laser Illumination

A comparison between the "Champion" solar cell under solar illumination and the three laser system is shown in Table 7.

Table 7.   Solar and Laser Illumination Comparison

	Sun	Laser	Units	%Difference
V_{oc}	2.76425	2.75339	Volts	0.3929
J_{sc}	19.8531	20.00003	mA/cm^2	0.7401
V_{max}	2.525	2.475	Volts	1.9802
J_{max}	19.4419	19.4836	mA/cm^2	0.2145
P_{max}	0.04909	0.0482219	W/cm^2	1.7698
Fill Factor	89.4527	87.5669	%	2.1082
Efficiency	36.2829	51.15	%	40.9755

The increase in cell efficiency is due to the fact that the laser system provided the solar cell with only the required energy at the correct frequencies.

E. CELL SHADOWING

In Michalopoulos' thesis it was demonstrated that a frequency response shift occurred in the middle layer (GaAs) of the triple-junction cell due to the shadowing effect from the top layer (InGaP). Figure 27 below illustrates that shift.
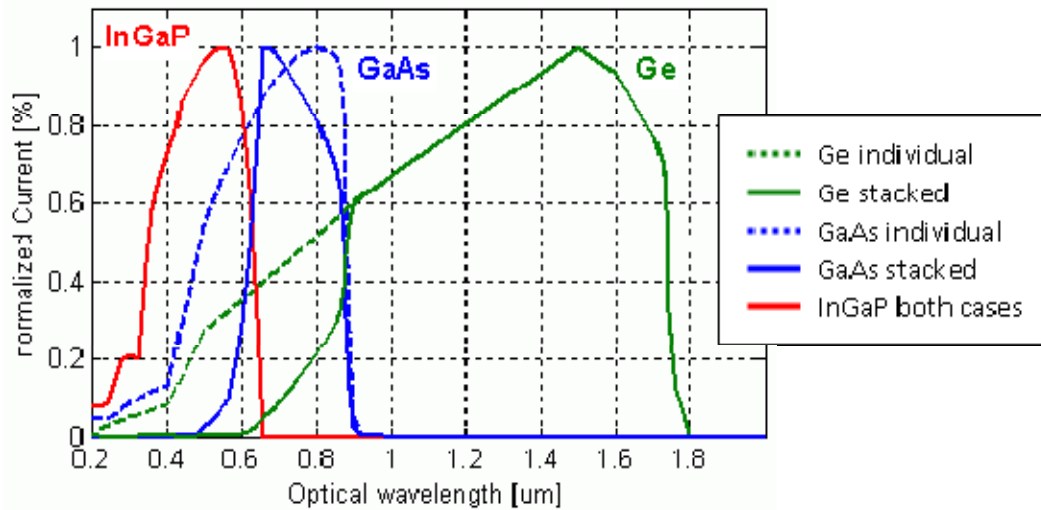
Figure 27. Cell Shadowing (From Michalopoulos 117)

This phenomenon occurs due to the fact that when the cells are illuminated by the sun individually they are exposed to a photon population of greater energy than necessary to cause electron excitation. These photons generate current that shift the peak response to the right when normalized. When the cell is then shadowed by a layer that absorbs these greater energy photons the curve shifts to the left. The effect of adding an InGaP cell on top of the GaAs cell essentially shifts the incident solar spectrum available to the GaAs cell for conversion. This is shown in Figure 28.
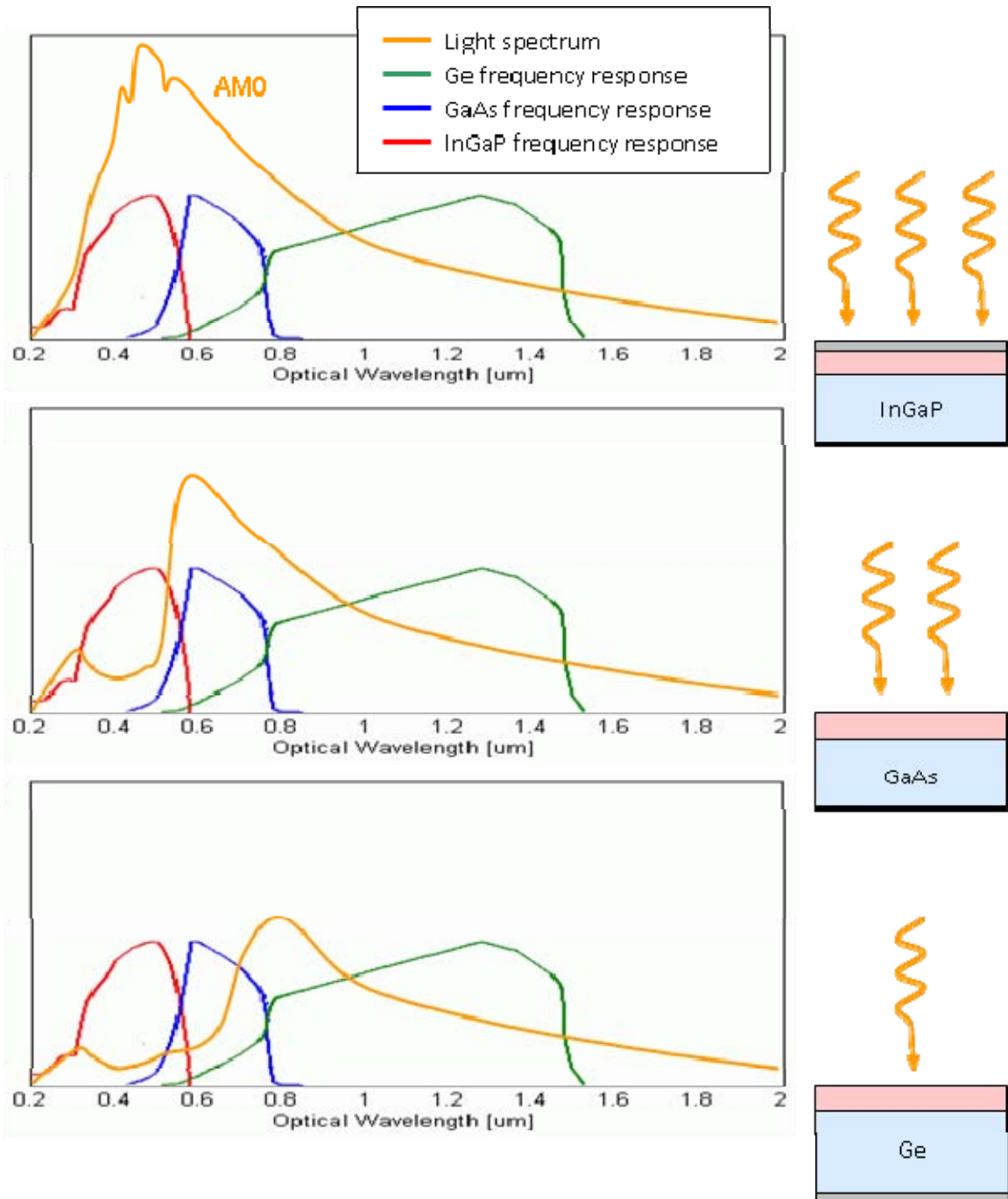
Figure 28.   Available Solar Spectrum Peak Shift (From Michalopoulos 121)

This figure shows that each layer is virtually transparent to photons of wavelength greater than (in other words energy less than) necessary to achieve electron excitation. This transparency to lower energy photons results in negligible frequency response shifting when using laser wavelengths longer than necessary for electron excitation for

each additional cell layer added. This explains why the short circuit current density obtained in the "Champion" triple-junction solar cell under laser illumination was approximately 20 mA/cm^2, which was the same when the cells were illuminated individually.

Cell shadowing does not seem to be a major concern when designing a laser system for power beaming. Currently the bandgap energies for the cell layers are separated by enough distance to preclude shadowing. However, as solar cell technology increases and the number of layers increases a word of caution is appropriate. As the peak frequency responses in each layer converge, shadowing may become more prevalent.

F.   SUMMARY

The three laser system designed will generate the equivalent of one sun if propagated to the solar arrays. The combined three laser system yielded a 51.15% efficiency, which equates to a requirement of only 972.4 W/m^2 to achieve the same cell outputs. Of course, these lasers are not currently available at the optimum frequencies and intensity to achieve this efficiency so the next step in the modeling process is to apply real world constraints. The 51.15% efficiency is a theoretical limit that would require a variable intensity FEL.

THIS PAGE INTENTIONALLY LEFT BLANK

VIII. AIRBORNE LASER EXPERIMENT

A.   CHAPTER OVERVIEW

An opportunity exists to use an existing air platform to conduct initial feasibility testing. The U.S. Missile Defense Agency (MDA) is responsible for management of the ABL program. The U.S. Air Force is executing the program from Kirtland AFB in Albuquerque, NM. The program has recently conducted live fire testing, successfully destroying missiles in-flight.

B.   PROGRAM DESCRIPTION

The ABL is outfitted on a Boeing 747-400F airframe and consists of three onboard lasers. The reported operating altitude for the mission is 40,000 ft or 12.2 kilometers.

Figure 29.   ABL Boeing 747-400F (From Boeing Web site 2010)

The turret for the laser system is located on the nose of the plane and consists of a 1.5 m aperture (see Figure 30).

Figure 30.   ABL Aperture (From Phillips Blog 2010)

The specifics of these lasers are not readily available in the unclassified realm, but inferences can be made for our discussion. The main laser is a continuous wave megawatt class Chemical Oxygen Iodine Laser (COIL) with an operating wavelength of 1.315 microns. It contains six laser modules in series to achieve megawatt powers. This implies that it has the capability of being somewhat scalable, if not all six modules were used. The laser was designed and built by Northrop Grumman Space Technology. The Tracking Illuminating Laser (TILL) is used to obtain target range and perform initial atmospheric characterization. The TILL is a diode pumped Yb:YAG laser, which typically operates at a wavelength of 1064 nm. The laser was designed and built by Raytheon Electronic Systems. The Beacon Illuminating Laser (BILL) is used for adaptive optics and was built by Northrop Grumman Space Technology. The BILL is kilowatt class and either solid state or electrically powered. ("ABL YAL," 2010)

C.   AIRBORNE LASER EXAMPLE

The ABL platform offers several unique opportunities. First, the operational altitude of approximately 12.2 km removes a great deal of atmosphere from the equation. This will limit the amount of power lost due to scattering. Also, the altitude will decrease the range between the laser source and the satellite. Second, ABL comes equipped with an extremely capable adaptive optics package, which limits the effect of air turbulence on the test. The test would feature one of the three lasers currently onboard the platform. These lasers are not capable of varying intensity in small step sizes. Instead, the test would involve a relatively constant power laser.

The following example will introduce real world constraints on power beaming by applying a specific wavelength and intensity laser. This example still requires several assumptions, but will begin to address the complexity of the challenge at hand. Using the ABL COIL laser to illuminate a hypothetical GEO communications satellite with Ge solar cells, the trade-off analysis will come to life. Recall that the peak spectral response for the Ge solar cell was 1510 nm, but unfortunately that wavelength laser is not available. Instead, the COIL will be used at 1315 nm, assuming a conservative power output of one megawatt since the actual output is classified. The first step was to determine the diffraction limited spot radius illuminated at GEO from the ABL platform. Using Equation 5.6 the radius was determined to be approximately 19 m, which equated to a total area of 1151 m^2. This example incorporates losses of 16% of the laser energy that fell outside the first zero of the laser diffraction pattern and a Strehl ratio of 0.85 for the adaptive optics package to account for losses associated with atmospheric turbulence. A conservative estimate of atmospheric transmittance of 65% (which discounts the fact that the aircraft is at altitude) is assumed (see Figure 7). The COIL laser would be capable of projecting 403 W/m^2 out to the GEO belt or approximately 30% of one sun. Figure 31 shows the Ge cell I-V curve when illuminated with the COIL.
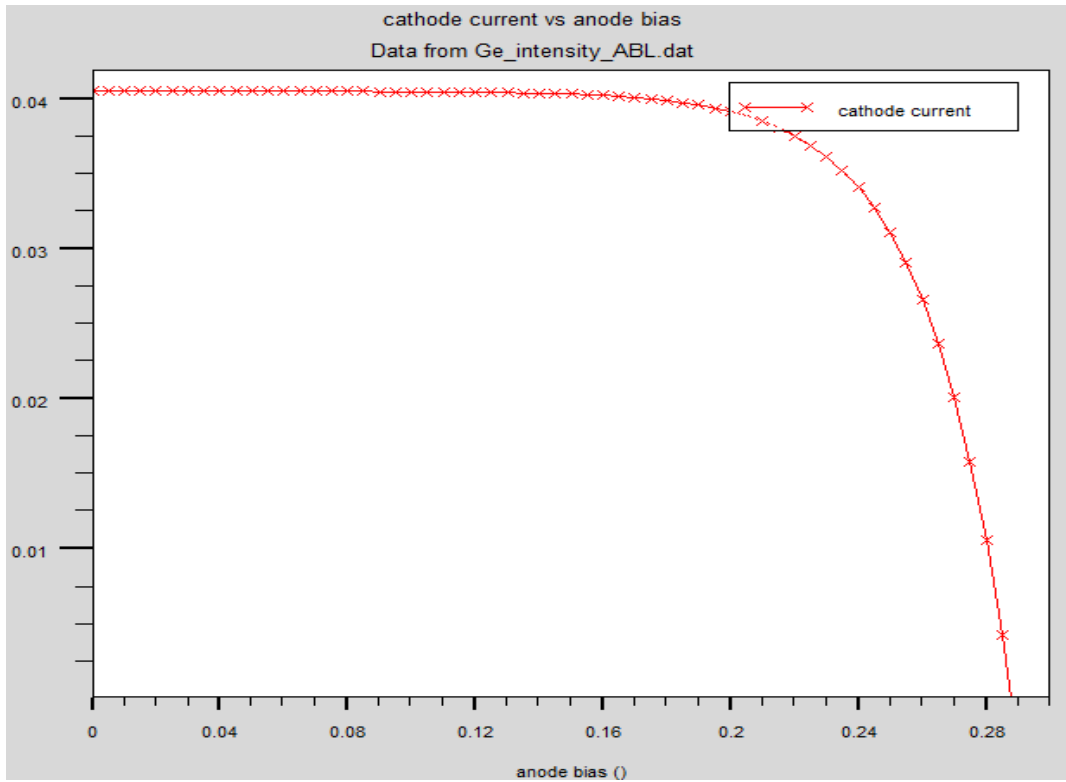
Figure 31.   ABL Germanium Solar Cell Example

Table 8 shows a side-by-side comparison of the Ge solar cell under solar, theoretical laser and ABL.

Table 8.   ABL Comparison

	Sun	Laser	ABL	Units
V_{oc}	0.30246	0.269605	0.28775	Volts
J_{sc}	71.6097	20.0346	40.5454	mA/cm^2
V_{max}	0.24	0.209999	0.229998	Volts
J_{max}	65.1267	18.03	36.1762	mA/cm^2
P_{max}	0.01563	0.003786	0.0083205	W/cm^2
Fill Factor	72.1658	70.0979	71.3165	%
Efficiency	11.5524	21.3915	20.6463	%

Although the ABL was not capable of providing the same output as the cell under solar illumination, it was able to approach the same output. The ABL was also able to achieve solar cell efficiency near that of the theoretical laser. One might expect the efficiency to drop significantly due to the fact that the cell was not provided the optimum wavelength of light, but the result can be explained using concentration effects. The theoretical laser was only applying 177 W/m^2 to the cell, whereas the ABL supplied 403 W/m^2, more than a factor of two. Solar cell efficiency has been demonstrated to increase as the intensity of the energy imparted on it increases. This can be seen today in terrestrial applications that use solar concentrators to achieve intensities on the order of 100s of suns by reflecting more light onto a solar cell. The only limitation on this concentrating effect is the ability to remove the excess heat generated in the substrate.

D.   FUTURE MODEL CURRENT STATUS

The examples to this point have limited the complexity of the overall power beaming challenge. A realistic power beaming challenge will have a target satellite that has a changing range and other than perpendicular angle of incidence. In order to vary these two parameters, code written in Matlab would need to be employed. Matlab code currently exists that has the ability to run the Silvaco Atlas code iterating the intensity and angle of incidence for each run as a function of time. The next step to be completed will be a STK model that would be capable of calculating the irradiance level at the satellite from a ground-based laser. The Matlab code would now need to read a data file outputted from STK to obtain the irradiance and angle of incidence and then subsequently write those values into the Silvaco program. This would allow the solar cell output parameters to be plotted as a function of time.

E.   SATELLITE SURVIVABILITY MODULE

The Satellite Survivability Module (SSM) for STK was developed by Ball Aerospace and Technologies Corporation for the Air Force Research Laboratory (AFRL). "The Satellite Survivability Module (SSM) is an end-to-end, physics-based, performance prediction model for directed energy engagement of orbiting spacecraft. Two engagement types are currently supported: laser engagement of the focal plane array of an imaging

71

spacecraft; and Radio Frequency (RF) engagement of spacecraft components." (Buehler 1) The SSM was created to model the effects of a ground-based laser attack on an orbiting imaging satellite. The module is capable of modeling the atmospheric effects on the propagation of the laser energy. It calculates the irradiance level at the satellite taking into account changing satellite range and atmospheric losses, which could then be outputted to a data file and subsequently read by the Matlab code previously described.

F.   SUMMARY

This chapter attempted to remove some of the assumptions that were made to simplify power beaming for preliminary analysis. This was done using the ABL to provide a real world example of a laser with a wavelength that was not theoretical for the illumination of a Ge solar cell at GEO. Next a description of the current status of the modeling process was presented. Finally, an STK module was described to explain how it could be applied for modeling power beaming.

IX. CONCLUSIONS

A. CONCLUSIONS

The effective replacement of the sun was accomplished using a three laser system designed to provide the same output of the solar cell. This system of lasers was not limited to the available frequencies and intensities of lasers available. Instead, the system of lasers devised was meant to achieve the highest efficiency of the solar cell while maintaining the same power output. In a perfect world the system would include variable frequency and intensity lasers, but applying real world constraints will decrease the efficiency of the solar cell.

B. FUTURE WORK RECOMMENDATIONS

In order to predict the satellite solar cell response to laser illumination or understand the results of a test, the simulation capabilities of several software packages will have to be employed. First, STK would need to be used to model the motion of the satellite with respect to the laser ground site. This will allow the user to incorporate the varying range of the target satellite. For a more complete understanding of the atmospheric effects on the laser beam the variations in atmosphere must be accounted for. This will account for the losses associated with absorption and scattering as the beam transverses the atmosphere. Finally, the angle of incidence must be understood to determine the amount of reflection. The Silvaco software could be used to vary the angle of incidence.

Another area for improvement would be the ability to model the thermal aspects of the solar cell. The efficiency of solar cells is highly dependent on operating temperature. Additionally, this simulation could help answer the question of whether the satellite's thermal control system could remove the heat generated from applying power of greater than one sun.

Although solar cell optimization was not the focus of this research, improvements to the solar cell model could be made to provide for more accurate results. For instance, the top contact for the solar cell should appear opaque to incoming light. This will

reduce the amount of light entering the cell between 2-10%. Also, the Silvaco software has the ability to incorporate anti-reflective coatings on the top of the solar cell to reduce the amount of reflected light, thereby permitting a greater percentage of light to enter the cell structure. Finally, radiation damage to on-orbit satellite solar arrays could be incorporated into the model. Preliminary work has already been performed in this area and would only need to be applied based on the cell's age and operating environment.

APPENDIX A. LIST OF SYMBOLS

Symbol	Description	Unit
B	Optical constant	cm^{-6}
c	Speed of light	m/s
c_o	Speed of light in a vacuum	m/s
d	Distance	m
E	Energy	eV
E_g	Energy bandgap	eV
f	Frequency	Hz
FF	Fill Factor	–
λ	Photon wavelength	m
h	Plank's constant	J·s
hν	Photon energy	eV
I	Current	A
I_{SC}	Short circuit current	A
I_{SP}	Specific Impulse	s
J_{SC}	Short circuit current density	mA/cm^2
k	Boltzmann's constant	J/K
kT	Thermal energy	eV
L	Length of the cavity	m
η	Power conversion efficiency	–
$η_{laser}$	Efficiency under laser illumination	–
$η_{solar}$	Efficiency under solar illumination	–
n	Number of electrons	–
n_r	Index of refraction	–
ν	Photon frequency	Hz
$Δν_{FSR}$	Longitudinal mode spacing	m
N_1	Number of electrons in state one	–
N_2	Number of electrons in state two	–
N_A	Acceptor/hole density concentration	cm^{-3}
N_D	Donor/electron density concentration	cm^{-3}
n_i^2	Majority · minority carrier concentration product	cm^{-3}
p	Number of holes	–
P	Power	W
P_{inc}	Incident Power	W
P_{max}	Maximum power	W
P_{sun}	Average solar density	W/cm^2
q	Charge	J

75

r_{lens}	Radius of lens	m
r_{spot}	Radius of spot	m
$SR(\lambda)$	Spectral Response at wavelength	A/W
T	Absolute temperature	^{o}K
V	Voltage	V
V_{bi}	Built-in voltage	V
V_{max}	Maximum voltage	V
V_{min}	Minimum voltage	V
V_{OC}	Open circuit current	V

APPENDIX B. SOME PHYSICAL CONSTANTS

Quantity	Symbol	Value
Boltzmann's constant	k	$1.38066 \cdot 10^{-23}$ J/K
Electron charge	q	$1.60218 \cdot 10^{-19}$ Cb
Electronvolt	eV	$1.60218 \cdot 10^{-19}$ J
Plank's constant	h	$6.6260755 \cdot 10^{-34}$ J·s
Light speed in vacuum	c_o	$2.99792458 \cdot 10^{-8}$ m/s

THIS PAGE INTENTIONALLY LEFT BLANK

APPENDIX C. UNITS

Quantity	Unit	Symbol	Equivalence
Length	meter	m	m
Mass	kilogram	kg	kg
Time	second	s	s
Current	ampere	A	A
Temperature	degree Kelvin	K	K
Surface	square meter	m^2	m^2
Volume	cube meter	m^3	m^3
Velocity	–	m/s	m/s
Frequency	Hertz	Hz	1/s
Energy	Joule	J	$Kg \cdot m^2/s^2$
Power	Watt	W	$N \cdot m/s$
Electric charge	Coulomb	Cb	$A \cdot s$
Electric potential	Volt	V	$Kg \cdot m^2 / A \cdot s^3$
Electric resistance	Ohm	Ω	$Kg \cdot m^2 / A^2 \cdot s^3$

THIS PAGE INTENTIONALLY LEFT BLANK

APPENDIX D. MAGNITUDE PREFIXES

Magnitude prefix	Symbol	Multiple factor
giga	G	$1 \times 10^{+9}$
mega	M	$1 \times 10^{+6}$
kilo	K	$1 \times 10^{+3}$
hecto	h	$1 \times 10^{+2}$
deka	da	$1 \times 10^{+1}$
-	-	1×10^{0}
deci	d	1×10^{-1}
centi	c	1×10^{-2}
milli	m	1×10^{-3}
micro	μ	1×10^{-6}
nano	n	1×10^{-9}
pico	p	1×10^{-12}
femto	f	1×10^{-15}

THIS PAGE INTENTIONALLY LEFT BLANK

APPENDIX E. ATLAS CODE

A.   TSUTAGAWA ORIGINAL CODE

```
#Michael Tsutagawa      16 Nov 2008    CHAMPION CELL - 36.28% Efficiency!!
#This model is an explicit InGaP/GaAs/Ge Triple Junction solar cell with Tunnel
Junction KATO OPTM 0.82InGaP/3.9umGaAs/ORIG300um Ge with BUFFER LAYERS.
# This cell is based on Michalopoulos' cell.  In addition, this cell has buffer
layers under the top and middle layers.
# The buffer layers were incorporated based on Agui's dual cell design and show
increased power out.
# The ORIGINAL BUILT cell (Voc=2.69247  &  Jsc=19.0779 ma/cm2   P=0.05136667
mW/cm2)
#Using the AM0nrel.spec file, the 0.75InGap/2.2umGaAs/ORIG300um Ge cell has
Voc=2.6925  &   Jsc=19.6084 ma/cm2   P=0.05279562 mW/cm2

#Change the Germanium bottom layer parameters to the ORIGINAL Ge parameters and
run. Expect more power due to better Ge cell.
#Thickened top InGap layer to 0.76um.  Expect more power.
#Using the AM0nrel.spec file, the 0.76InGap/2.2umGaAs/ORIG300um Ge cell has
Voc=2.69213  &   Jsc=19.6459 ma/cm2   P=0.05288932 mW/cm2
#This Bates top and middle layer plus Original Ge bottom layer beats previous
cell!!

#Using the AM0nrel.spec file, the 0.77InGap/2.3umGaAs/ORIG300um Ge cell has
Voc=2.69069  &   Jsc=19.6826 ma/cm2   P=0.05295977 mW/cm2
#Using the AM0nrel.spec file, the 0.79InGap/2.5umGaAs/ORIG300um Ge cell has
Voc=2.68787  &   Jsc=19.7532 ma/cm2   P=0.05309403 mW/cm2
#Using the AM0nrel.spec file, the 0.8InGap/2.5umGaAs/ORIG300um  Ge cell has
Voc=2.68753  &   Jsc=19.7873 ma/cm2   P=0.05317896 mW/cm2
#Using the AM0nrel.spec file, the 0.81InGap/2.6umGaAs/ORIG300um Ge cell has
Voc=2.68621  &   Jsc=19.8206  ma/cm2   P=0.05324229 mW/cm2
#Using the AM0nrel.spec file, the 0.82InGap/2.7umGaAs/ORIG300um Ge cell has
Voc=2.68496  &   Jsc=19.8532  ma/cm2   P=0.05330505 mW/cm2
#Using the AM0nrel.spec file, this 0.82InGap(doped 5e19)/2.7umGaAs(doped
5e19)/ORIG300um Ge(doped 3e18)cell has   Voc=2.7735 & Jsc=19.8531  ma/cm2
P=0.05506257 mW/cm2
#Using the AM0nrel.spec file, the 0.82InGap(doped 5e19)/2.7umGaAs(doped
5e19)/ORIG300um Ge(Emitter & Substrate doped 3e18)cell has
# Voc=2.7736 & Jsc=19.8531  ma/cm2  P=0.05506456 mW/cm2    Pmax=0.0489605
# Vmax=2.52998 Jmax=19.3521 ma/cm2  FF=0.889147  Eff=0.361866

#At 300K, using the AM0nrel.spec file, this 0.82InGap(doped
5e19)/3.9umGaAs(doped 5e19)/ORIG300um Ge(Emitter & Substrate doped 3e18)cell
has
# Voc=2.76425 & Jsc=19.8531 ma/cm2  P=0.05487893 mW/cm2    Pmax=0.0490907
# Vmax=2.525    Jmax=19.4419 ma/cm2  FF=0.894527  Eff=0.362829

# Main Silvaco ATLAS Structure
go atlas
# Definition of constants
# Mesh
#   X-Mesh
#   Y-Mesh
#   QT Mesh
# Regions
# Electrodes
# Doping
# Material Properties
```

```
# Models
# Light beams
# Solving

#Define the X-Mesh.  Must start from left to right, or from lesser to greater
values.
#mesh width=1
mesh width=200000
#mesh space.mult=1
# X-mesh:  surface=500 um2= 1/200000 cm2
x.mesh loc=-250 spac=50
x.mesh loc=0     spac=10
x.mesh loc=250  spac=50


#Define the Y-Mesh.  Must start from surface of the device to the back, or go
from lesser to greater value with up as negative.
# Vacuum
y.mesh loc=-0.87  spac=0.003
# Window (0.01 um)
y.mesh loc=-0.86  spac=0.003
# Emitter (0.17 um)
y.mesh loc=-0.69  spac=0.003
# Base (0.63 um)
y.mesh loc=-0.34  spac=0.03
y.mesh loc=-0.06  spac=0.003
# BSF (0.01 um)
y.mesh loc=-0.05  spac=0.003
# Buffer (0.03 um)
y.mesh loc=-0.02  spac=0.002

# Tunnel Emitter (0.015)
y.mesh loc=-0.005 spac=0.001
# Tunnel Base (0.015)
y.mesh loc=0.01    spac=0.001


# Window (0.01 um)
y.mesh loc=0.02    spac=0.003
# Emitter (0.01 um)
y.mesh loc=0.03    spac=0.003
# Base (3.87 um)
y.mesh loc=2.815   spac=0.03
y.mesh loc=3.90    spac=0.003
# BSF (0.01 um)
y.mesh loc=3.91    spac=0.003
# Buffer (0.3 um)
y.mesh loc=4.21    spac=0.002

# Tunnel Emitter (0.015)
y.mesh loc=4.225   spac=0.001
# Tunnel Base (0.015)
y.mesh loc=4.24    spac=0.001

# Window (0.05 um) - ORIGINAL Cell parameters
y.mesh loc=4.29    spac=0.01
# Emitter (0.1 um)
y.mesh loc=4.39    spac=0.01
# Substrate (300 um)
y.mesh loc=304.39 spac=50

# Window (0.01 um) - BATES OPTM parameters
#y.mesh loc=2.39   spac=0.01
# Emitter (4 um)
```

```
#y.mesh loc=6.39    spac=0.01
# Substrate (300 um)
#y.mesh loc=306.39 spac=50


###################
# REGIONS
###################
# Vacuum
region num=1 material=Vacuum x.min=-250 x.max=250  y.min=-0.92  y.max=-0.87
#Window AlInP (=InAsP)
region num=2 material=InAsP  x.min=-250 x.max=250  y.min=-0.87  y.max=-0.86
#Emitter
region num=3 material=InGaP  x.min=-250 x.max=250  y.min=-0.86  y.max=-0.69
#Base
region num=4 material=InGaP  x.min=-250 x.max=250  y.min=-0.69  y.max=-0.06
#BSF
region num=5 material=InGaP  x.min=-250 x.max=250  y.min=-0.06  y.max=-0.05
#Buffer AlInP (=InAsP)
region num=6 material=InAsP  x.min=-250 x.max=250  y.min=-0.05  y.max=-0.02

#Tunnel Emitter
region num=7 material=InGaP  x.min=-250 x.max=250  y.min=-0.02  y.max=-0.005
#Tunnel Base
region num=8 material=InGaP  x.min=-250 x.max=250  y.min=-0.005 y.max=0.01

#Window AlInP (=InAsP)
region num=9 material=InAsP  x.min=-250 x.max=250  y.min=0.01   y.max=0.02
#Emitter
region num=10 material=GaAs  x.min=-250 x.max=250  y.min=0.02   y.max=0.03
#Base
region num=11 material=GaAs  x.min=-250 x.max=250  y.min=0.03   y.max=3.90
#BSF
region num=12 material=InGaP x.min=-250 x.max=250  y.min=3.90   y.max=3.91
#Buffer
region num=13 material=GaAs  x.min=-250 x.max=250  y.min=3.91   y.max=4.21

#Tunnel Emitter
region num=14 material=GaAs  x.min=-250 x.max=250  y.min=4.21   y.max=4.225
#Tunnel Base
region num=15 material=GaAs  x.min=-250 x.max=250  y.min=4.225 y.max=4.24

#Window
region num=16 material=GaAs  x.min=-250 x.max=250  y.min=4.24   y.max=4.29
#Emitter
region num=17 material=Ge    x.min=-250 x.max=250  y.min=4.29   y.max=4.39
#Substrate
region num=18 material=Ge    x.min=-250 x.max=250  y.min=4.39   y.max=304.39

####################
# ELECTRODES - Use 2% of cell width for optimal grid contact width (500x0.02 =
10um)
####################
electrode name=cathode     x.min=-5   x.max=5   y.min=-0.87  y.max=-0.87
electrode name=tunneltop  x.min=-250 x.max=250 y.min=-0.02  y.max=0.01
electrode name=tunnelbot  x.min=-250 x.max=250 y.min=4.21   y.max=4.24
electrode name=anode       x.min=-250 x.max=250 y.min=304.39 y.max=304.39

###################
# DOPING - n-emitter on p-base
###################
# Window - Realistic from 1e20
doping uniform region=2 n.type conc=5e19
```

85

```
# Emitter
doping uniform region=3 n.type conc=4.64e17
# Base
doping uniform region=4 p.type conc=1e17
# BSF - Realistic from 1e20
doping uniform region=5 p.type conc=5e19
# Buffer
doping uniform region=6 p.type conc=1e18

# Tunnel Emitter
doping uniform region=7 p.type conc=8e18
# Tunnel Base
doping uniform region=8 n.type conc=1e19

# Window
doping uniform region=9 n.type conc=4.64e17
# Emitter
doping uniform region=10 n.type conc=4.64e15
# Base
doping uniform region=11 p.type conc=1e17
# BSF - Realistic from 1e20
doping uniform region=12 p.type conc=5e19
# Buffer - May want to change to 1e18.
doping uniform region=13 p.type conc=7e18

# Tunnel Emitter
doping uniform region=14 p.type conc=8e18
# Tunnel Base
doping uniform region=15 n.type conc=1e19

# Window
doping uniform region=16 n.type conc=7e18
# Emitter - Changed from 2e18
doping uniform region=17 n.type conc=3e18
# Substrate - Changed from 1e17
doping uniform region=18 p.type conc=3e18

#####################
# MATERIAL PROPERTIES
#####################
material TAUN=1e-7 TAUP=1e-7 COPT=1.5e-10 AUGN=8.3e-32 AUGP=1.8e-31

# Vacuum
material material=Vacuum real.index=3.3 imag.index=0

# InGaP
material material=InGaP EG300=1.9 PERMITTIVITY=11.62 AFFINITY=4.16
material material=InGaP MUN=1945 MUP=141
material material=InGaP NC300=1.3e20 NV300=1.28e19
material material=InGaP index.file=InGaP-1.9.opt

# GaAs
material material=GaAs EG300=1.42 PERMITTIVITY=13.1 AFFINITY=4.07
material material=GaAs MUN=8800 MUP=400
material material=GaAs NC300=4.7e17 NV300=7e18
material material=GaAs index.file=GaAs.opt

# Ge
material material=Ge EG300=0.67 PERMITTIVITY=16 AFFINITY=4
material material=Ge MUN=3900 MUP=1800
material material=Ge NC300=1.04e19 NV300=6e18
material material=Ge index.file=Ge.opt
```

```
# AlInP (=InAsP)
material material=InAsP EG300=2.4 PERMITTIVITY=11.7 AFFINITY=4.2
material material=InAsP MUN=2291 MUP=142
material material=InAsP NC300=1.08e20 NV300=1.28e19
material material=InAsP index.file=AlInP.opt

#Gold
material material=Gold real.index=1.2 imag.index=1.8


####################
# MODELS
####################
models srh temp=300 print


####################
# CONTACTS
####################
contact name=tunneltop resist=1e17
contact name=tunnelbot resist=1e17


####################
# LIGHTBEAMS - Calculates the position of the light source and defines the
beam.
####################
beam num=1 x.origin=0 y.origin=-5 angle=90 back.refl \
      power.file=AM0nrel.spec wavel.start=0.12 wavel.end=2.4 wavel.num=1500

#Output and Display the Structure file
struct outfile=$StructFile
#tonyplot $StructFile


####################
# SOLVING I-V CURVE
####################
method gummel newton maxtraps=10 itlimit=25 climit=1 dvmax=0.1


log outf=Triple_KATO_OPTM_0.82InGaP_3.9GaAs_ORIG300Ge_Realistic_Doping_300K.log
solve initial
#Beam strength of 1.0 sun
solve b1=1.0
solve vanode=0.0 name=anode vstep=0.05 vfinal=2.4
solve vanode=2.4 name=anode vstep=0.005 vfinal=3

extract init
infile="Triple_KATO_OPTM_0.82InGaP_3.9GaAs_ORIG300Ge_Realistic_Doping_300K.log"
extract name="Jsc" y.val from curve(v."anode", i."anode") where x.val=0.1
extract name="Voc" x.val from curve(v."anode", i."anode") where y.val=0.0
extract name="iv"  curve(v."anode", i."cathode")
outfile="Triple_KATO_OPTM_0.82InGaP_3.9GaAs_ORIG300Ge_Realistic_Doping_300K.dat
"

extract name="Power" curve(v."anode", (v."anode" * i."anode")) outf="Power.dat"
# Min since negative values
extract name="Pmax" min(curve(v."anode", (v."anode" * i."anode")))
extract name="Vmax" x.val from curve(v."anode", (v."anode"*i."anode") ) \
      where y.val=$"Pmax"
extract name="Jmax" $"Pmax"/$"Vmax"
extract name="FF" $"Pmax"/($"Jsc"*$"Voc")
#Use AMO of 0.1353 W/cm2
extract name="Eff" $Pmax/0.1353
```

87

```
#################
#OUTPUT
#################
tonyplot Triple_KATO_OPTM_0.82InGaP_3.9GaAs_ORIG300Ge_Realistic_Doping_300K.dat
save
outf=Triple_KATO_OPTM_0.82InGaP_3.9GaAs_ORIG300Ge_Realistic_Doping_300K.log

log off
```

B.   DIVIDED CHAMPION INGAP FREQUENCY RESPONSE

```
# Jamie VanDyke Freq Response of Michael Tsutagawa's Champion Cell InGaP Layer

# Main Silvaco ATLAS Structure
go atlas
# Definition of constants
# Mesh
#   X-Mesh
#   Y-Mesh
#   QT Mesh
# Regions
# Electrodes
# Doping
# Material Properties
# Models
# Light beams
# Solving

#Define the X-Mesh.  Must start from left to right, or from lesser to greater
values.
#mesh width=1
mesh width=200000
#mesh space.mult=1
# X-mesh:  surface=500 um2= 1/200000 cm2
x.mesh loc=-250 spac=50
x.mesh loc=0    spac=10
x.mesh loc=250  spac=50

#Define the Y-Mesh.  Must start from surface of the device to the back, or go
from lesser to greater value with up as negative.
# Vacuum
y.mesh loc=-0.87  spac=0.003
# Window (0.01 um)
y.mesh loc=-0.86  spac=0.003
# Emitter (0.17 um)
y.mesh loc=-0.69  spac=0.003
# Base (0.63 um)
y.mesh loc=-0.34  spac=0.03
y.mesh loc=-0.06  spac=0.003
# BSF (0.01 um)
y.mesh loc=-0.05  spac=0.003
# Buffer (0.03 um)
y.mesh loc=-0.02  spac=0.002

#################
# REGIONS
#################
# Vacuum
region num=1 material=Vacuum x.min=-250 x.max=250  y.min=-0.92  y.max=-0.87
#Window AlInP (=InAsP)
region num=2 material=InAsP  x.min=-250 x.max=250  y.min=-0.87  y.max=-0.86
```

```
#Emitter
region num=3 material=InGaP  x.min=-250 x.max=250  y.min=-0.86  y.max=-0.69
#Base
region num=4 material=InGaP  x.min=-250 x.max=250  y.min=-0.69  y.max=-0.06
#BSF
region num=5 material=InGaP  x.min=-250 x.max=250  y.min=-0.06  y.max=-0.05
#Buffer AlInP (=InAsP)
region num=6 material=InAsP  x.min=-250 x.max=250  y.min=-0.05  y.max=-0.02


####################
# ELECTRODES - Use 2% of cell width for optimal grid contact width (500x0.02 =
10um)
####################
electrode name=cathode    x.min=-5   x.max=5   y.min=-0.87  y.max=-0.87
electrode name=anode      x.min=-250 x.max=250 y.min=-0.02 y.max=-0.02


###################
# DOPING - n-emitter on p-base
###################
# Window - Realistic from 1e20
doping uniform region=2 n.type conc=5e19
# Emitter
doping uniform region=3 n.type conc=4.64e17
# Base
doping uniform region=4 p.type conc=1e17
# BSF - Realistic from 1e20
doping uniform region=5 p.type conc=5e19
# Buffer
doping uniform region=6 p.type conc=1e18


####################
# MATERIAL PROPERTIES
####################
material TAUN=1e-7 TAUP=1e-7 COPT=1.5e-10 AUGN=8.3e-32 AUGP=1.8e-31

# Vacuum
material material=Vacuum real.index=3.3 imag.index=0

# InGaP
material material=InGaP EG300=1.9 PERMITTIVITY=11.62 AFFINITY=4.16
material material=InGaP MUN=1945 MUP=141
material material=InGaP NC300=1.3e20 NV300=1.28e19
material material=InGaP index.file=InGaP-1.9.opt

# GaAs
material material=GaAs EG300=1.42 PERMITTIVITY=13.1 AFFINITY=4.07
material material=GaAs MUN=8800 MUP=400
material material=GaAs NC300=4.7e17 NV300=7e18
material material=GaAs index.file=GaAs.opt

# Ge
material material=Ge EG300=0.67 PERMITTIVITY=16 AFFINITY=4
material material=Ge MUN=3900 MUP=1800
material material=Ge NC300=1.04e19 NV300=6e18
material material=Ge index.file=Ge.opt

# AlInP (=InAsP)
material material=InAsP EG300=2.4 PERMITTIVITY=11.7 AFFINITY=4.2
material material=InAsP MUN=2291 MUP=142
material material=InAsP NC300=1.08e20 NV300=1.28e19
material material=InAsP index.file=AlInP.opt
```

89

```
#Gold
material material=Gold real.index=1.2 imag.index=1.8


####################
# MODELS
####################
models srh temp=300 print


####################
# LIGHTBEAMS - Calculates the position of the light source and defines the
beam.
####################
beam num=1 x.origin=0 y.origin=-5 angle=90 back.refl \
        power.file=AM0nrel_unity.spec wavel.start=0.35 wavel.end=0.6
wavel.num=250


# Solving
# Get frequency response
solve init


log outfile=InGaP-freq.log
solve b1=1 lambda=0.35
solve b1=1 lambda=0.355
solve b1=1 lambda=0.36
solve b1=1 lambda=0.365
solve b1=1 lambda=0.37
solve b1=1 lambda=0.375
solve b1=1 lambda=0.38
solve b1=1 lambda=0.385
solve b1=1 lambda=0.39
solve b1=1 lambda=0.395
solve b1=1 lambda=0.4
solve b1=1 lambda=0.405
solve b1=1 lambda=0.410
solve b1=1 lambda=0.415
solve b1=1 lambda=0.42
solve b1=1 lambda=0.425
solve b1=1 lambda=0.43
solve b1=1 lambda=0.435
solve b1=1 lambda=0.44
solve b1=1 lambda=0.445
solve b1=1 lambda=0.45
solve b1=1 lambda=0.455
solve b1=1 lambda=0.46
solve b1=1 lambda=0.465
solve b1=1 lambda=0.47
solve b1=1 lambda=0.475
solve b1=1 lambda=0.48
solve b1=1 lambda=0.485
solve b1=1 lambda=0.49
solve b1=1 lambda=0.495
solve b1=1 lambda=0.5
solve b1=1 lambda=0.505
solve b1=1 lambda=0.51
solve b1=1 lambda=0.515
solve b1=1 lambda=0.52
solve b1=1 lambda=0.525
solve b1=1 lambda=0.53
solve b1=1 lambda=0.535
solve b1=1 lambda=0.54
solve b1=1 lambda=0.545
solve b1=1 lambda=0.55
```

```
solve b1=1 lambda=0.555
solve b1=1 lambda=0.56
solve b1=1 lambda=0.565
solve b1=1 lambda=0.57
solve b1=1 lambda=0.575
solve b1=1 lambda=0.58
solve b1=1 lambda=0.585
solve b1=1 lambda=0.59
solve b1=1 lambda=0.595
solve b1=1 lambda=0.6

tonyplot InGaP-freq.log

log off
```

C.   DIVIDED CHAMPION GAAS FREQUENCY RESPONSE

```
# Jamie VanDyke Freq Response of Michael Tsutagawa's Champion Cell GaAs Layer

# Main Silvaco ATLAS Structure
go atlas
# Definition of constants
# Mesh
#    X-Mesh
#    Y-Mesh
#    QT Mesh
# Regions
# Electrodes
# Doping
# Material Properties
# Models
# Light beams
# Solving

#Define the X-Mesh.  Must start from left to right, or from lesser to greater
values.
#mesh width=1
mesh width=200000
#mesh space.mult=1
# X-mesh:  surface=500 um2= 1/200000 cm2
x.mesh loc=-250 spac=50
x.mesh loc=0     spac=10
x.mesh loc=250   spac=50

#Define the Y-Mesh.  Must start from surface of the device to the back, or go
from lesser to greater value with up as negative.
# Vacuum
y.mesh loc=-0.87  spac=0.003
# Window (0.01 um)
y.mesh loc=-0.86  spac=0.003

# Emitter (0.01 um)
y.mesh loc=-0.85   spac=0.003
# Base (3.87 um)
y.mesh loc=1.935  spac=0.03
y.mesh loc=3.02    spac=0.003
# BSF (0.01 um)
y.mesh loc=3.03    spac=0.003
# Buffer (0.3 um)
y.mesh loc=3.33    spac=0.002
```

91

```
####################
# REGIONS
####################
# Vacuum
region num=1 material=Vacuum x.min=-250 x.max=250  y.min=-0.92  y.max=-0.87

#Window AlInP (=InAsP)
region num=2 material=InAsP  x.min=-250 x.max=250  y.min=-0.87   y.max=-0.86
#Emitter
region num=3 material=GaAs  x.min=-250 x.max=250  y.min=-0.86   y.max=-0.85
#Base
region num=4 material=GaAs  x.min=-250 x.max=250  y.min=-0.85   y.max=3.02
#BSF
region num=5 material=InGaP x.min=-250 x.max=250  y.min=3.02   y.max=3.03
#Buffer
region num=6 material=GaAs  x.min=-250 x.max=250  y.min=3.03   y.max=3.33

####################
# ELECTRODES - Use 2% of cell width for optimal grid contact width (500x0.02 =
10um)
####################
electrode name=cathode    x.min=-5   x.max=5   y.min=-0.87  y.max=-0.87
electrode name=anode      x.min=-250 x.max=250 y.min=3.33 y.max=3.33

####################
# DOPING - n-emitter on p-base
####################
# Window
doping uniform region=2 n.type conc=4.64e17
# Emitter
doping uniform region=3 n.type conc=4.64e15
# Base
doping uniform region=4 p.type conc=1e17
# BSF - Realistic from 1e20
doping uniform region=5 p.type conc=5e19
# Buffer - May want to change to 1e18.
doping uniform region=6 p.type conc=7e18

####################
# MATERIAL PROPERTIES
####################
material TAUN=1e-7 TAUP=1e-7 COPT=1.5e-10 AUGN=8.3e-32 AUGP=1.8e-31

# Vacuum
material material=Vacuum real.index=3.3 imag.index=0

# InGaP
material material=InGaP EG300=1.9 PERMITTIVITY=11.62 AFFINITY=4.16
material material=InGaP MUN=1945 MUP=141
material material=InGaP NC300=1.3e20 NV300=1.28e19
material material=InGaP index.file=InGaP-1.9.opt

# GaAs
material material=GaAs EG300=1.42 PERMITTIVITY=13.1 AFFINITY=4.07
material material=GaAs MUN=8800 MUP=400
material material=GaAs NC300=4.7e17 NV300=7e18
material material=GaAs index.file=GaAs.opt

# Ge
material material=Ge EG300=0.67 PERMITTIVITY=16 AFFINITY=4
material material=Ge MUN=3900 MUP=1800
```

```
material material=Ge NC300=1.04e19 NV300=6e18
material material=Ge index.file=Ge.opt

# AlInP (=InAsP)
material material=InAsP EG300=2.4 PERMITTIVITY=11.7 AFFINITY=4.2
material material=InAsP MUN=2291 MUP=142
material material=InAsP NC300=1.08e20 NV300=1.28e19
material material=InAsP index.file=AlInP.opt

#Gold
material material=Gold real.index=1.2 imag.index=1.8


####################
# MODELS
####################
models srh temp=300 print


####################
# LIGHTBEAMS - Calculates the position of the light source and defines the
beam.
####################
beam num=1 x.origin=0 y.origin=-5 angle=90 back.refl \
      power.file=AM0nrel_unity.spec wavel.start=0.35 wavel.end=0.9
wavel.num=480

#Output and Display the Structure file
struct outfile=$StructFile
#tonyplot $StructFile

# Solving
# Get frequency response
solve init

log outfile=GaAs-freq.log
solve b1=1 lambda=0.35
solve b1=1 lambda=0.355
solve b1=1 lambda=0.36
solve b1=1 lambda=0.365
solve b1=1 lambda=0.37
solve b1=1 lambda=0.375
solve b1=1 lambda=0.38
solve b1=1 lambda=0.385
solve b1=1 lambda=0.39
solve b1=1 lambda=0.395
solve b1=1 lambda=0.4
solve b1=1 lambda=0.405
solve b1=1 lambda=0.410
solve b1=1 lambda=0.415
solve b1=1 lambda=0.42
solve b1=1 lambda=0.425
solve b1=1 lambda=0.43
solve b1=1 lambda=0.435
solve b1=1 lambda=0.44
solve b1=1 lambda=0.445
solve b1=1 lambda=0.45
solve b1=1 lambda=0.455
solve b1=1 lambda=0.46
solve b1=1 lambda=0.465
solve b1=1 lambda=0.47
solve b1=1 lambda=0.475
solve b1=1 lambda=0.48
solve b1=1 lambda=0.485
```

```
solve b1=1 lambda=0.49
solve b1=1 lambda=0.495
solve b1=1 lambda=0.5
solve b1=1 lambda=0.505
solve b1=1 lambda=0.51
solve b1=1 lambda=0.515
solve b1=1 lambda=0.52
solve b1=1 lambda=0.525
solve b1=1 lambda=0.53
solve b1=1 lambda=0.535
solve b1=1 lambda=0.54
solve b1=1 lambda=0.545
solve b1=1 lambda=0.55
solve b1=1 lambda=0.555
solve b1=1 lambda=0.56
solve b1=1 lambda=0.565
solve b1=1 lambda=0.57
solve b1=1 lambda=0.575
solve b1=1 lambda=0.58
solve b1=1 lambda=0.585
solve b1=1 lambda=0.59
solve b1=1 lambda=0.595
solve b1=1 lambda=0.6
solve b1=1 lambda=0.605
solve b1=1 lambda=0.61
solve b1=1 lambda=0.615
solve b1=1 lambda=0.62
solve b1=1 lambda=0.625
solve b1=1 lambda=0.63
solve b1=1 lambda=0.635
solve b1=1 lambda=0.64
solve b1=1 lambda=0.645
solve b1=1 lambda=0.65
solve b1=1 lambda=0.655
solve b1=1 lambda=0.66
solve b1=1 lambda=0.665
solve b1=1 lambda=0.67
solve b1=1 lambda=0.675
solve b1=1 lambda=0.68
solve b1=1 lambda=0.685
solve b1=1 lambda=0.69
solve b1=1 lambda=0.695
solve b1=1 lambda=0.7
solve b1=1 lambda=0.705
solve b1=1 lambda=0.71
solve b1=1 lambda=0.715
solve b1=1 lambda=0.72
solve b1=1 lambda=0.725
solve b1=1 lambda=0.73
solve b1=1 lambda=0.735
solve b1=1 lambda=0.74
solve b1=1 lambda=0.745
solve b1=1 lambda=0.75
solve b1=1 lambda=0.755
solve b1=1 lambda=0.76
solve b1=1 lambda=0.765
solve b1=1 lambda=0.77
solve b1=1 lambda=0.775
solve b1=1 lambda=0.78
solve b1=1 lambda=0.785
solve b1=1 lambda=0.79
solve b1=1 lambda=0.795
```

```
solve b1=1 lambda=0.8
solve b1=1 lambda=0.805
solve b1=1 lambda=0.81
solve b1=1 lambda=0.815
solve b1=1 lambda=0.82
solve b1=1 lambda=0.825
solve b1=1 lambda=0.83
solve b1=1 lambda=0.835
solve b1=1 lambda=0.84
solve b1=1 lambda=0.845
solve b1=1 lambda=0.85
solve b1=1 lambda=0.855
solve b1=1 lambda=0.86
solve b1=1 lambda=0.865
solve b1=1 lambda=0.87
solve b1=1 lambda=0.875
solve b1=1 lambda=0.88
solve b1=1 lambda=0.885
solve b1=1 lambda=0.89
solve b1=1 lambda=0.895
solve b1=1 lambda=0.9

tonyplot GaAs-freq.log

log off
```

D.   DIVIDED CHAMPION GE FREQUENCY RESPONSE

```
# Jamie VanDyke Freq Response of Michael Tsutagawa's Champion Cell Ge Layer

# Main Silvaco ATLAS Structure
go atlas
# Definition of constants
# Mesh
#   X-Mesh
#   Y-Mesh
#   QT Mesh
# Regions
# Electrodes
# Doping
# Material Properties
# Models
# Light beams
# Solving

#Define the X-Mesh.  Must start from left to right, or from lesser to greater
values.
#mesh width=1
mesh width=200000
#mesh space.mult=1
# X-mesh:  surface=500 um2= 1/200000 cm2
x.mesh loc=-250 spac=50
x.mesh loc=0     spac=10
x.mesh loc=250   spac=50

#Define the Y-Mesh.  Must start from surface of the device to the back, or go
from lesser to greater value with up as negative.
# Vacuum
y.mesh loc=4.28  spac=0.003

# Window (0.05 um) - ORIGINAL Cell parameters
```

```
y.mesh loc=4.29    spac=0.01
# Emitter (0.1 um)
y.mesh loc=4.39    spac=0.01
# Substrate (300 um)
y.mesh loc=304.39 spac=50


###################
# REGIONS
###################
# Vacuum
region num=1 material=Vacuum x.min=-250 x.max=250  y.min=4.23  y.max=4.28
#Window
region num=2 material=GaAs  x.min=-250 x.max=250  y.min=4.24   y.max=4.29
#Emitter
region num=3 material=Ge    x.min=-250 x.max=250  y.min=4.29   y.max=4.39
#Substrate
region num=4 material=Ge    x.min=-250 x.max=250  y.min=4.39   y.max=304.39


######################
# ELECTRODES - Use 2% of cell width for optimal grid contact width (500x0.02 =
10um)
######################
electrode name=cathode    x.min=-5   x.max=5   y.min=4.29  y.max=4.29
electrode name=anode      x.min=-250 x.max=250 y.min=304.39 y.max=304.39


####################
# DOPING - n-emitter on p-base
####################
# Window
doping uniform region=2 n.type conc=7e18
# Emitter - Changed from 2e18
doping uniform region=3 n.type conc=3e18
# Substrate - Changed from 1e17
doping uniform region=4 p.type conc=3e18


#####################
# MATERIAL PROPERTIES
#####################
material TAUN=1e-7 TAUP=1e-7 COPT=1.5e-10 AUGN=8.3e-32 AUGP=1.8e-31


# Vacuum
material material=Vacuum real.index=3.3 imag.index=0


# InGaP
material material=InGaP EG300=1.9 PERMITTIVITY=11.62 AFFINITY=4.16
material material=InGaP MUN=1945 MUP=141
material material=InGaP NC300=1.3e20 NV300=1.28e19
material material=InGaP index.file=InGaP-1.9.opt


# GaAs
material material=GaAs EG300=1.42 PERMITTIVITY=13.1 AFFINITY=4.07
material material=GaAs MUN=8800 MUP=400
material material=GaAs NC300=4.7e17 NV300=7e18
material material=GaAs index.file=GaAs.opt


# Ge
material material=Ge EG300=0.67 PERMITTIVITY=16 AFFINITY=4
material material=Ge MUN=3900 MUP=1800
material material=Ge NC300=1.04e19 NV300=6e18
material material=Ge index.file=Ge.opt


# AlInP (=InAsP)
```

```
material material=InAsP EG300=2.4 PERMITTIVITY=11.7 AFFINITY=4.2
material material=InAsP MUN=2291 MUP=142
material material=InAsP NC300=1.08e20 NV300=1.28e19
material material=InAsP index.file=AlInP.opt

#Gold
material material=Gold real.index=1.2 imag.index=1.8


####################
# MODELS
####################
models srh temp=300 print

####################
# LIGHTBEAMS - Calculates the position of the light source and defines the
beam.
####################
beam num=1 x.origin=0 y.origin=-5 angle=90 back.refl \
       power.file=AM0nrel_unity.spec wavel.start=0.35 wavel.end=1.7
wavel.num=880

# Solving
# Get frequency response
solve init

log outfile=Ge-freq.log
solve b1=1 lambda=0.35
solve b1=1 lambda=0.355
solve b1=1 lambda=0.36
solve b1=1 lambda=0.365
solve b1=1 lambda=0.37
solve b1=1 lambda=0.375
solve b1=1 lambda=0.38
solve b1=1 lambda=0.385
solve b1=1 lambda=0.39
solve b1=1 lambda=0.395
solve b1=1 lambda=0.4
solve b1=1 lambda=0.405
solve b1=1 lambda=0.410
solve b1=1 lambda=0.415
solve b1=1 lambda=0.42
solve b1=1 lambda=0.425
solve b1=1 lambda=0.43
solve b1=1 lambda=0.435
solve b1=1 lambda=0.44
solve b1=1 lambda=0.445
solve b1=1 lambda=0.45
solve b1=1 lambda=0.455
solve b1=1 lambda=0.46
solve b1=1 lambda=0.465
solve b1=1 lambda=0.47
solve b1=1 lambda=0.475
solve b1=1 lambda=0.48
solve b1=1 lambda=0.485
solve b1=1 lambda=0.49
solve b1=1 lambda=0.495
solve b1=1 lambda=0.5
solve b1=1 lambda=0.505
solve b1=1 lambda=0.51
solve b1=1 lambda=0.515
solve b1=1 lambda=0.52
solve b1=1 lambda=0.525
```

```
solve b1=1 lambda=0.53
solve b1=1 lambda=0.535
solve b1=1 lambda=0.54
solve b1=1 lambda=0.545
solve b1=1 lambda=0.55
solve b1=1 lambda=0.555
solve b1=1 lambda=0.56
solve b1=1 lambda=0.565
solve b1=1 lambda=0.57
solve b1=1 lambda=0.575
solve b1=1 lambda=0.58
solve b1=1 lambda=0.585
solve b1=1 lambda=0.59
solve b1=1 lambda=0.595
solve b1=1 lambda=0.6
solve b1=1 lambda=0.605
solve b1=1 lambda=0.61
solve b1=1 lambda=0.615
solve b1=1 lambda=0.62
solve b1=1 lambda=0.625
solve b1=1 lambda=0.63
solve b1=1 lambda=0.635
solve b1=1 lambda=0.64
solve b1=1 lambda=0.645
solve b1=1 lambda=0.65
solve b1=1 lambda=0.655
solve b1=1 lambda=0.66
solve b1=1 lambda=0.665
solve b1=1 lambda=0.67
solve b1=1 lambda=0.675
solve b1=1 lambda=0.68
solve b1=1 lambda=0.685
solve b1=1 lambda=0.69
solve b1=1 lambda=0.695
solve b1=1 lambda=0.7
solve b1=1 lambda=0.705
solve b1=1 lambda=0.71
solve b1=1 lambda=0.715
solve b1=1 lambda=0.72
solve b1=1 lambda=0.725
solve b1=1 lambda=0.73
solve b1=1 lambda=0.735
solve b1=1 lambda=0.74
solve b1=1 lambda=0.745
solve b1=1 lambda=0.75
solve b1=1 lambda=0.755
solve b1=1 lambda=0.76
solve b1=1 lambda=0.765
solve b1=1 lambda=0.77
solve b1=1 lambda=0.775
solve b1=1 lambda=0.78
solve b1=1 lambda=0.785
solve b1=1 lambda=0.79
solve b1=1 lambda=0.795
solve b1=1 lambda=0.8
solve b1=1 lambda=0.805
solve b1=1 lambda=0.81
solve b1=1 lambda=0.815
solve b1=1 lambda=0.82
solve b1=1 lambda=0.825
solve b1=1 lambda=0.83
solve b1=1 lambda=0.835
```

```
solve b1=1 lambda=0.84
solve b1=1 lambda=0.845
solve b1=1 lambda=0.85
solve b1=1 lambda=0.855
solve b1=1 lambda=0.86
solve b1=1 lambda=0.865
solve b1=1 lambda=0.87
solve b1=1 lambda=0.875
solve b1=1 lambda=0.88
solve b1=1 lambda=0.885
solve b1=1 lambda=0.89
solve b1=1 lambda=0.895
solve b1=1 lambda=0.9
solve b1=1 lambda=0.905
solve b1=1 lambda=0.91
solve b1=1 lambda=0.915
solve b1=1 lambda=0.92
solve b1=1 lambda=0.925
solve b1=1 lambda=0.93
solve b1=1 lambda=0.935
solve b1=1 lambda=0.94
solve b1=1 lambda=0.945
solve b1=1 lambda=0.95
solve b1=1 lambda=0.955
solve b1=1 lambda=0.96
solve b1=1 lambda=0.965
solve b1=1 lambda=0.97
solve b1=1 lambda=0.975
solve b1=1 lambda=0.98
solve b1=1 lambda=0.985
solve b1=1 lambda=0.99
solve b1=1 lambda=0.995
solve b1=1 lambda=1.000
solve b1=1 lambda=1.005
solve b1=1 lambda=1.01
solve b1=1 lambda=1.015
solve b1=1 lambda=1.02
solve b1=1 lambda=1.025
solve b1=1 lambda=1.03
solve b1=1 lambda=1.035
solve b1=1 lambda=1.04
solve b1=1 lambda=1.045
solve b1=1 lambda=1.05
solve b1=1 lambda=1.055
solve b1=1 lambda=1.06
solve b1=1 lambda=1.065
solve b1=1 lambda=1.07
solve b1=1 lambda=1.075
solve b1=1 lambda=1.08
solve b1=1 lambda=1.085
solve b1=1 lambda=1.09
solve b1=1 lambda=1.095
solve b1=1 lambda=1.100
solve b1=1 lambda=1.105
solve b1=1 lambda=1.11
solve b1=1 lambda=1.115
solve b1=1 lambda=1.12
solve b1=1 lambda=1.125
solve b1=1 lambda=1.13
solve b1=1 lambda=1.135
solve b1=1 lambda=1.14
solve b1=1 lambda=1.145
```

```
solve b1=1 lambda=1.15
solve b1=1 lambda=1.155
solve b1=1 lambda=1.16
solve b1=1 lambda=1.165
solve b1=1 lambda=1.17
solve b1=1 lambda=1.175
solve b1=1 lambda=1.18
solve b1=1 lambda=1.185
solve b1=1 lambda=1.19
solve b1=1 lambda=1.195
solve b1=1 lambda=1.200
solve b1=1 lambda=1.205
solve b1=1 lambda=1.21
solve b1=1 lambda=1.215
solve b1=1 lambda=1.22
solve b1=1 lambda=1.225
solve b1=1 lambda=1.23
solve b1=1 lambda=1.235
solve b1=1 lambda=1.24
solve b1=1 lambda=1.245
solve b1=1 lambda=1.25
solve b1=1 lambda=1.255
solve b1=1 lambda=1.26
solve b1=1 lambda=1.265
solve b1=1 lambda=1.27
solve b1=1 lambda=1.275
solve b1=1 lambda=1.28
solve b1=1 lambda=1.285
solve b1=1 lambda=1.29
solve b1=1 lambda=1.295
solve b1=1 lambda=1.300
solve b1=1 lambda=1.305
solve b1=1 lambda=1.31
solve b1=1 lambda=1.315
solve b1=1 lambda=1.32
solve b1=1 lambda=1.325
solve b1=1 lambda=1.33
solve b1=1 lambda=1.335
solve b1=1 lambda=1.34
solve b1=1 lambda=1.345
solve b1=1 lambda=1.35
solve b1=1 lambda=1.355
solve b1=1 lambda=1.36
solve b1=1 lambda=1.365
solve b1=1 lambda=1.37
solve b1=1 lambda=1.375
solve b1=1 lambda=1.38
solve b1=1 lambda=1.385
solve b1=1 lambda=1.39
solve b1=1 lambda=1.395
solve b1=1 lambda=1.4
solve b1=1 lambda=1.405
solve b1=1 lambda=1.41
solve b1=1 lambda=1.415
solve b1=1 lambda=1.42
solve b1=1 lambda=1.425
solve b1=1 lambda=1.43
solve b1=1 lambda=1.435
solve b1=1 lambda=1.44
solve b1=1 lambda=1.445
solve b1=1 lambda=1.45
solve b1=1 lambda=1.455
```

```
solve b1=1 lambda=1.46
solve b1=1 lambda=1.465
solve b1=1 lambda=1.47
solve b1=1 lambda=1.475
solve b1=1 lambda=1.48
solve b1=1 lambda=1.485
solve b1=1 lambda=1.49
solve b1=1 lambda=1.495
solve b1=1 lambda=1.500
solve b1=1 lambda=1.505
solve b1=1 lambda=1.51
solve b1=1 lambda=1.515
solve b1=1 lambda=1.52
solve b1=1 lambda=1.525
solve b1=1 lambda=1.53
solve b1=1 lambda=1.535
solve b1=1 lambda=1.54
solve b1=1 lambda=1.545
solve b1=1 lambda=1.55
solve b1=1 lambda=1.555
solve b1=1 lambda=1.56
solve b1=1 lambda=1.565
solve b1=1 lambda=1.57
solve b1=1 lambda=1.575
solve b1=1 lambda=1.58
solve b1=1 lambda=1.585
solve b1=1 lambda=1.59
solve b1=1 lambda=1.595
solve b1=1 lambda=1.600
solve b1=1 lambda=1.605
solve b1=1 lambda=1.61
solve b1=1 lambda=1.615
solve b1=1 lambda=1.62
solve b1=1 lambda=1.625
solve b1=1 lambda=1.63
solve b1=1 lambda=1.635
solve b1=1 lambda=1.64
solve b1=1 lambda=1.645
solve b1=1 lambda=1.65
solve b1=1 lambda=1.655
solve b1=1 lambda=1.66
solve b1=1 lambda=1.665
solve b1=1 lambda=1.67
solve b1=1 lambda=1.675
solve b1=1 lambda=1.68
solve b1=1 lambda=1.685
solve b1=1 lambda=1.69
solve b1=1 lambda=1.695
solve b1=1 lambda=1.700

tonyplot  Ge-freq.log

log off
```

E.   INGAP INTENSITY DETERMINATION

```
# Jamie VanDyke Laser Simulation for InGaP Layer of Michael Tsutagawa's
Champion Cell
```

```
# This model is an explicit InGaP/GaAs/Ge Triple Junction solar cell with
Tunnel Junction KATO OPTM 0.82InGaP/3.9umGaAs/ORIG300um Ge with BUFFER LAYERS.
# This cell is based on Michalopoulos' cell.  In addition, this cell has buffer
layers under the top and middle layers.
# The buffer layers were incorporated based on Agui's dual cell design and show
increased power out.

#At 300K, using the AM0nrel.spec file cell outputs
# Voc= 1.41965 V  Jsc= 19.8526 mA/cm2  Pmax= 0.025073 W/cm2
# Vmax= 1.3 V  Jmax= 19.2868 mA/cm2  FF= 88.9623 %  Eff= 18.5313 %

#At 300K, using a 554 +/-1 nm laser at X.X W/cm2 intensity cell outputs
# Voc=   Jsc=  mA/cm2  Pmax=  W/cm2
# Vmax=   Jmax=  mA/cm2 FF= % Eff= %


# Main Silvaco ATLAS Structure
go atlas
# Definition of constants
# Mesh
#   X-Mesh
#   Y-Mesh
#   QT Mesh
# Regions
# Electrodes
# Doping
# Material Properties
# Models
# Light beams
# Solving

#Define the X-Mesh.  Must start from left to right, or from lesser to greater
values.
#mesh width=1
mesh width=200000
#mesh space.mult=1
# X-mesh:  surface=500 um2= 1/200000 cm2
x.mesh loc=-250 spac=50
x.mesh loc=0     spac=10
x.mesh loc=250  spac=50

#Define the Y-Mesh.  Must start from surface of the device to the back, or go
from lesser to greater value with up as negative.
# Vacuum
y.mesh loc=-0.87  spac=0.003
# Window (0.01 um)
y.mesh loc=-0.86  spac=0.003
# Emitter (0.17 um)
y.mesh loc=-0.69  spac=0.003
# Base (0.63 um)
y.mesh loc=-0.34  spac=0.03
y.mesh loc=-0.06  spac=0.003
# BSF (0.01 um)
y.mesh loc=-0.05  spac=0.003

##################
# REGIONS
##################
# Vacuum
region num=1 material=Vacuum x.min=-250 x.max=250  y.min=-0.92  y.max=-0.87
#Window AlInP (=InAsP)
region num=2 material=InAsP  x.min=-250 x.max=250  y.min=-0.87  y.max=-0.86
```

```
#Emitter
region num=3 material=InGaP  x.min=-250 x.max=250  y.min=-0.86  y.max=-0.69
#Base
region num=4 material=InGaP  x.min=-250 x.max=250  y.min=-0.69  y.max=-0.06
#BSF
region num=5 material=InGaP  x.min=-250 x.max=250  y.min=-0.06  y.max=-0.05
#Buffer AlInP (=InAsP)
region num=6 material=InAsP  x.min=-250 x.max=250  y.min=-0.05  y.max=-0.02


####################
# ELECTRODES - Use 2% of cell width for optimal grid contact width (500x0.02 =
10um)
####################
electrode name=cathode    x.min=-5   x.max=5   y.min=-0.87  y.max=-0.87
electrode name=anode      x.min=-250 x.max=250 y.min=-0.02 y.max=-0.02


###################
# DOPING - n-emitter on p-base
####################
# Window - Realistic from 1e20
doping uniform region=2 n.type conc=5e19
# Emitter
doping uniform region=3 n.type conc=4.64e17
# Base
doping uniform region=4 p.type conc=1e17
# BSF - Realistic from 1e20
doping uniform region=5 p.type conc=5e19
# Buffer
doping uniform region=6 p.type conc=1e18


####################
# MATERIAL PROPERTIES
####################
material TAUN=1e-7 TAUP=1e-7 COPT=1.5e-10 AUGN=8.3e-32 AUGP=1.8e-31

# Vacuum
material material=Vacuum real.index=3.3 imag.index=0

# InGaP
material material=InGaP EG300=1.9 PERMITTIVITY=11.62 AFFINITY=4.16
material material=InGaP MUN=1945 MUP=141
material material=InGaP NC300=1.3e20 NV300=1.28e19
material material=InGaP index.file=InGaP-1.9.opt

# GaAs
material material=GaAs EG300=1.42 PERMITTIVITY=13.1 AFFINITY=4.07
material material=GaAs MUN=8800 MUP=400
material material=GaAs NC300=4.7e17 NV300=7e18
material material=GaAs index.file=GaAs.opt

# Ge
material material=Ge EG300=0.67 PERMITTIVITY=16 AFFINITY=4
material material=Ge MUN=3900 MUP=1800
material material=Ge NC300=1.04e19 NV300=6e18
material material=Ge index.file=Ge.opt

# AlInP (=InAsP)
material material=InAsP EG300=2.4 PERMITTIVITY=11.7 AFFINITY=4.2
material material=InAsP MUN=2291 MUP=142
material material=InAsP NC300=1.08e20 NV300=1.28e19
material material=InAsP index.file=AlInP.opt
```

103

```
#Gold
material material=Gold real.index=1.2 imag.index=1.8


####################
# MODELS
####################
models srh temp=300 print


####################
# LIGHTBEAMS - Calculates the position of the light source and defines the
beam.
####################
beam num=1 x.origin=0 y.origin=-5 angle=90 back.refl \
      power.file=AM0nrel553.spec wavel.start=0.553 wavel.end=0.555 wavel.num=1

#Output and Display the Structure file
struct outfile=$StructFile
#tonyplot $StructFile


####################
# SOLVING I-V CURVE
####################
method gummel newton maxtraps=10 itlimit=25 climit=1 dvmax=0.1


log outf=InGaP_intensity.log
solve initial
#Beam strength of 1.0 sun
solve b1=1.0
solve vanode=0.0 name=anode vstep=0.05 vfinal=1
solve vanode=1.0 name=anode vstep=0.005 vfinal=1.4

extract init infile="InGaP_intensity.log"
extract name="Jsc" y.val from curve(v."anode", i."cathode") where x.val=0.05
extract name="Voc" x.val from curve(v."anode", i."cathode") where y.val=0.0
extract name="iv"  curve(v."anode", i."cathode") outfile="InGaP_intensity.dat"

extract name="Power" curve(v."anode", (v."anode" * i."cathode"))
outfile="Power.dat"
# Min since negative values
extract name="Pmax" max(curve(v."anode", (v."anode" * i."cathode")))
extract name="Vmax" x.val from curve(v."anode", (v."anode"*i."cathode") ) \
      where y.val=$"Pmax"
extract name="Jmax" $"Pmax"/$"Vmax"
extract name="FF" $"Pmax"/($"Jsc"*$"Voc")
#Use Power Incident of 0.0472 W/cm2
extract name="Eff" $Pmax/0.0472


#################
#OUTPUT
#################
tonyplot Power.dat
tonyplot InGaP_intensity.dat


log off
```

F.   GAAS INTENSITY DETERMINATION

```
# Jamie VanDyke Laser Simulation for GaAs Layer of Michael Tsutagawa's Champion
Cell
```

```
#At 300K, using the AM0nrel.spec file cell outputs
# Voc= 1.08034 V  Jsc= 39.3149 mA/cm2  Pmax= 0.0342071 W/cm2
# Vmax= 0.919988 V  Jmax= 37.1821 mA/cm2  FF= 80.5376 %  Eff= 25.2824 %

#At 300K, using a 861 +/-1 nm laser at 14.97 W/cm2 intensity cell outputs
# Voc= 1.0625 V  Jsc= 19.9968 mA/cm2  Pmax= 0.0178733 W/cm2
# Vmax= 0.929985 V  Jmax= 19.2189 mA/cm2  FF= 84.1231 %  Eff= 59.6971 %

# Main Silvaco ATLAS Structure
go atlas
# Definition of constants
# Mesh
#   X-Mesh
#   Y-Mesh
#   QT Mesh
# Regions
# Electrodes
# Doping
# Material Properties
# Models
# Light beams
# Solving

#Define the X-Mesh.  Must start from left to right, or from lesser to greater
values.
#mesh width=1
mesh width=200000
#mesh space.mult=1
# X-mesh:  surface=500 um2= 1/200000 cm2
x.mesh loc=-250 spac=50
x.mesh loc=0     spac=10
x.mesh loc=250  spac=50

#Define the Y-Mesh.  Must start from surface of the device to the back, or go
from lesser to greater value with up as negative.
# Vacuum
y.mesh loc=-0.87  spac=0.003
# Window (0.01 um)
y.mesh loc=-0.86  spac=0.003

# Emitter (0.01 um)
y.mesh loc=-0.85   spac=0.003
# Base (3.87 um)
y.mesh loc=1.935  spac=0.03
y.mesh loc=3.02    spac=0.003
# BSF (0.01 um)
y.mesh loc=3.03    spac=0.003
# Buffer (0.3 um)
y.mesh loc=3.33    spac=0.002

##################
# REGIONS
##################
# Vacuum
region num=1 material=Vacuum x.min=-250 x.max=250  y.min=-0.92  y.max=-0.87

#Window AlInP (=InAsP)
region num=2 material=InAsP  x.min=-250 x.max=250  y.min=-0.87   y.max=-0.86
#Emitter
region num=3 material=GaAs  x.min=-250 x.max=250  y.min=-0.86   y.max=-0.85
#Base
region num=4 material=GaAs  x.min=-250 x.max=250  y.min=-0.85   y.max=3.02
```

105

```
#BSF
region num=5 material=InGaP x.min=-250 x.max=250  y.min=3.02   y.max=3.03
#Buffer
region num=6 material=GaAs  x.min=-250 x.max=250  y.min=3.03   y.max=3.33

#####################
# ELECTRODES - Use 2% of cell width for optimal grid contact width (500x0.02 =
10um)
#####################
electrode name=cathode     x.min=-5   x.max=5   y.min=-0.87  y.max=-0.87
electrode name=anode       x.min=-250 x.max=250 y.min=3.33 y.max=3.33

####################
# DOPING - n-emitter on p-base
####################
# Window
doping uniform region=2 n.type conc=4.64e17
# Emitter
doping uniform region=3 n.type conc=4.64e15
# Base
doping uniform region=4 p.type conc=1e17
# BSF - Realistic from 1e20
doping uniform region=5 p.type conc=5e19
# Buffer - May want to change to 1e18.
doping uniform region=6 p.type conc=7e18

####################
# MATERIAL PROPERTIES
####################
material TAUN=1e-7 TAUP=1e-7 COPT=1.5e-10 AUGN=8.3e-32 AUGP=1.8e-31

# Vacuum
material material=Vacuum real.index=3.3 imag.index=0

# InGaP
material material=InGaP EG300=1.9 PERMITTIVITY=11.62 AFFINITY=4.16
material material=InGaP MUN=1945 MUP=141
material material=InGaP NC300=1.3e20 NV300=1.28e19
material material=InGaP index.file=InGaP-1.9.opt

# GaAs
material material=GaAs EG300=1.42 PERMITTIVITY=13.1 AFFINITY=4.07
material material=GaAs MUN=8800 MUP=400
material material=GaAs NC300=4.7e17 NV300=7e18
material material=GaAs index.file=GaAs.opt

# Ge
material material=Ge EG300=0.67 PERMITTIVITY=16 AFFINITY=4
material material=Ge MUN=3900 MUP=1800
material material=Ge NC300=1.04e19 NV300=6e18
material material=Ge index.file=Ge.opt

# AlInP (=InAsP)
material material=InAsP EG300=2.4 PERMITTIVITY=11.7 AFFINITY=4.2
material material=InAsP MUN=2291 MUP=142
material material=InAsP NC300=1.08e20 NV300=1.28e19
material material=InAsP index.file=AlInP.opt

#Gold
material material=Gold real.index=1.2 imag.index=1.8

####################
```

```
# MODELS
####################
models srh temp=300 print

####################
# LIGHTBEAMS - Calculates the position of the light source and defines the
beam.
####################
beam num=1 x.origin=0 y.origin=-5 angle=90 back.refl \
      power.file=AM0nrel861.spec wavel.start=0.86 wavel.end=0.862 wavel.num=1

#Output and Display the Structure file
struct outfile=$StructFile
#tonyplot $StructFile

####################
# SOLVING I-V CURVE
####################
method gummel newton maxtraps=10 itlimit=25 climit=1 dvmax=0.1

log outf=GaAs_intensity.log
solve initial
#Beam strength of 1.0 sun
solve b1=1.0
solve vanode=0.0 name=anode vstep=0.05 vfinal=0.6
solve vanode=0.6 name=anode vstep=0.005 vfinal=1.1

extract init infile="GaAs_intensity.log"
extract name="Jsc" y.val from curve(v."anode", i."cathode") where x.val=0.05
extract name="Voc" x.val from curve(v."anode", i."cathode") where y.val=0.0
extract name="iv"  curve(v."anode", i."cathode") outfile="GaAs_intensity.dat"

extract name="Power" curve(v."anode", (v."anode" * i."cathode"))
outf="Power.dat"
# Maximum of curve
extract name="Pmax" max(curve(v."anode", (v."anode" * i."cathode")))
extract name="Vmax" x.val from curve(v."anode", (v."anode"*i."cathode") ) \
      where y.val=$"Pmax"
extract name="Jmax" $"Pmax"/$"Vmax"
extract name="FF" $"Pmax"/($"Jsc"*$"Voc")
#Use Power Incident of 0.02994 W/cm2
extract name="Eff" $Pmax/0.02994

#################
#OUTPUT
#################
tonyplot GaAs_intensity.dat
tonyplot Power.dat

log off
```

G.   GE INTENSITY DETERMINATION

```
# Jamie VanDyke Laser Simulation for Ge Layer of Michael Tsutagawa's Champion
Cell

#At 300K, using the AM0nrel.spec file cell outputs
# Voc= 0.302459 V  Jsc= 71.6097 mA/cm2  Pmax= 0.01563 W/cm2
# Vmax= 0.24 V  Jmax= 65.1267 mA/cm2  FF= 72.1658 %  Eff= 11.5524 %

#At 300K, using a 1511 +/-1 nm laser at 8.85 W/cm2 intensity cell outputs
```

```
# Voc= 0.269605 V  Jsc= 20.0346 mA/cm2  Pmax= 0.0037863 W/cm2
# Vmax= 0.209999 V  Jmax= 18.03 mA/cm2  FF= 70.0979 %  Eff= 21.3915 %


# Main Silvaco ATLAS Structure
go atlas
# Definition of constants
# Mesh
#   X-Mesh
#   Y-Mesh
#   QT Mesh
# Regions
# Electrodes
# Doping
# Material Properties
# Models
# Light beams
# Solving

#Define the X-Mesh.  Must start from left to right, or from lesser to greater
values.
#mesh width=1
mesh width=200000
#mesh space.mult=1
# X-mesh:  surface=500 um2= 1/200000 cm2
x.mesh loc=-250 spac=50
x.mesh loc=0    spac=10
x.mesh loc=250  spac=50


#Define the Y-Mesh.  Must start from surface of the device to the back, or go
from lesser to greater value with up as negative.
# Vacuum
y.mesh loc=4.28  spac=0.003

# Window (0.05 um) - ORIGINAL Cell parameters
y.mesh loc=4.29   spac=0.01
# Emitter (0.1 um)
y.mesh loc=4.39   spac=0.01
# Substrate (300 um)
y.mesh loc=304.39 spac=50

##################
# REGIONS
##################
# Vacuum
region num=1 material=Vacuum x.min=-250 x.max=250  y.min=4.23  y.max=4.28
#Window
region num=2 material=GaAs  x.min=-250 x.max=250  y.min=4.24   y.max=4.29
#Emitter
region num=3 material=Ge    x.min=-250 x.max=250  y.min=4.29   y.max=4.39
#Substrate
region num=4 material=Ge    x.min=-250 x.max=250  y.min=4.39   y.max=304.39

####################
# ELECTRODES - Use 2% of cell width for optimal grid contact width (500x0.02 =
10um)
####################
electrode name=cathode    x.min=-5   x.max=5   y.min=4.29  y.max=4.29
electrode name=anode      x.min=-250 x.max=250 y.min=304.39 y.max=304.39

###################
# DOPING - n-emitter on p-base
```

108

```
####################
# Window
doping uniform region=2 n.type conc=7e18
# Emitter - Changed from 2e18
doping uniform region=3 n.type conc=3e18
# Substrate - Changed from 1e17
doping uniform region=4 p.type conc=3e18


####################
# MATERIAL PROPERTIES
####################
material TAUN=1e-7 TAUP=1e-7 COPT=1.5e-10 AUGN=8.3e-32 AUGP=1.8e-31

# Vacuum
material material=Vacuum real.index=3.3 imag.index=0

# InGaP
material material=InGaP EG300=1.9 PERMITTIVITY=11.62 AFFINITY=4.16
material material=InGaP MUN=1945 MUP=141
material material=InGaP NC300=1.3e20 NV300=1.28e19
material material=InGaP index.file=InGaP-1.9.opt

# GaAs
material material=GaAs EG300=1.42 PERMITTIVITY=13.1 AFFINITY=4.07
material material=GaAs MUN=8800 MUP=400
material material=GaAs NC300=4.7e17 NV300=7e18
material material=GaAs index.file=GaAs.opt

# Ge
material material=Ge EG300=0.67 PERMITTIVITY=16 AFFINITY=4
material material=Ge MUN=3900 MUP=1800
material material=Ge NC300=1.04e19 NV300=6e18
material material=Ge index.file=Ge.opt

# AlInP (=InAsP)
material material=InAsP EG300=2.4 PERMITTIVITY=11.7 AFFINITY=4.2
material material=InAsP MUN=2291 MUP=142
material material=InAsP NC300=1.08e20 NV300=1.28e19
material material=InAsP index.file=AlInP.opt

#Gold
material material=Gold real.index=1.2 imag.index=1.8

####################
# MODELS
####################
models srh temp=300 print

####################
# LIGHTBEAMS - Calculates the position of the light source and defines the
beam.
####################
beam num=1 x.origin=0 y.origin=-5 angle=90 back.refl \
      power.file=AM0nrel1510.spec wavel.start=1.51 wavel.end=1.512 wavel.num=1

#Output and Display the Structure file
struct outfile=$StructFile
#tonyplot $StructFile


####################
# SOLVING I-V CURVE
####################
```

```
method gummel newton maxtraps=10 itlimit=25 climit=1 dvmax=0.1

log outf=Ge_intensity.log
solve initial
#Beam strength of 1.0 sun
solve b1=1.0
solve vanode=0.0 name=anode vstep=0.05 vfinal=0.12
solve vanode=0.12 name=anode vstep=0.005 vfinal=0.3

extract init infile="Ge_intensity.log"
extract name="Jsc" y.val from curve(v."anode", i."cathode") where x.val=0.1
extract name="Voc" x.val from curve(v."anode", i."cathode") where y.val=0.0
extract name="iv"  curve(v."anode", i."cathode") outfile="Ge_intensity.dat"

extract name="Power" curve(v."anode", (v."anode" * i."cathode"))
outfile="Power.dat"
# Max of curve
extract name="Pmax" max(curve(v."anode", (v."anode" * i."cathode")))
extract name="Vmax" x.val from curve(v."anode", (v."anode"*i."cathode") ) \
      where y.val=$"Pmax"
extract name="Jmax" $"Pmax"/$"Vmax"
extract name="FF" $"Pmax"/($"Jsc"*$"Voc")
#Use Power Incident of 0.0177 W/cm2
extract name="Eff" $Pmax/0.0177

#################
#OUTPUT
#################
tonyplot Ge_intensity.dat

log off
```

H.   CHAMPION UNDER LASER ILLUMINATION

```
# Jamie VanDyke Laser Simulation for Michael Tsutagawa's Champion Cell

#At 300K, using the AM0nrel.spec file cell outputs
# Voc= 2.76425 V  Jsc= 19.8531 mA/cm2  Pmax= 0.0490907 W/cm2
# Vmax= 2.525 V  Jmax= 19.4419 mA/cm2  FF= 89.4527 %  Eff= 36.2829 %

#At 300K, using AM0nrel1.spec file cell outputs
# Voc= 2.75339 V  Jsc= 20.0003 mA/cm2  Pmax= 0.0482219 W/cm2
# Vmax= 2.475 V  Jmax= 19.4836 mA/cm2  FF= 87.5669 %  Eff= 51.15 %

# Main Silvaco ATLAS Structure
go atlas
# Definition of constants
# Mesh
#   X-Mesh
#   Y-Mesh
#   QT Mesh
# Regions
# Electrodes
# Doping
# Material Properties
# Models
# Light beams
# Solving

#Define the X-Mesh.  Must start from left to right, or from lesser to greater
values.
```

110

```
#mesh width=1
mesh width=200000
#mesh space.mult=1
# X-mesh:  surface=500 um2= 1/200000 cm2
x.mesh loc=-250 spac=50
x.mesh loc=0    spac=10
x.mesh loc=250  spac=50


#Define the Y-Mesh.  Must start from surface of the device to the back, or go
from lesser to greater value with up as negative.
# Vacuum
y.mesh loc=-0.87  spac=0.003
# Window (0.01 um)
y.mesh loc=-0.86  spac=0.003
# Emitter (0.17 um)
y.mesh loc=-0.69  spac=0.003
# Base (0.63 um)
y.mesh loc=-0.34  spac=0.03
y.mesh loc=-0.06  spac=0.003
# BSF (0.01 um)
y.mesh loc=-0.05  spac=0.003
# Buffer (0.03 um)
y.mesh loc=-0.02  spac=0.002

# Tunnel Emitter (0.015)
y.mesh loc=-0.005 spac=0.001
# Tunnel Base (0.015)
y.mesh loc=0.01    spac=0.001

# Window (0.01 um)
y.mesh loc=0.02    spac=0.003
# Emitter (0.01 um)
y.mesh loc=0.03    spac=0.003
# Base (3.87 um)
y.mesh loc=2.815  spac=0.03
y.mesh loc=3.90    spac=0.003
# BSF (0.01 um)
y.mesh loc=3.91    spac=0.003
# Buffer (0.3 um)
y.mesh loc=4.21    spac=0.002

# Tunnel Emitter (0.015)
y.mesh loc=4.225  spac=0.001
# Tunnel Base (0.015)
y.mesh loc=4.24    spac=0.001

# Window (0.05 um) - ORIGINAL Cell parameters
y.mesh loc=4.29    spac=0.01
# Emitter (0.1 um)
y.mesh loc=4.39    spac=0.01
# Substrate (300 um)
y.mesh loc=304.39 spac=50


#################
# REGIONS
#################
# Vacuum
region num=1 material=Vacuum x.min=-250 x.max=250  y.min=-0.92  y.max=-0.87
#Window AlInP (=InAsP)
region num=2 material=InAsP  x.min=-250 x.max=250  y.min=-0.87  y.max=-0.86
#Emitter
region num=3 material=InGaP  x.min=-250 x.max=250  y.min=-0.86  y.max=-0.69
```

```
#Base
region num=4 material=InGaP  x.min=-250 x.max=250  y.min=-0.69  y.max=-0.06
#BSF
region num=5 material=InGaP  x.min=-250 x.max=250  y.min=-0.06  y.max=-0.05
#Buffer AlInP (=InAsP)
region num=6 material=InAsP  x.min=-250 x.max=250  y.min=-0.05  y.max=-0.02

#Tunnel Emitter
region num=7 material=InGaP  x.min=-250 x.max=250  y.min=-0.02  y.max=-0.005
#Tunnel Base
region num=8 material=InGaP  x.min=-250 x.max=250  y.min=-0.005 y.max=0.01

#Window AlInP (=InAsP)
region num=9 material=InAsP  x.min=-250 x.max=250  y.min=0.01   y.max=0.02
#Emitter
region num=10 material=GaAs  x.min=-250 x.max=250  y.min=0.02   y.max=0.03
#Base
region num=11 material=GaAs  x.min=-250 x.max=250  y.min=0.03   y.max=3.90
#BSF
region num=12 material=InGaP x.min=-250 x.max=250  y.min=3.90   y.max=3.91
#Buffer
region num=13 material=GaAs  x.min=-250 x.max=250  y.min=3.91   y.max=4.21

#Tunnel Emitter
region num=14 material=GaAs  x.min=-250 x.max=250  y.min=4.21   y.max=4.225
#Tunnel Base
region num=15 material=GaAs  x.min=-250 x.max=250  y.min=4.225  y.max=4.24

#Window
region num=16 material=GaAs  x.min=-250 x.max=250  y.min=4.24   y.max=4.29
#Emitter
region num=17 material=Ge    x.min=-250 x.max=250  y.min=4.29   y.max=4.39
#Substrate
region num=18 material=Ge    x.min=-250 x.max=250  y.min=4.39   y.max=304.39

#####################
# ELECTRODES - Use 2% of cell width for optimal grid contact width (500x0.02 =
10um)
#####################
electrode name=cathode    x.min=-5   x.max=5   y.min=-0.87  y.max=-0.87
electrode name=tunneltop  x.min=-250 x.max=250 y.min=-0.02  y.max=0.01
electrode name=tunnelbot  x.min=-250 x.max=250 y.min=4.21   y.max=4.24
electrode name=anode      x.min=-250 x.max=250 y.min=304.39 y.max=304.39

####################
# DOPING - n-emitter on p-base
####################
# Window - Realistic from 1e20
doping uniform region=2 n.type conc=5e19
# Emitter
doping uniform region=3 n.type conc=4.64e17
# Base
doping uniform region=4 p.type conc=1e17
# BSF - Realistic from 1e20
doping uniform region=5 p.type conc=5e19
# Buffer
doping uniform region=6 p.type conc=1e18

# Tunnel Emitter
doping uniform region=7 p.type conc=8e18
# Tunnel Base
doping uniform region=8 n.type conc=1e19
```

112

```
# Window
doping uniform region=9 n.type conc=4.64e17
# Emitter
doping uniform region=10 n.type conc=4.64e15
# Base
doping uniform region=11 p.type conc=1e17
# BSF - Realistic from 1e20
doping uniform region=12 p.type conc=5e19
# Buffer - May want to change to 1e18.
doping uniform region=13 p.type conc=7e18

# Tunnel Emitter
doping uniform region=14 p.type conc=8e18
# Tunnel Base
doping uniform region=15 n.type conc=1e19

# Window
doping uniform region=16 n.type conc=7e18
# Emitter - Changed from 2e18
doping uniform region=17 n.type conc=3e18
# Substrate - Changed from 1e17
doping uniform region=18 p.type conc=3e18


#####################
# MATERIAL PROPERTIES
#####################
material TAUN=1e-7 TAUP=1e-7 COPT=1.5e-10 AUGN=8.3e-32 AUGP=1.8e-31

# Vacuum
material material=Vacuum real.index=3.3 imag.index=0

# InGaP
material material=InGaP EG300=1.9 PERMITTIVITY=11.62 AFFINITY=4.16
material material=InGaP MUN=1945 MUP=141
material material=InGaP NC300=1.3e20 NV300=1.28e19
material material=InGaP index.file=InGaP-1.9.opt

# GaAs
material material=GaAs EG300=1.42 PERMITTIVITY=13.1 AFFINITY=4.07
material material=GaAs MUN=8800 MUP=400
material material=GaAs NC300=4.7e17 NV300=7e18
material material=GaAs index.file=GaAs.opt

# Ge
material material=Ge EG300=0.67 PERMITTIVITY=16 AFFINITY=4
material material=Ge MUN=3900 MUP=1800
material material=Ge NC300=1.04e19 NV300=6e18
material material=Ge index.file=Ge.opt

# AlInP (=InAsP)
material material=InAsP EG300=2.4 PERMITTIVITY=11.7 AFFINITY=4.2
material material=InAsP MUN=2291 MUP=142
material material=InAsP NC300=1.08e20 NV300=1.28e19
material material=InAsP index.file=AlInP.opt

#Gold
material material=Gold real.index=1.2 imag.index=1.8

####################
# MODELS
####################
```

```
models srh temp=300 print

#####################
# CONTACTS
#####################
contact name=tunneltop resist=1e17
contact name=tunnelbot resist=1e17

#####################
# LIGHTBEAMS - Calculates the position of the light source and defines the
beam.
#####################
beam num=1 x.origin=0 y.origin=-5 angle=90 back.refl \
      power.file=AM0nrel1.spec wavel.start=0.553 wavel.end=0.555 wavel.num=1
beam num=2 x.origin=0 y.origin=-5 angle=90 back.refl \
      power.file=AM0nrel1.spec wavel.start=0.860 wavel.end=0.862 wavel.num=1
beam num=3 x.origin=0 y.origin=-5 angle=90 back.refl \
      power.file=AM0nrel1.spec wavel.start=1.51 wavel.end=1.512 wavel.num=1
#Output and Display the Structure file
struct outfile=$StructFile
#tonyplot $StructFile


#####################
# SOLVING I-V CURVE
#####################
method gummel newton maxtraps=10 itlimit=25 climit=1 dvmax=0.1

log outf=Combined_laser.log
solve initial
#Beam strength of 1.0 sun
solve b1=1.0 b2=1.0 b3=1.0
solve vanode=0.0 name=anode vstep=0.05 vfinal=2.4
solve vanode=2.4 name=anode vstep=0.005 vfinal=2.8

extract init infile="Combined_laser.log"
extract name="Jsc" y.val from curve(v."anode", i."cathode") where x.val=0.05
extract name="Voc" x.val from curve(v."anode", i."cathode") where y.val=0.0
extract name="iv"  curve(v."anode", i."cathode") outfile="Combined_laser.dat"

extract name="Power" curve(v."anode", (v."anode" * i."cathode"))
outf="Power.dat"
# Max of curve
extract name="Pmax" max(curve(v."anode", (v."anode" * i."cathode")))
extract name="Vmax" x.val from curve(v."anode", (v."anode"*i."cathode") ) \
      where y.val=$"Pmax"
extract name="Jmax" $"Pmax"/$"Vmax"
extract name="FF" $"Pmax"/($"Jsc"*$"Voc")
#Use Power Incident of 0.09434 W/cm2
extract name="Eff" $Pmax/0.09434

#################
#OUTPUT
#################
tonyplot Combined_laser.dat

log off
```

114

LIST OF REFERENCES

"Adaptive Optics," Wikipedia, 14 May 2010,
    http://en.wikipedia.org/wiki/Adaptive_optics, (31 May 2010).

Air Force Technology Web site, "ABL YAL 1A Airborne Laser, USA,"
    http://www.airforce-technology.com/projects/abl/, (31 May 2010).

ATLAS User's Manual, vols 1–2, SILVACO International, 2000.

Bates, Andrew D. "Novel Optimization Techniques For Multi-junction Solar Cell
    Design Using Silvaco Atlas," Master's thesis, Naval Postgraduate School,
    Monterey, CA, June, 2004.

Boeing, "Airborne Laser Test Bed," http://www.boeing.com/defense-
    space/military/abl/index.html, (31 May 2010).

Boeing, "Boeing Completes Preliminary Design of Free Electron Laser Weapon System,"
    http://boeing.mediaroom.com/index.php?s=43&item=1126, March 2010 (23 May
    2010).

Buelher, Patrick, Joshua Smith Modeling Laser Effects on Imaging Spacecraft Using the
    SSM. Ball Aerospace and Technologies Corp., Albuquerque, New Mexico, 2006.

Buelher, Patrick, Joshua Smith Satellite Survivability Module (SSM) Version 2.0. Ball
    Aerospace and Technologies Corp., Albuquerque, New Mexico, 2007.

Chase, Charles T. "Annealing of Defect Sites in Radiation Damaged Indium Phosphide
    Solar Cells Through Laser Illumination," Master's thesis, Naval Postgraduate
    School, Monterey, CA, December, 1995.

Davenport, Bradley P. "Advanced Thermophotovoltaic Cells Modeling, Optimized For
    Use In Radioisotope Thermoelectric Generators (RTGS) For Mars and Deep
    Space Mission," Master's thesis, Naval Postgraduate School, Monterey, CA, June
    2004.

"Free Electron Laser," Wikipedia, 7 February 2010,
    http://en.wikipedia.org/wiki/Free_electron_laser, (31 May 2010).

Guoan, Christopher M. "Ground-Based high Energy Power Beaming Support of
    Spacecraft Power Requirements," Master's thesis, Naval Postgraduate School,
    Monterey, CA, June 2006.

Kuhn, Kelin J. Laser Engineering. New Jersey: Prentice Hall, 1998.

Landis, Geoffrey A. "Photovoltaic Receivers for Laser Beamed Power in Space," NASA Contractor Report 189075, presented at 22nd IEEE Photovoltaic Specialists Conference, Las Vegas, NV 7-11October 1991.

Landis, Geoffrey A. "Laser Beamed Power: Satellite Demonstration Applications," Paper IAF-92-0600, 43rd IAF Congress, Washington DC, September 1992.

Landis, Geoffrey A. "Satellite Eclipse Power by Ground-Based Laser Illumination," NASA Glenn Research Center, Ohio, August 1990.

Landis, Geoffrey, A. "Space Power by Ground-Based Laser Illumination," Intersociety Energy Conversion Engineering Conference, September 15, 1991.

Landis, Geoffrey A., Mark Stavnes, Steve Oleson, and John Bozek, "Space Transfer with Ground-Based Laser / Electric Propulsion," Paper AIAA-92-3213, NASA Glenn Research Center, Ohio, July 1992.

Lavery, Jeffrey B. "Quantum Tunneling Model of a P-N Juntion in SILVACO," Master's thesis, Naval Postgraduate School, Monterey, CA, September 2008.

Luce, Richard C. "Spacecraft Power Beaming and Solar Cell Annealing Using High-Energy Lasers," Master's thesis, Naval Postgraduate School, Monterey, CA, December 2002.

"Memory Effect," Wikipedia, 23 January 2010, http://en.wikipedia.org/wiki/Memory_effect, (31 May 2010).

Michael, Sherif. Personal discussions, Naval Postgraduate School Department of Electrical and Computer Engineering, Space Systems Academic Group.

Michael, Sherif. EC3230 Lecture Notes. Naval Postgraduate School, 2009.

Michalopoulos, Panayiotis, "A Novel Approach For The Development and Optimization of State-of-the-Art Photovoltaic Devices Using Silvaco," Master's thesis, Naval Postgraduate School, Monterey, CA, March 2002.

"Mode-locking," Wikipedia, 28 April 2010, http://en.wikipedia.org/wiki/Mode-locking, (31 May 2010).

Phillips Blog, http://phillips.blogs.com/goc/page/2/, (23 May 2010).

Silfvast, William T. Laser Fundamentals.   United Kingdom: Cambridge University Press, 2004.

SILVACO International Web site, www.silvaco.com, (31 May 2010).

Tsutagawa, Michael H. "Triple Junction InGaP/GaAs/Ge Solar Cell Optimization Using Silvaco Atlas," Master's thesis, Naval Postgraduate School, Monterey, CA, December 2008.

Wertz, James R. and Wiley J. Larson. <u>Space Mission Analysis and Design</u>. 3rd edition. California: Microcosm Press, 1999.

THIS PAGE INTENTIONALLY LEFT BLANK

INITIAL DISTRIBUTION LIST

1.   Defense Technical Information Center
        Ft. Belvoir, Virginia

2.   Dudley Knox Library
        Naval Postgraduate School
        Monterey, California